UiT
THE ARCTIC
UNIVERSITY
OF NORWAY

Faculty of Science and Technology
Department of Mathematics and Statistics

A bidirectional pulse propagation model for extreme nonlinear optics: derivation and implementation.

Magdalena Korzeniowska

Master thesis in Applied Mathematics MAT-3900, May 2020

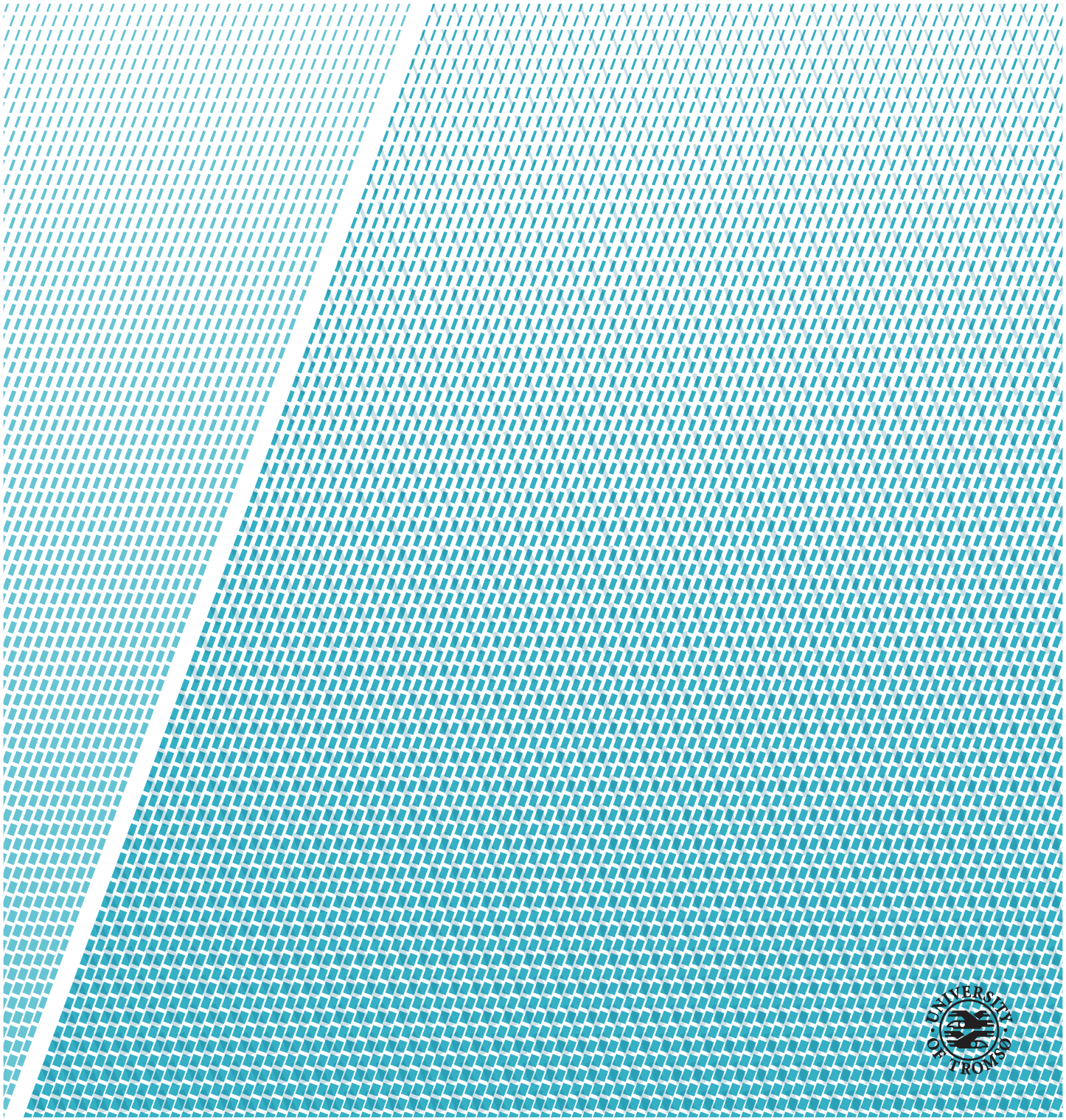

"And God said, *Let there be light*, and there was light."
–Genesis 1:3

Abstract

With growing capabilities of high-intensity laser beams to generate ultra-short pulses of light, the simulation of pulse propagation in nonlinear media is expected to catch up with the front-line experimental setups. Among the challenges of nonlinear material response modeling is the ability to capture the back-scatter effect - a phenomenon inherently elusive for the well-established methods of unidirectional type. In this paper we consider a bidirectional shooting method proposed by P. Jakobsen in "Bidirectional pulse propagation equation for extreme nonlinear optics.", Physica Scripta, 89:095502, 2014.

We derive the method for a Transverse Magnetic (TM) field, propagating in a material slab with a Kerr-type nonlinear polarization response, and delimited by two material interfaces. By performing a proof-of-concept implementation of the method, we demonstrate that it is indeed capable of reconstructing the expected quantitative and qualitative properties of the modeled physical system, including reflection from interfaces and third harmonic generation. Nevertheless, we find that both the accuracy of the solution, as well as the convergence of the iterative process, are negatively impacted by an increase in the relative scale of the nonlinearity coefficient. That points to the limitations of the underlying implementation and, potentially, the BPPE method itself. In that context we conclude with a brief discussion of the interdependence between the BPPE method and its numerical incarnations.

Acknowledgements

I would like to thank my supervisor, professor Per Kristen Jakobsen, for digressing in a most-inspiring way.

Contents

List of Figures

List of Tables

List of Acronyms

AST	Artificial Source Test
BC	Boundary Condition
BPPE	Bidirectional Pulse Propagation Equation
DFT	Discrete Fourier Transform
EM	Electromagnetic
FFT	Fast Fourier Transform
FT	Fourier Transform
FTC	Fundamental Theorem of Calculus
FWHM	Full Width at Half Maximum
IFFT	Inverse Fast Fourier Transform
IFT	Inverse Fourier Transform
LHS	Left-Hand Side
RHS	Right-Hand Side
SI	International System of Units
TE	Transverse Electric
TM	Transverse Magnetic
UPPE	Unidirectional Pulse Propagation Equation

Part I

Model derivation

1

Introduction

Modeling laser pulse propagation through material media has become more challenging in the recent years, as the physically available lasers became capable of generating ultra-intense, $\sim 10^{16}\left[W/cm^2\right]$, and ultra-short, $\sim 10^{-18}\,[s]$, pulses of light. Such extreme conditions can easily excite new degrees of freedom in the underlying system, leading to the emergence of complex interactions between the external electric field and the response of the material. In consequence, nonlinear polarization effects are induced in the material, causing non-negligible scattering of light, and hence changing the direction of light propagation.

A mathematical tool widely used in the modeling of pulse propagation, and a well-established one too, is a Unidirectional Pulse Propagation Equation (UPPE) method [10], with generalizations presented in [8] and [9]. It is a spectral method, suited for capturing nonlinear effects and multiple harmonic generation in nonlinear media. However, as the name suggest, the assumptions of the method break down as soon as there is a significant back-propagation of light involved. That includes not only the back-scattering effect, but also the reflection from material interfaces.

In response to that weakness, a bidirectional extension of the UPPE method was proposed in [6], called a BPPE method. The method takes advantage of a certain redundancy in the eigenmode representation of the solution, and poses an additional constraint on the amplitudes of the eigenmodes. This constraint is the key leverage that allows to introduce the back-propagation capability into

the method. That new, key feature is then employed in an iterative-shooting regime approximating the light propagation solution.

The applicability of the BPPE method is backed with the results of concrete simulation experiments in [3]. In this paper we derive the BPPE method for a Transverse Magnetic (TM)-field propagating in a material medium with a Kerr-type nonlinear response, and in presence of two material interfaces delimiting the material slab. We also present a validation technique for the BPPE method, a proof-of-concept numerical implementation, and the corresponding simulation results.

* * *

This paper is structured as follows. After presenting the modeling assumptions, we proceed to deriving a pulse-propagation model from Maxwell's equations. We show how the system of differential equations in time can be reformulated into an explicit system of first order differential equations in space, such that a boundary problem can be posed for the propagation of the electric field state, from an initial boundary into the rest of the spatial domain. We solve the problem in spectral domain, deriving a system of coupled differential equations for the amplitudes of the eigenmodes, called a BPPE system.

We continue with addressing the issue of traversing material interfaces. Departing from the continuity conditions for the TM-field, we derive three continuity equations, describing how the transition into and out-of the material slab is performed. We also impose conditions guaranteeing that the solutions to the model represent actual physical processes.

With all tools at hand, in Chapter 6 we present the full BPPE model, the core of this thesis paper. We perform scaling of the model, and make a choice of physical scales and parameters for the represented physical system. To accompany the model, in the following chapter we present a dedicated Artificial Source Test (AST). The testing technique was originally presented in [7] for a Transverse Electric (TE)-mode. We adapt it to incorporate the particularities of the TM-mode.

In the second part of this paper we present the numerical implementation of the BPPE method and the AST. We focus on particular implementation choices made. Then, we introduce the scope of the simulations performed, and present their results. We present two major simulation cases, with different emphasis on the nonlinear Kerr-effect.

The paper concludes with a discussion of the findings from the simulation part, proposing also a way forward, both for the BPPE method, as well as for the underlying implementation.

2

Modeling assumptions

2.1 Physical setup

The physical setup that we consider in this paper is presented in Figure 2.1. It consists of a material slab placed in a vacuum. There are two material interfaces perpendicular to the z-axis, one at point $z = a$, and the other at $z = b$. The slab is conceptually infinite in x-direction, there are no horizontal material interfaces. We distinguish between the two faces of each interface, marking them with $z = a^-$ and $z = b^-$ for the left-hand sides, and $z = a^+$, $z = b^+$ for the right hand sides. This is formally introduced in interface-transition section 4.1.2. Interface point $z = a$ is also denoted as z_a, and for point $z = b$ we use z_b.

Further, we consider an electromagnetic pulse entering the slab at point $z = a^-$, propagating through the slab, and exiting the slab at point $z = b^+$. Due to the nonlinear polarization effect, some portion of the electromagnetic radiation is expected to be back-scattered inside the slab, traveling in the opposite direction. Internal reflection from the material interface is also expected, due to the difference in the refractive indices of vacuum and the slab material. The back-scattered or reflected light exits the slab back at the first interface $z = a$.

Further discussion about light propagation in material slab are included in section 5.3, and then continued in section 6.1.2, put into the perspective of BPPE method.

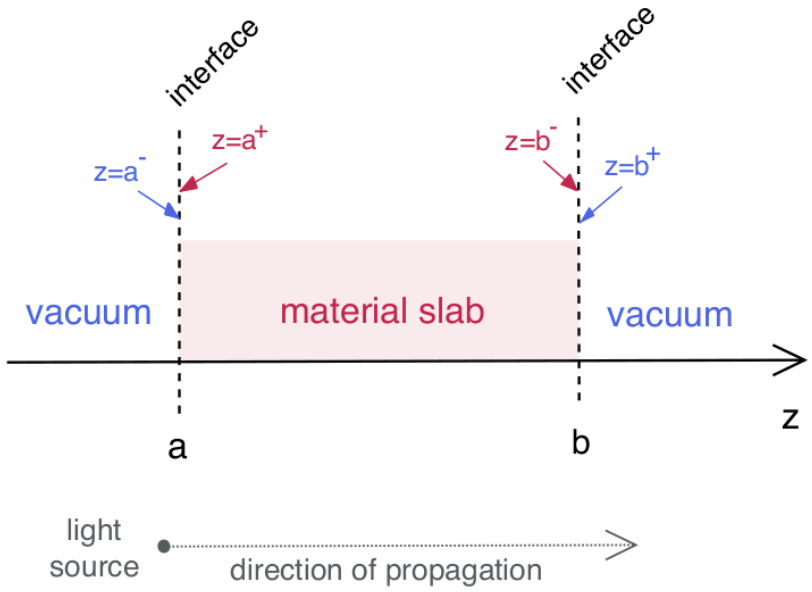

Figure 2.1: Physical setup.

2.2 TM field

In this paper we consider only the TM mode of an electromagnetic field. As indicated in [6], analogous derivations can be made for general electromagnetic fields. Such derivations are to a certain extent provided in [5].

We model the electromagnetic wave as a plane wave, where the electric and magnetic field components are perpendicular to each other. For the TM field, as the name suggests, the magnetic field component is perpendicular to the direction of propagation of the electromagnetic wave. Assuming a Cartesian coordinate system, and placing the magnetic field vector parallel to the y-axis, we must have the electric field vector lying in the xz-plane, as shown in Figure 2.2. We assume the direction of propagation along the z-axis.

The TM field and the nonlinear polarization can be written in component form as:

$$\begin{aligned} \boldsymbol{E}(z,x,t) &= e_1(z,x,t)\,\hat{\imath} \\ &= e_2(z,x,t)\,\hat{k}, \\ \boldsymbol{B}(z,x,t) &= b(z,x,t)\,\hat{\jmath}, \\ \boldsymbol{P}_{NL}(z,x,t) &= p_1(z,x,t)\,\hat{\imath} \\ &= p_2(z,x,t)\,\hat{k}, \end{aligned} \tag{2.1}$$

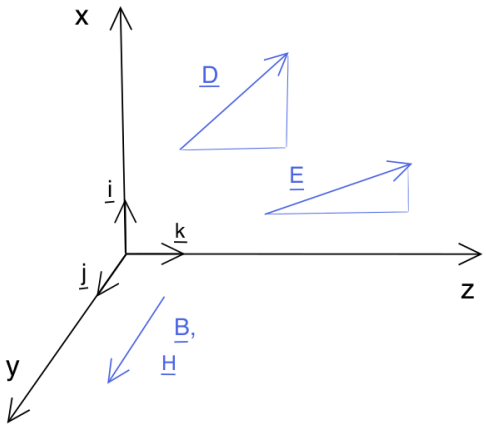

Figure 2.2: TM-field components.

where $\hat{\imath}, \hat{\jmath}$ and $\hat{k}$ are unit vectors along $x, y,$ and z axes respectively. We note that magnetic field $\boldsymbol{B}$ has only one component. We delay writing out the components of the electric flux density vector $\boldsymbol{D}$ until section 3.1.

2.3 Polarization model

Electromagnetic field present in a non-vacuum medium interacts with the electrically charged particles of the medium by exerting an electromagnetic force on them. In a dielectric material, the electrons are bound to atoms and do not flow freely through the medium (no electric current). Nevertheless, they can be pulled out from their equilibrium points by the acting force, causing polarization of the medium.

The redistribution of electrons gives rise to a new electric field in the medium. This new electric field interacts with the external electric field applied to the dielectric in the first place. That, in turn, modifies the polarization of the medium even further, and so on. The interaction between the two electric fields becomes intertwined.

We consider a polarization vector $\boldsymbol{P}(t, x, y, z)$ to be a sum of linear and nonlinear functions of electric field $\boldsymbol{E}(t, x, y, z)$. Dropping the dependence on arguments we have:

$$\boldsymbol{P} = \epsilon_0 (\boldsymbol{P}_L + \boldsymbol{P}_{NL}), \tag{2.2}$$

where

$$\boldsymbol{P}_L = \mathcal{L}(\boldsymbol{E}),$$
$$\mathcal{L}(\cdot) = \int_{-\infty}^{t} dt' \; \chi(t - t', z) \; (\cdot), \tag{2.3}$$
$$\boldsymbol{P}_{NL} = \eta \boldsymbol{E}^2 \boldsymbol{E}, \tag{2.4}$$

and η is a relatively small number, making the nonlinear polarization influence much less profound. Such model, where the impact of nonlinear polarization is much smaller than the impact of linear polarization, is reasonable in the context of short-wave optics. We go back to determining the actual scale of the nonlinearity factor η in section 6.2.3.

The linear polarization is determined by linear operator (2.3). This operator performs a convolution of the electric field at previous times with time-dependent susceptibility χ. Susceptibility of a dielectric material is a dimensionless quantity, reflecting how easily the material polarizes in response to an electric field.

The nonlinear polarization component (2.4) is of the form of *Kerr-type* nonlinearity. This is the only nonlinearity type that we consider in this paper.

2.4 Dispersion model

The dispersive properties of the material slab are of relevance in our considerations. Different frequency modes travel through a dispersive medium with different phase velocities, causing a *dispersion* of a temporal signal. This is modeled by a frequency-dependent refractive index.

In Chapter 3 and Appendix B we show how the refractive index arises from susceptibility when solving the light propagation model based on Maxwell's equations. Primarily, we consider linear susceptibility operator and a linear refractive index $n(\omega)$. For the refractive index we assume a particular model, which we present in this section as one of the modeling assumptions. In order to account for the nonlinear polarization Kerr effect, we also introduce, in section 6.2.3, a concept of *nonlinear* refractive index n_2. This nonlinear index is then incorporated into the overall nonlinearity coefficient η.

For modeling dispersion we use *Lorentz oscillator model* and write the susceptibility $\widehat{\chi}$ as a function of frequency ω as

$$\widehat{\chi}(\omega) = \frac{\omega_p^2}{\omega_r^2 - \omega^2 - i\gamma\omega}, \tag{2.5}$$

where

ω_p is plasma frequency, and $\omega_p^2 = \frac{q^2 N}{\epsilon_0 m_e}$, where q is electron charge, N is electron density, m_e is mass of electron,

ω_r is resonance frequency,

$\gamma = \frac{2}{\tau}$, where τ is pulse duration, or width in time domain.

Given susceptibility, we model the *complex* refractive index $n_c(\omega)$ as

$$\begin{aligned} n_c^2(\omega) = (n(\omega) + i\alpha(\omega))^2 &= 1 + \widehat{\chi}(\omega) \\ &= 1 + \mathrm{Re}\{\widehat{\chi}(\omega)\} + i\,\mathrm{Im}\{\widehat{\chi}(\omega)\}, \end{aligned} \tag{2.6}$$

where $n(\omega)$ and $\alpha(\omega)$ are the real refractive index and the absorption coefficient respectively. Separating out the real and imaginary parts of equation (2.6) we get

$$\begin{aligned} \epsilon_{Re} &= 1 + \mathrm{Re}\{\widehat{\chi}(\omega)\} = 1 + \frac{\omega_p^2\left(\omega_r^2 - \omega^2\right)}{\left(\omega_r^2 - \omega^2\right)^2 + \omega^2\gamma^2}, \\ \epsilon_{Im} &= \mathrm{Im}\{\widehat{\chi}(\omega)\} = \frac{\omega_p^2\gamma\omega}{\left(\omega_r^2 - \omega^2\right)^2 + \omega^2\gamma^2}. \end{aligned}$$

With that we write the refractive index and the absorption coefficient as

$$\begin{aligned} n(\omega) &= \sqrt{\frac{1}{2}\left(\epsilon_{Re} + \sqrt{\epsilon_{Re}^2 + \epsilon_{Im}^2}\right)}, \\ \alpha(\omega) &= \sqrt{\frac{1}{2}\left(-\epsilon_{Re} + \sqrt{\epsilon_{Re}^2 + \epsilon_{Im}^2}\right)}. \end{aligned} \tag{2.7}$$

For particular values of parameters ω_p, ω_r, γ those two functions of ω can be graphed. We do this in scaling section 6.3.3. We also show there that the absorption coefficient $\alpha(\omega)$ is negligible under the chosen parameter set, giving

$$n_c(\omega) \approx \mathrm{Re}\{n_c(\omega)\} = n(\omega).$$

Thus, throughout this paper, we associate refractive index with the real refractive index $n(\omega)$, defined as in (2.7).

3

Light propagation

3.1 Maxwell's equations in component form

For modeling of electromagnetism we naturally depart from Maxwell's equations. We consider an isotropic, homogeneous, and non-magnetic material with no free charges or currents[1]. Maxwell's equations are given as

$$\begin{aligned} \nabla \times \boldsymbol{E} + \partial_t \boldsymbol{B} &= 0, \\ \nabla \times \boldsymbol{H} - \partial_t \boldsymbol{D} &= 0, \\ \nabla \cdot \boldsymbol{B} &= 0, \\ \nabla \cdot \boldsymbol{D} &= 0, \end{aligned} \tag{3.1}$$

and using (2.2) we also have

$$\begin{aligned} \boldsymbol{H} &= \frac{1}{\mu_0}\boldsymbol{B}, \\ \boldsymbol{D} &= \epsilon_0 \boldsymbol{E} + \boldsymbol{P} \\ &= \epsilon_0 \left(\boldsymbol{E} + \boldsymbol{P}_L + \boldsymbol{P}_{NL}\right) \\ &= \epsilon_0 \left(\boldsymbol{E} + \mathcal{L}(\boldsymbol{E}) + \eta \boldsymbol{E}^2 \boldsymbol{E}\right) \\ &= \epsilon_0 (1 + \mathcal{L})(\boldsymbol{E}) + \epsilon_0 \eta \boldsymbol{E}^2 \boldsymbol{E}, \end{aligned}$$

1. nothing is assumed about the dispersive properties of the material yet

which in component form becomes

$$\begin{aligned}
\boldsymbol{H} &= \frac{1}{\mu_0} b, \\
\boldsymbol{D} &= \epsilon_0 (1 + \mathcal{L}) \begin{bmatrix} e_1 \\ e_2 \end{bmatrix} + \epsilon_0 \begin{bmatrix} p_1 \\ p_2 \end{bmatrix} && (3.2) \\
&= \epsilon_0 (1 + \mathcal{L}) \begin{bmatrix} e_1 \\ e_2 \end{bmatrix} + \epsilon_0 \eta \left(e_1^2 + e_2^2 \right) \begin{bmatrix} e_1 \\ e_2 \end{bmatrix} = \begin{bmatrix} d_1 \\ d_2 \end{bmatrix}. && (3.3)
\end{aligned}$$

Inserting polarization and electromagnetic field components (2.1) and (3.2) into Maxwell's equations (3.1) we get

$$\begin{aligned}
\boldsymbol{\nabla} \times \boldsymbol{E} &= \cancelto{0}{\left(\partial_y e_2 \right)} \hat{\imath} + (\partial_z e_1 - \partial_x e_2) \hat{\jmath} - \cancelto{0}{\left(\partial_y e_1 \right)} \hat{k}, \\
\partial_t \boldsymbol{B} &= \partial_t b \, \hat{\jmath} \\
&\Rightarrow (\partial_z e_1 - \partial_x e_2 + \partial_t b) \hat{\jmath} = 0,
\end{aligned}$$

$$\begin{aligned}
\boldsymbol{\nabla} \times \boldsymbol{H} &= \frac{1}{\mu_0} \left(-\partial_z b \, \hat{\imath} + \partial_x b \, \hat{k} \right), \\
\partial_t \boldsymbol{D} &= \epsilon_0 \partial_t \left[(1 + \mathcal{L}) \begin{bmatrix} e_1 \\ e_2 \end{bmatrix} + \begin{bmatrix} p_1 \\ p_2 \end{bmatrix} \right] \\
&\Rightarrow \left(-\frac{1}{\mu_0} \partial_z b \right) \hat{\imath} = (\epsilon_0 \partial_t \left[(1 + \mathcal{L}) e_1 + p_1 \right]) \hat{\imath}, \\
&\qquad \left(\frac{1}{\mu_0} \partial_x b \right) \hat{k} = (\epsilon_0 \partial_t \left[(1 + \mathcal{L}) e_2 + p_2 \right]) \hat{k},
\end{aligned}$$

$$\boldsymbol{\nabla} \cdot \boldsymbol{B} = \cancelto{0}{\partial_y b} \Rightarrow \quad 0 = 0,$$

$$\boldsymbol{\nabla} \cdot \boldsymbol{D} = \epsilon_0 \partial_x \left[(1 + \mathcal{L}) e_1 + p_1 \right] + \epsilon_0 \partial_z \left[(1 + \mathcal{L}) e_2 + p_2 \right] = 0.$$

We gather the above results into a systems of Maxwell's equations for TM mode in component form

$$\begin{aligned}
\partial_z e_1 - \partial_x e_2 + \partial_t b &= 0, && (3.4) \\
-\partial_z b &= \frac{1}{c^2} \partial_t \left[(1 + \mathcal{L}) e_1 + p_1 \right], && (3.5) \\
\partial_x b &= \frac{1}{c^2} \partial_t \left[(1 + \mathcal{L}) e_2 + p_2 \right], && (3.6) \\
\partial_x (1 + \mathcal{L}) e_1 + \partial_z (1 + \mathcal{L}) e_2 &= -\partial_x p_1 - \partial_z p_2, && (3.7)
\end{aligned}$$

where we have used that $\epsilon_0 \mu_0 = \frac{1}{c^2}$.

In order to propagate the initial state along z, we write the above equations as an explicit ∂_z-propagation system

$$\partial_z e_1 = \partial_x e_2 - \partial_t b, \tag{3.8}$$
$$\partial_z (1 + \mathcal{L}) e_2 = -\partial_x (1 + \mathcal{L}) e_1 - \partial_x p_1 - \partial_z p_2, \tag{3.9}$$
$$\partial_z b = -\frac{1}{c^2} \partial_t \left[(1 + \mathcal{L}) e_1 + p_1 \right], \tag{3.10}$$

with an additional constraint

$$\partial_x b - \frac{1}{c^2} \partial_t \left[(1 + \mathcal{L}) e_2 + p_2 \right] = 0. \tag{3.11}$$

For the system (3.8)-(3.10) to be explicit in ∂_z, we must handle the $\partial_z p_2$ term on the Right-Hand Side (RHS) of equation (3.9). We do it in section 3.2.1.

We now take a look at the constraint (3.11). Taking ∂_z of (3.11) and inserting equations (3.10) and (3.9) we get

$$\begin{aligned}
&\partial_{xz} b - \frac{1}{c^2} \partial_{tz} \left[(1 + \mathcal{L}) e_2 + p_2 \right] \\
&\quad = \partial_x \left(-\frac{1}{c^2} \partial_t \left[(1 + \mathcal{L}) e_1 + p_1 \right] \right) - \frac{1}{c^2} \partial_{tz} \left[(1 + \mathcal{L}) e_2 + p_2 \right] \\
&\quad = -\frac{1}{c^2} \partial_t \left[(1 + \mathcal{L}) \partial_x e_1 + (1 + \mathcal{L}) \partial_z e_2 + \partial_x p_1 + \partial_z p_2 \right] \\
&\quad = 0.
\end{aligned} \tag{3.12}$$

Thus we have obtained that constraint (3.11) is conserved by the system (3.8) - (3.10). However, that result bases on the assumption of differentiability of $(1 + \mathcal{L}) e_2$ in the z-direction. Whether that assumption is acceptable, given arbitrary refractive index step at the material interface, is not yet guaranteed at this point. We come back to this matter in Chapter 4, where we look into the conditions for crossing the material interfaces.

3.2 Solving the system of Maxwell's equations

3.2.1 Explicit ∂_z-system

For solving the system (3.8)-(3.10) numerically with an explicit method, we need the system to be explicit in z. What is problematic about the current form of the system, is the $\partial_z p_2$ term on the RHS of (3.9), making the system implicit with respect to z.

Let us expand $\partial_z p_2$ according to (2.4)

$$\begin{aligned}
\partial_z p_2 &= \eta \partial_z \left(e_1^2 + e_2^2\right) e_2 \\
&= \eta \left[\partial_z \left(e_1^2 + e_2^2\right) e_2 + \left(e_1^2 + e_2^2\right) \partial_z e_2\right] \\
&= \eta \left[e_2 \left(\partial_z e_1^2 + \partial_z e_2^2\right) + \left(e_1^2 + e_2^2\right) \partial_z e_2\right] \\
&= \eta \left[e_2 \left(2e_1\, \partial_z e_1 + 2e_2\, \partial_z e_2\right) + \left(e_1^2 + e_2^2\right) \partial_z e_2\right] \\
&= \eta \left[2e_1 e_2 \partial_z e_1 + 2e_2^2\, \partial_z e_2 + e_1^2 \partial_z e_2 + e_2^2 \partial_z e_2\right] \\
&= \eta \left[2e_1 e_2 \partial_z e_1 + \partial_z e_2 \left(3e_2^2 + e_1^2\right)\right] .
\end{aligned} \tag{3.13}$$

We can now transform (3.9) as follows

$$\partial_z e_2 = -\partial_x e_1 - (1 + \mathcal{L})^{-1} \left[\partial_x p_1 + \partial_z p_2\right] \tag{3.14}$$

and substitute it for $\partial_z e_2$ in (3.13)

$$\partial_z p_2 = \eta \left[2e_1 e_2 \partial_z e_1 + \left(3e_2^2 + e_1^2\right) \left(-\partial_x e_1 - (1 + \mathcal{L})^{-1} \left[\partial_x p_1 + \partial_z p_2\right]\right)\right] . \tag{3.15}$$

We obtained a rather inconvenient form, where $\partial_z p_2$ on the Left-Hand Side (LHS) is dependent on $\partial_z p_2$ on the RHS. We recall, however, that we assumed the nonlinear polarization components p_1 and p_2 to be perturbations, as in (2.4), with η being a relatively small number[2]. We can proceed to expanding $\partial_z p_2$ on the RHS of (3.15) recursively, using (3.13) and (3.14), and with each expansion we get an additional factor of η coming from the perturbations expansion. Neglecting the product of small quantities, with a factor η^2 or smaller, we obtain that (3.13) can be approximated as

$$\partial_z p_2 = \eta \left[2e_1 e_2 \partial_z e_1 + \left(3e_2^2 + e_1^2\right) \left(-\partial_x e_1\right)\right] . \tag{3.16}$$

By choosing to perform this linear approximation, we managed to eliminate $\partial_z e_2$ dependence from the RHS of (3.9). Using (3.16) in (3.9) gives a system which can be solved explicitly, given that the initial values of e_1, $\partial_z e_1$ and e_2 are known.

3.2.2 Normal modes

The strategy for solving the system of Maxwell's equations (3.8)-(3.10) is to express its solutions in terms of the normal modes, in spectral domain.

First, we eliminate the magnetic field from the system by taking cross derivatives. Taking ∂_z of (3.8) and substituting that into the ∂_t of (3.10) gives the

2. the size of η is established in the process of scaling

first equation of (3.17). Equation (3.9) is the second equation of (3.17).

$$\begin{aligned}\partial_{zz}e_1 &= \partial_{xz}e_2 - \partial_{tz}b \\ &= \partial_{xz}e_2 + \frac{1}{c^2}\partial_{tt}\left[(1+\mathcal{L})e_1 + p_1\right], \\ \partial_z e_2 &= -\partial_x e_1 - (1+\mathcal{L})^{-1}\left[\partial_x p_1 + \partial_z p_2\right].\end{aligned} \tag{3.17}$$

Linearizing system (3.17) as indicated in section 3.2.1 we obtain

$$\begin{aligned}\partial_{zz}e_1 &= \partial_{xz}e_2 + \frac{1}{c^2}\partial_{tt}\left[(1+\mathcal{L})e_1 + p_1\right], \\ \partial_z e_2 &= -\partial_x e_1.\end{aligned} \tag{3.18}$$

System (3.18) is linear to the leading order. We will now find the complete set of modes solving this system. For a homogeneous medium we can take the Fourier Transform (FT) of (3.18) in space and time, obtaining an algebraic system to be solved, instead of a differential one. Doing so we get

$$\begin{aligned}-k^2\widehat{e_1} &= -\xi k\widehat{e_2} - \left(\frac{\omega}{c}\right)^2 n^2(\omega)\widehat{e_1}, \\ ik\widehat{e_2} &= -i\xi\widehat{e_1},\end{aligned} \tag{3.19}$$

where

- k is the longitudinal wave number,
- ξ is the transverse wave number,
- $\widehat{\ }$ denotes an element transformed by FT to spectral domain, according to the FT conventions presented in Appendix A,
- $\mathcal{F}\{(1+\mathcal{L})e_1\}$ is presented in Appendix B, and it leads to the emergence of refractive index $n(\omega)$.

We now rearrange system (3.19) and solve for different values of parameter

k^3

$$\begin{aligned}
&\widehat{e_1}\left[\left(\frac{\omega}{c}n(\omega)\right)^2 - k^2\right] = -\xi k\widehat{e_2}, \\
&\qquad -\xi\widehat{e_1} = k\widehat{e_2} \quad \Rightarrow \quad \widehat{e_2} = -\frac{\xi}{k}\widehat{e_1}, \quad k \neq 0 \qquad (3.20)\\
&\qquad\qquad \Downarrow \\
&\widehat{e_1}\left[\left(\frac{\omega}{c}n(\omega)\right)^2 - k^2\right] = -\xi k\left(-\frac{\xi}{k}\widehat{e_1}\right), \quad k \neq 0 \\
&\qquad\qquad \Downarrow \\
&\left(\frac{\omega}{c}n(\omega)\right)^2 - k^2 = \xi^2, \quad k \neq 0.
\end{aligned}$$

Denoting

$$\beta(\omega, \xi) = \sqrt{\left(\frac{\omega}{c}n(\omega)\right)^2 - \xi^2} \qquad (3.21)$$

we get that for $k \neq 0$

$$k^2 = \beta^2 \quad \Rightarrow \quad k = \pm\beta.$$

Thus, in order to solve system (3.19) for $\widehat{e_1}$, $\widehat{e_2}$, we need to consider three cases for the values of k:

$$k = +\beta; \quad k = -\beta; \quad k = 0.$$

For $k = \pm\beta$, system (3.19) is over-determined and we have certain freedom in choosing the solutions $\widehat{e_1}$, $\widehat{e_2}$, and thus in choosing the basis for the solution space.

Using (3.20) let us have for

- $\underline{k = +\beta}$:

$$\left.\begin{matrix}\widehat{e_1} = \beta \\ \widehat{e_2} = -\xi\end{matrix}\right\} \quad \Rightarrow \quad \widehat{\boldsymbol{e}} = \begin{bmatrix}\beta \\ -\xi\end{bmatrix},$$

- $\underline{k = -\beta}$:

$$\left.\begin{matrix}\widehat{e_1} = \beta \\ \widehat{e_2} = \xi\end{matrix}\right\} \quad \Rightarrow \quad \widehat{\boldsymbol{e}} = \begin{bmatrix}\beta \\ \xi\end{bmatrix},$$

- $\underline{k = 0}$:

$$\left.\begin{matrix}\widehat{e_1} = 0 \\ \widehat{e_2} = 1 \quad \text{(arbitrary)}\end{matrix}\right\} \quad \Rightarrow \quad \widehat{\boldsymbol{e}} = \begin{bmatrix}0 \\ 1\end{bmatrix}. \qquad (3.22)$$

3. Of the three parameters k, ξ, ω, only two are independent (free parameters). It is customary in optics to relate $k = k(\xi, \omega)$.

For each of the three cases of k-values we obtained in (3.22) the basis vectors for the normal mode expansions. We will use those vectors to express the solutions to our system of Maxwell's equations in section 3.2.4.

3.2.3 Digression on the direction of propagation

In this section we relate the the ∂_z-propagation of the differential system, with the direction of propagation (travel) of the electromagnetic wave.

Without a loss of generality we chose a coordinate system such that the material interface plane is perpendicular to z-axis, as depicted in Figure 3.1.

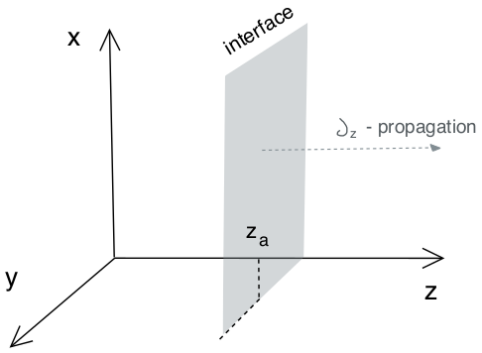

Figure 3.1: Placement of interface plane $\perp$ to z-axis.

Assuming some Boundary Condition (BC) at z_a, we know the state of the electric field at z_a for all times t, and along the x-axis. Hence, the respective derivatives ∂_t and ∂_x are known and we can *propagate* the state from z_a plane to all other planes along z-direction, using our explicit ∂_z-system.

The BC state can be arbitrary, so it is possible to model different incidence angles of the incoming laser pulse by choosing the BC carefully. Figure 3.2 indicates how BCs for perpendicular and oblique incident angles differ.

For a perpendicular incidence angle, all points along x oscillate in phase and the corresponding electromagnetic wave propagates along the z-direction. The state of such system is *uniform* in x-direction.

For an oblique incidence angle, different points along x experience a different stage of oscillation. Such state is *non-uniform* in x. The direction of wave-propagation has both x and z components, but the *propagation* of the BC-state from z_a to other planes along z is done using the same ∂_z-propagation system.

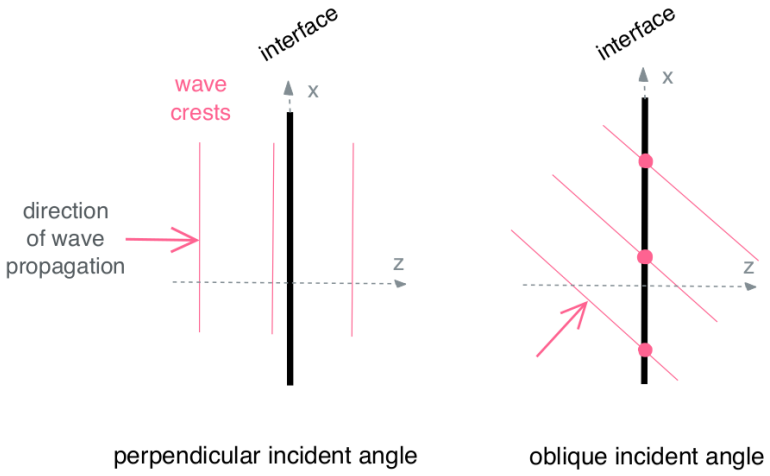

Figure 3.2: Laser-beam incident angles.

3.2.4 Expressing solutions in terms of normal modes

With the three basis vectors (3.22) we express the solutions to system (3.17) as the superposition of z-dependent Fourier modes. Following the conventions in Appendix A for the Inverse Fourier Transform (IFT)s in x and t we get

$$\begin{aligned}\boldsymbol{e}(z,t,x) &= \frac{1}{\sqrt{2\pi}^2}\int_{-\infty}^{+\infty} d\omega \int_{-\infty}^{+\infty} d\xi\ \widehat{\boldsymbol{e}}(z,\omega,\xi)\ e^{i(\xi x-\omega t)} \\ &= \frac{1}{\sqrt{2\pi}^2}\int_{-\infty}^{+\infty} d\omega \int_{-\infty}^{+\infty} d\xi\ \left\{A_+(z,\omega,\xi)\begin{bmatrix}\beta\\-\xi\end{bmatrix}e^{i\beta z}\right. \\ &\qquad + A_-(z,\omega,\xi)\begin{bmatrix}\beta\\\xi\end{bmatrix}e^{-i\beta z} \\ &\qquad \left. + Q(z,\omega,\xi)\begin{bmatrix}0\\1\end{bmatrix}\right\}\ e^{i(\xi x-\omega t)}, \end{aligned} \tag{3.23}$$

where A_+, A_- and Q are Fourier coefficients, representing the amplitudes of the wave modes.

We follow here the same conventions as in [6]. Under those conventions we have different sign in the Fourier modes for temporal and spatial FTs. As confusing as that might be, it results in a more intuitive direction of wave travel. For an increasing time, the $k > 0$ wave mode *travels to* the right, while the $k < 0$ mode *travels to* the left along z. That makes A_+ the amplitude fo the right-traveling wave, and A_- the amplitude of the left-traveling wave. Q is the amplitude of a *transversely*-traveling mode.

3.2.5 The issue of physical interpretation

We note the fact that when expressing a physical electric field through equation (3.23), we have to integrate over negative temporal frequencies ω. We present here a justification of such approach.

In order for the electric field to be real (as opposed to imaginary), and thus *physical*, we must have the following relations met for the complex amplitudes

$$\begin{aligned} A_-(z,\omega,\xi) &= A_+^*(z,-\omega,-\xi), \\ A_+(z,\omega,\xi) &= A_-^*(z,-\omega,-\xi), \\ Q(z,\omega,\xi) &= Q^*(z,-\omega,-\xi). \end{aligned} \tag{3.24}$$

The solution representation (3.23) can be written as a sum of integrals over the *physical* frequency range $\omega \geq 0$, and the *non-physical* frequency range $\omega \leq 0$. We drop the dependence on arguments and obtain

$$\begin{aligned} \boldsymbol{e} &= \frac{1}{\sqrt{2\pi}^2}\int_{-\infty}^{+\infty} d\omega \int_{-\infty}^{+\infty} d\xi \left\{ A_+ \begin{bmatrix} \beta \\ -\xi \end{bmatrix} e^{i\beta z} + A_- \begin{bmatrix} \beta \\ \xi \end{bmatrix} e^{-i\beta z} + Q \begin{bmatrix} 0 \\ 1 \end{bmatrix} \right\} e^{i(\xi x - \omega t)} \\ &= \frac{1}{2\pi}\int_{-\infty}^{+\infty} d\xi \left[\int_0^{+\infty} d\omega \left\{ A_+ \begin{bmatrix} \beta \\ -\xi \end{bmatrix} e^{i\beta z} + A_- \begin{bmatrix} \beta \\ \xi \end{bmatrix} e^{-i\beta z} + Q \begin{bmatrix} 0 \\ 1 \end{bmatrix} \right\} e^{i(\xi x - \omega t)} \right. \\ &\qquad \left. + \int_{-\infty}^{0} d\omega \left\{ A_+ \begin{bmatrix} \beta \\ -\xi \end{bmatrix} e^{i\beta z} + A_- \begin{bmatrix} \beta \\ \xi \end{bmatrix} e^{-i\beta z} + Q \begin{bmatrix} 0 \\ 1 \end{bmatrix} \right\} e^{i(\xi x - \omega t)} \right]. \end{aligned}$$

Using now relations (3.24), we modify the negative frequency range for the positive one, introducing the complex conjugates of the complex amplitudes

$$\begin{aligned} \boldsymbol{e} &= \frac{1}{2\pi}\int_{-\infty}^{+\infty} d\xi \left[\int_0^{+\infty} d\omega \left\{ A_+ \begin{bmatrix} \beta \\ -\xi \end{bmatrix} e^{i\beta z} + A_- \begin{bmatrix} \beta \\ \xi \end{bmatrix} e^{-i\beta z} + Q \begin{bmatrix} 0 \\ 1 \end{bmatrix} \right\} e^{i(\xi x - \omega t)} \right. \\ &\qquad \left. + \int_0^{+\infty} d\omega \left\{ A_-^* \begin{bmatrix} \beta \\ -\xi \end{bmatrix} e^{-i\beta z} + A_+^* \begin{bmatrix} \beta \\ \xi \end{bmatrix} e^{i\beta z} + Q^* \begin{bmatrix} 0 \\ 1 \end{bmatrix} \right\} e^{-i(\xi x - \omega t)} \right] \\ &= \frac{1}{2\pi}\int_{-\infty}^{+\infty} d\xi \int_0^{+\infty} d\omega \left[\left\{ A_+ \begin{bmatrix} \beta \\ -\xi \end{bmatrix} e^{i\beta z} + A_- \begin{bmatrix} \beta \\ \xi \end{bmatrix} e^{-i\beta z} + Q \begin{bmatrix} 0 \\ 1 \end{bmatrix} \right\} e^{i(\xi x - \omega t)} + (*) \right], \end{aligned}$$

where $(*)$ denotes the complex conjugate. We obtained a form where the integration argument is a sum of a complex number and its complex conjugate. Making assumptions (3.24) about the physicality of the electromagnetic field we managed to transform the solution expansion (3.23) into the form which does not include integrating over negative temporal frequencies $\omega \leq 0$. We thus know, that the solutions of this form are physical[4].

4. There is still an issue of the existence of a physical magnetic field b accompanying such electric field. We address this matter in section 5.2

3.2.6 Redundancy

Relations (3.24) bind the complex conjugates of the opposite frequency ranges, so effectively out of the six unknowns: A_+, A_+^*, A_-, A_-^*, Q, Q^*, only three are truly independent. The electric field considered in this paper has only two components in TM mode, while there are three unknown amplitude coefficients in expansion (3.23). This allows us to pose one additional condition without restricting the solutions to the system (3.17) in any way.

Anticipating derivations of section 6.1, we choose to set this additional condition to

$$\partial_z A_+ e^{i\beta z} + \partial_z A_- e^{-i\beta z} = 0. \tag{3.25}$$

3.2.7 Spectral representation of Maxwell's equations

We now use the normal modes expansion (3.23) in the system of equations (3.17). First, we write out the two components of the electric field in terms of their respective IFTs. We drop the dependence on arguments henceforth.

$$e_1 = \frac{1}{\sqrt{2\pi}^2} \int_{-\infty}^{+\infty} d\omega \int_{-\infty}^{+\infty} d\xi \overbrace{\left\{ A_+ \beta e^{i\beta z} + A_- \beta e^{-i\beta z} \right\}}^{\widehat{e_1}} e^{i(\xi x - \omega t)} \tag{3.26}$$

$$e_2 = \frac{1}{\sqrt{2\pi}^2} \int_{-\infty}^{+\infty} d\omega \int_{-\infty}^{+\infty} d\xi \underbrace{\left\{ -A_+ \xi e^{i\beta z} + A_- \xi e^{-i\beta z} + Q \right\}}_{\widehat{e_2}} e^{i(\xi x - \omega t)}. \tag{3.27}$$

The required ∂_z derivatives of e_1, e_2 in Fourier domain take the form

$$\begin{aligned} \widehat{\partial_z e_1} &= \partial_z \left\{ \beta \left(A_+ e^{i\beta z} + A_- e^{-i\beta z} \right) \right\} \\ &= \beta \left[\partial_z A_+ e^{i\beta z} + \partial_z A_- e^{-i\beta z} + i\beta \left(A_+ e^{i\beta z} - A_- e^{-i\beta z} \right) \right] \\ &= i\beta^2 \left(A_+ e^{i\beta z} - A_- e^{-i\beta z} \right) + \underbrace{\partial_z A_+ e^{i\beta z} + \partial_z A_- e^{-i\beta z}}_{=0 \text{ by } (3.25)}, \end{aligned} \tag{3.28}$$

$$\begin{aligned} \widehat{\partial_{zz} e_1} &= i\beta^2 \partial_z \left(A_+ e^{i\beta z} - A_- e^{-i\beta z} \right) \\ &= i\beta^2 \left[\partial_z A_+ e^{i\beta z} - \partial_z A_- e^{-i\beta z} + i\beta \left(A_+ e^{i\beta z} + A_- e^{-i\beta z} \right) \right] \\ &= \underbrace{i^2 \beta^3}_{-\beta^3} \left(A_+ e^{i\beta z} + A_- e^{-i\beta z} \right) + 2i\beta^2 \, \partial_z A_+ e^{i\beta z}, \end{aligned} \tag{3.29}$$

$$\begin{aligned}\widehat{\partial_z e_2} &= \partial_z \left\{\xi\left(-A_+e^{i\beta z} + A_-e^{-i\beta z}\right) + Q\right\}\\ &= \xi\left[-\partial_z A_+e^{i\beta z} + \partial_z A_-e^{-i\beta z} - i\beta\left(A_+e^{i\beta z} + A_-e^{-i\beta z}\right)\right] + \partial_z Q\\ &= -i\beta\xi\left(A_+e^{i\beta z} + A_-e^{-i\beta z}\right) + 2\xi\ \partial_z A_-e^{-i\beta z} + \partial_z Q. \qquad (3.30)\end{aligned}$$

In order to bring the system of Maxwell's equations into spectral domain, we insert the spectral z-derivatives (3.28), (3.29) and (3.30) into the system (3.17)

$$\begin{aligned}&-\beta^3\left(A_+e^{i\beta z} + A_-e^{-i\beta z}\right) + 2i\beta^2\ \partial_z A_+e^{i\beta z}\\ &-i\xi\left[-i\beta\xi\left(A_+e^{i\beta z} + A_-e^{-i\beta z}\right) - 2\xi\ \partial_z A_+e^{i\beta z} + \partial_z Q\right]\\ &\qquad -\left[-\frac{\omega^2}{c^2}n^2(\omega)\beta\left(A_+e^{i\beta z} + A_-e^{-i\beta z}\right)\right] = \widehat{NL_1},\\ &-i\beta\xi\left(A_+e^{i\beta z} + A_-e^{-i\beta z}\right) - 2\xi\partial_z A_+e^{i\beta z} + \partial_z Q\\ &\qquad +i\xi\beta\left(A_+e^{i\beta z} + A_-e^{-i\beta z}\right) = \widehat{NL_2},\end{aligned}$$

where for the FT of operator $(1+\mathcal{L})$ gives rise to the refractive index $n(\omega)$ as derived in Appendix B, and

$$\widehat{NL_1} = \mathcal{F}\left\{\frac{1}{c^2}\partial_{tt}p_1\right\} = -\frac{\omega^2}{c^2}\widehat{p_1}, \qquad (3.31)$$

$$\widehat{NL_2} = \mathcal{F}\left\{-(1+\mathcal{L})^{-1}\left[\partial_x p_1 + \partial_z p_2\right]\right\} = -\frac{1}{n^2(\omega)}\left(i\xi\widehat{p_1} + \partial_z\widehat{p_2}\right). \qquad (3.32)$$

Performing algebraic transformations and using $\beta^2 = \left(\frac{\omega}{c}n(\omega)\right)^2 - \xi^2$, according to (3.21), we get

$$\begin{aligned}&\cancelto{0}{\left[-\beta^2 - \xi^2 + \left(\frac{\omega}{c}n(\omega)\right)^2\right]}\beta\left(A_+e^{i\beta z} + A_-e^{-i\beta z}\right)\\ &\qquad +2i\left(\beta^2+\xi^2\right)\ \partial_z A_+e^{i\beta z} - i\xi\partial_z Q = \widehat{NL_1},\\ &\cancelto{0}{(-i\xi + i\xi)\beta}\left(A_+e^{i\beta z} + A_-e^{-i\beta z}\right) - 2\xi\partial_z A_+e^{i\beta z} + \partial_z Q = \widehat{NL_2}\end{aligned}$$

$$\Downarrow$$

$$\begin{aligned}2i\left(\beta^2+\xi^2\right)\ \partial_z A_+e^{i\beta z} - i\xi\partial_z Q &= \widehat{NL_1},\\ -2\xi\partial_z A_+e^{i\beta z} + \partial_z Q &= \widehat{NL_2}. \qquad (3.33)\end{aligned}$$

The system of equations (3.33) is a spectral representation of the system of equations (3.17), which in turn corresponds to the Maxwell's equations for the TM mode with magnetic field eliminated.

3.3 BPPE system

3.3.1 The differential system

We simplify system (3.33) by addition and subtraction to the following form

$$\begin{aligned}
&\left[2i\left(\beta^2+\xi^2\right)-2i\xi^2\right]\partial_z A_+ e^{i\beta z}\cancel{(-i\xi+i\xi)}\,\partial_z Q = \widehat{NL_1}+i\xi\widehat{NL_2},\\
&\left[-2\xi-i\frac{\xi}{\cancel{\beta^2}}\cancel{\left[2i\left(\beta^2+\xi^2\right)-2i\xi^2\right]}\right]\partial_z A_+ e^{i\beta z}\\
&\qquad\qquad +\partial_z Q\cancel{\left(1-i\frac{\xi}{\beta^2}\cdot 0\right)} = \widehat{NL_2}-i\frac{\xi}{\beta^2}\left(\widehat{NL_1}+i\xi\widehat{NL_2}\right)\\
&\qquad\qquad\qquad\qquad\Downarrow
\end{aligned}$$

$$\begin{aligned}
2i\beta^2\partial_z A_+ e^{i\beta z} = &\quad \widehat{NL_1}+i\xi\widehat{NL_2} &&\overset{def.}{=} \widehat{NL_A},\\
\partial_z Q = &\quad -i\frac{\xi}{\beta^2}\widehat{NL_2}+\left(1+\frac{\xi^2}{\beta^2}\right)\widehat{NL_2} &&\overset{def.}{=} \widehat{NL_Q}.
\end{aligned} \tag{3.34}$$

System (3.34) is valid for entire ω range, both its positive and negative values. Transform the system for negative frequencies ω by using complex conjugates and relations (3.24) we get

$$\begin{aligned}
2i\beta^2\partial_z A_+(\omega\le 0)\,e^{i\beta z} &= \widehat{NL_A}(\omega\le 0),\\
\partial_z Q(\omega\le 0) &= \widehat{NL_Q}(\omega\le 0)\\
&\downarrow (*)\\
-2i\beta^2\partial_z A_+^*(\omega\le 0)\,e^{-i\beta z} &= \widehat{NL_A}^*(\omega\le 0),\\
\partial_z Q^*(\omega\le 0) &= \widehat{NL_Q}^*(\omega\le 0)\\
&\downarrow \text{relations (3.24)}\\
-2i\beta^2\partial_z A_-(\omega\ge 0)\,e^{-i\beta z} &= \widehat{NL_A}(\omega\ge 0),\\
\partial_z Q(\omega\ge 0) &= \widehat{NL_Q}(\omega\ge 0).
\end{aligned}$$

We obtained a system similar to (3.34), with the second equation exactly the same, but the first equation involving A_- instead of A_+. Putting those equations together we obtain a system of three equations, describing all three unknown spectral amplitudes A_+, A_- and Q

$$\begin{aligned}
2i\beta^2\partial_z A_+ e^{i\beta z} &= \widehat{NL_A},\\
-2i\beta^2\partial_z A_- e^{-i\beta z} &= \widehat{NL_A},\\
\partial_z Q &= \widehat{NL_Q}.
\end{aligned} \tag{3.35}$$

We call system (3.35) a BPPE system. It is the core mechanism of the model presented in this paper.

Under the assumption that nonlinear polarization is only a *perturbation* to the linear polarization vector (as discussed in section 3.2.1), system (3.35) is equivalent to the full Maxwell's equations (3.8)-(3.10).

Constraint (3.11) is preserved by the system as long as $(1+\mathcal{L})e_2$ is differentiable at all points along z-axis considered by the model, including interfaces in particular. In Chapter 4 we show that $(1+\mathcal{L})e_2$ is indeed differentiable at the interfaces.

3.3.2 The nonlinearity term

Let us look closer into the nonlinearity on the RHS of system (3.35). Using (3.31) and (3.32) in (3.34) we write

$$\begin{aligned}
\widehat{NL_A} &= \widehat{NL_1} + i\xi\widehat{NL_2} \\
&= -\frac{\omega^2}{c^2}\widehat{p_1} - \frac{i\xi}{n^2(\omega)}\left(i\xi\widehat{p_1} + \partial_z\widehat{p_2}\right) \\
&= \widehat{p_1}\left(\frac{\xi^2}{n^2(\omega)} - \frac{\omega^2}{c^2}\right) - \frac{i\xi}{n^2(\omega)}\partial_z\widehat{p_2} \\
&= -\frac{1}{n^2(\omega)}\left(\beta^2\widehat{p_1} + i\xi\partial_z\widehat{p_2}\right), \qquad (3.36) \\
\widehat{NL_Q} &= -i\frac{\xi}{\beta^2}\widehat{NL_2} + \left(1+\frac{\xi^2}{\beta^2}\right)\widehat{NL_2} \\
&= \cancel{\frac{i\xi\omega^2}{\beta^2c^2}\widehat{p_1}} - \left(1+\frac{\xi^2}{\beta^2}\right)\frac{1}{n^2(\omega)}\left(\cancel{i\xi\widehat{p_1}} + \partial_z\widehat{p_2}\right) \\
&= -\frac{\omega^2}{\beta^2c^2}\partial_z\widehat{p_2}, \qquad (3.37)
\end{aligned}$$

where in the first equation above we have used

$$\begin{gathered}
\frac{\omega^2 n^2(\omega)}{c^2} - \xi^2 = \beta^2 \\
\Downarrow \\
\frac{\xi^2}{n^2(\omega)} - \frac{\omega^2}{c^2} = -\frac{\beta^2}{n^2(\omega)},
\end{gathered}$$

and in the second equation we used that

$$-\left(1+\frac{\xi^2}{\beta^2}\right)\frac{1}{n^2(\omega)}ß\xi = i\xi\frac{(\beta^2+\xi^2)}{\beta^2 n^2(\omega)}$$
$$= i\xi\frac{\omega^2 \cancel{n^2(\omega)}}{c^2\beta^2\cancel{n^2(\omega)}} = i\xi\frac{\omega^2}{c^2\beta^2}.$$

With p_1 as in (3.3) and $\partial_z p_2$ as in (3.16), both nonlinearities $\widehat{NL_A}$ and $\widehat{NL_Q}$ are functions of electric field components e_1 and e_2 and their derivatives. The constructing algorithm is presented below.

Algorithm: Computing nonlinear RHS's $\widehat{NL_A}$ and $\widehat{NL_Q}$

1. Build $\widehat{e_1}$, $\widehat{e_2}$, $\widehat{\partial_z e_1}$ according to formulas (3.26), (3.27), (3.28), and $\widehat{\partial_x e_1} = i\xi\beta\left(A_+ e^{i\beta z} + A_- e^{-i\beta z}\right)$.

2. Take the IFTs of the quantities obtained in previous step.

3. Construct p_1, p_2, $\partial_z p_2$ according to (3.3) and (3.16).

4. Take the FTs of the nonlinearities in previous step to obtain $\widehat{p_1}$, $\widehat{p_2}$, $\widehat{\partial_z p_2}$.

5. Construct the RHS nonlinearities $\widehat{NL_A}$, $\widehat{NL_Q}$ according to (3.36) and (3.37).

Note that if we totally neglect $\partial_z\widehat{p_2}$ to be equal to zero then $\widehat{NL_Q} = 0$.

4

Material interfaces

4.1 Interface continuity conditions

4.1.1 Continuity of electric field components

For an electromagnetic wave crossing a material interface

i) the normal components of $\boldsymbol{D}$ and $\boldsymbol{B}$ (and hence $\boldsymbol{H}$) are continuous,

ii) the tangential components of $\boldsymbol{E}$ and $\boldsymbol{H}$ (and hence $\boldsymbol{B}$) are continuous.

To complete, neither the normal component of $\boldsymbol{E}$ nor the tangential component of $\boldsymbol{D}$ is required to be continuous. Those continuity restrictions are summarized in Table 4.1.

	$\boldsymbol{E}$	$\boldsymbol{D}$	$\boldsymbol{B}$	$\boldsymbol{H}$
$\parallel$	✓	×	✓	✓
$\perp$	×	✓	✓	✓

Table 4.1: Continuity restrictions for EM field components at interface.

In our considerations we reduced Maxwell's equations to the electric field only, making $\boldsymbol{E}$ and $\boldsymbol{D}$ the only relevant vectors. For a TM field those vectors have both normal and tangential components, but we have to ensure the continuity

only of the $\| \boldsymbol{E}$ and $\perp \boldsymbol{D}$ components when crossing the material interface. In component form, following (2.1) and (3.3), we have to ensure the continuity of

$$e_1(z,x,t), \tag{4.1}$$
$$d_2(z,x,t) = \epsilon_0(1+\mathcal{L})e_2 + \epsilon_0 \underbrace{\eta\left(e_1^2+e_2^2\right)e_2}_{p_2} \tag{4.2}$$

components.

Note, that by ensuring the continuity of $d_2 = \epsilon_0(1+\mathcal{L})e_2 + p_2$ we ensure that the constraint (3.11) is conserved across the interface - something that we could not do before, due to the fact that the differentiability of $(1+\mathcal{L})e_2$ at the interface could not have been assumed.

Note also, that neither $\epsilon_0(1+\mathcal{L})e_2$ nor p_2 alone need to be continuous across the interface, so the derivatives $\partial_z\epsilon_0(1+\mathcal{L})e_2$ or $\partial_z p_2$ may not exist at the interface. This situation allows us to consider the dynamical system only inside or outside the slab, not *at* the interface. In order to be able to step across the interface, in section 4.1.2 we derive the transformations according to the continuity conditions presented in this section.

4.1.2 Transition across interfaces

For propagating system (3.17) across the material interface, we need the continuity conditions for the components e_1, $\partial_z e_1$, e_2. We will be expressing those conditions in spectral domain, to fit with the spectral Maxwell's equations (3.35).

We consider a laser pulse propagating from left to right along z-axis, and traversing the interface at point $z=a$. We denote the electric field approaching the interface at $z=a$ from the left side as

$$e_1(a^-,x,t) = \lim_{z\to a^-} e_1(z,x,t),$$

and from the right side

$$e_1\left(a^+,x,t\right) = \lim_{z\to a^+} e_1(z,x,t).$$

By analogy similar applies to other electric field components and their derivatives, as well as spectral amplitudes and nonlinearities. For compactness, often only the dependence on z is maintained, omitting the other two variables x and t, or ξ and ω. When we do not specify which interface point is meant,

distinguishing only between the state at its two sides, we write

e_1^- - meaning e_1 in the limit of approaching the interface from the LHS,
e_1^+ - meaning e_1 in the limit of approaching the interface from the RHS.

In our scenario, the amplitude of the electric field is known on the LHS of the interface, and we aim to express the unknown amplitude on the RHS in terms of the known one. The continuity of a physical field requires that the limits approaching from either side are the same. For passing e_1 across the interface we use equation (4.1) which gives

$$e_1\left(a^+, x, t\right) = e_1\left(a^-, x, t\right). \tag{4.3}$$

For e_2 we use (4.2) which gives

$$\begin{aligned} &\epsilon_0(1+\mathcal{L}^+)e_2\left(a^+, x, t\right) + \epsilon_0 p_2\left(a^+, x, t\right) \\ &= \epsilon_0(1+\mathcal{L}^-)e_2\left(a^-, x, t\right) + \epsilon_0 p_2\left(a^-, x, t\right), \end{aligned} \tag{4.4}$$

where we remind that for Kerr-type nonlinearity

$$\begin{aligned} p_1 &= \eta\left(e_1^2 + e_2^2\right)e_1, \\ p_2 &= \eta\left(e_1^2 + e_2^2\right)e_2. \end{aligned} \tag{4.5}$$

Finally, for $\partial_z e_1$, we use (3.8). As long as there are no magnetic interfaces at z_a, then b is continuous across the interface and we have

$$\begin{aligned} &\partial_z e_1\left(a^+, x, t\right) - \partial_x e_2\left(a^+, x, t\right) \\ &= \partial_z e_1\left(a^-, x, t\right) - \partial_x e_2\left(a^+, x, t\right). \end{aligned} \tag{4.6}$$

Continuity conditions (4.3), (4.4), (4.6) are three equations for the three unknowns: $e_1\left(a^+, x, t\right)$, $e_2\left(a^+, x, t\right)$, $\partial_z e_1\left(a^+, x, t\right)$.

We now take those equations into spectral domain by taking FT in x and t, and by inserting the relevant mode expansions (3.26) and (3.27). We index $n(\omega)$ and $\beta(\omega, \xi)$ as shown in Figure 4.1, in order to distinguish values of those functions inside and outside of the slab.

Taking equation (4.3) into spectral domain and inserting the mode expansions yields

$$\widehat{e_1}\left(a^+, \xi, \omega\right) = \widehat{e_1}\left(a^-, \xi, \omega\right)$$

$$\Updownarrow$$

$$\begin{aligned} &\beta_1 A_+\left(a^+, \xi, \omega\right) e^{i\beta_1 z} + \beta_1 A_-\left(a^+, \xi, \omega\right) e^{-i\beta_1 z} \\ &= \beta_0 A_+\left(a^-, \xi, \omega\right) e^{i\beta_0 z} + \beta_0 A_-\left(a^-, \xi, \omega\right) e^{-i\beta_0 z}. \end{aligned} \tag{4.7}$$

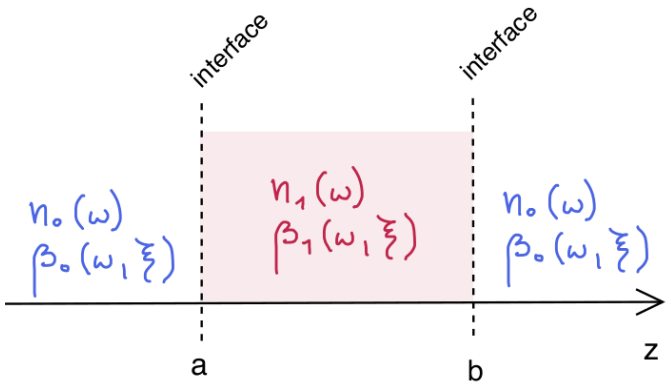

Figure 4.1: Indexing outside and inside the material slab.

Taking equation (4.4) into spectral domain and inserting the mode expansions yields

$$\begin{aligned}&\epsilon_0 n_1^2(\omega)\widehat{e_2}\left(a^+,\xi,\omega\right)+\epsilon_0\widehat{p_2}\left(a^+,\xi,\omega\right)\\&=\epsilon_0 n_0^2(\omega)\widehat{e_2}\left(a^-,\xi,\omega\right)+\epsilon_0\widehat{p_2}\left(a^-,\xi,\omega\right)\end{aligned}$$

$$\Updownarrow$$

$$\begin{aligned}&\cancel{\epsilon_0}^{1} n_1^2(\omega)\left[-\xi A_+\left(a^+,\xi,\omega\right)e^{i\beta_1 z}+\xi A_-\left(a^+,\xi,\omega\right)e^{-i\beta_1 z}+Q\left(a^+,\xi,\omega\right)\right]\\&\quad+\widehat{p_2}\left(a^+,\xi,\omega\right)\\&=\cancel{\epsilon_0}^{1} n_0^2(\omega)\left[-\xi A_+\left(a^-,\xi,\omega\right)e^{i\beta_0 z}+\xi A_-\left(a^-,\xi,\omega\right)e^{-i\beta_0 z}+Q\left(a^-,\xi,\omega\right)\right]\\&\quad+\widehat{p_2}\left(a^-,\xi,\omega\right).\end{aligned}\tag{4.8}$$

Taking equation (4.6) into spectral domain and inserting the mode expansions yields

$$\begin{aligned}&\partial_z\widehat{e_1}\left(a^+,x,t\right)-i\xi\widehat{e_2}\left(a^+,x,t\right)\\&=\partial_z\widehat{e_1}\left(a^-,x,t\right)-i\xi\widehat{e_2}\left(a^+,x,t\right)\end{aligned}$$

$$\Updownarrow$$

$$\begin{aligned}&\partial_z\left\{\beta_1 A_+\left(a^+,\xi,\omega\right)e^{i\beta_1 z}+\beta_1 A_-\left(a^+,\xi,\omega\right)e^{-i\beta_1 z}\right\}\\&\quad-i\xi\left[-\xi A_+\left(a^+,\xi,\omega\right)e^{i\beta_1 z}+\xi A_-\left(a^+,\xi,\omega\right)e^{-i\beta_1 z}+Q\left(a^+,\xi,\omega\right)\right]\\&=\partial_z\left\{\beta_0 A_+\left(a^-,\xi,\omega\right)e^{i\beta_0 z}+\beta_0 A_-\left(a^-,\xi,\omega\right)e^{-i\beta_0 z}\right\}\\&\quad-i\xi\left[-\xi A_+\left(a^-,\xi,\omega\right)e^{i\beta_0 z}+\xi A_-\left(a^-,\xi,\omega\right)e^{-i\beta_0 z}+Q\left(a^-,\xi,\omega\right)\right]\end{aligned}$$

$$\Updownarrow$$

$$\begin{aligned}
&\beta_1 \partial_z A_+\left(a^+,\xi,\omega\right) e^{i\beta_1 z} + i\beta_1^2 A_+\left(a^+,\xi,\omega\right) e^{i\beta_1 z} \\
&\quad + \beta_1 \partial_z A_-\left(a^+,\xi,\omega\right) e^{-i\beta_1 z} - i\beta_1^2 A_-\left(a^+,\xi,\omega\right) e^{-i\beta_1 z} \\
&\quad + i\xi^2 A_+\left(a^+,\xi,\omega\right) e^{i\beta_1 z} - i\xi^2 A_-\left(a^+,\xi,\omega\right) e^{-i\beta_1 z} - i\xi Q\left(a^+,\xi,\omega\right) \\
&= \beta_0 \partial_z A_+\left(a^-,\xi,\omega\right) e^{i\beta_0 z} + i\beta_0^2 A_+\left(a^-,\xi,\omega\right) e^{i\beta_0 z} \\
&\quad + \beta_0 \partial_z A_-\left(a^-,\xi,\omega\right) e^{-i\beta_0 z} - i\beta_0^2 A_-\left(a^-,\xi,\omega\right) e^{-i\beta_0 z} \\
&\quad + i\xi^2 A_+\left(a^-,\xi,\omega\right) e^{i\beta_0 z} - i\xi^2 A_-\left(a^-,\xi,\omega\right) e^{-i\beta_0 z} - i\xi Q\left(a^-,\xi,\omega\right)
\end{aligned}$$

$$\Updownarrow \text{ using (3.25)}$$

$$\begin{aligned}
&i\left(\beta_1^2+\xi^2\right)\left[A_+\left(a^+,\xi,\omega\right) e^{i\beta_1 z} - A_-\left(a^+,\xi,\omega\right) e^{-i\beta_1 z}\right] - i\xi Q\left(a^+,\xi,\omega\right) \\
&= i\left(\beta_0^2+\xi^2\right)\left[A_+\left(a^-,\xi,\omega\right) e^{i\beta_0 z} - A_-\left(a^-,\xi,\omega\right) e^{-i\beta_0 z}\right] - i\xi Q\left(a^-,\xi,\omega\right)
\end{aligned}$$

$$\Updownarrow \text{ using (3.21)}$$

$$\begin{aligned}
&\overbrace{\left(\beta_1^2+\xi^2\right)}^{\left[\frac{\omega}{c} n_1(\omega)\right]^2}\left[A_+\left(a^+,\xi,\omega\right) e^{i\beta_1 z} - A_-\left(a^+,\xi,\omega\right) e^{-i\beta_1 z}\right] - \xi Q\left(a^+,\xi,\omega\right) \\
&= \underbrace{\left(\beta_0^2+\xi^2\right)}_{\left[\frac{\omega}{c} n_0(\omega)\right]^2}\left[A_+\left(a^-,\xi,\omega\right) e^{i\beta_0 z} - A_-\left(a^-,\xi,\omega\right) e^{-i\beta_0 z}\right] - \xi Q\left(a^-,\xi,\omega\right).
\end{aligned} \tag{4.9}$$

Equations (4.7), (4.8), (4.9) constitute the three conditions for traversing interface in a continuous manner. By analogy, similar relations can be derived for the other interface at $z = b$, where the light beam exits the slab.

Note that spectral amplitudes A_+, A_- and Q are not *physical* quantities, and thus they themselves are not expected to be continuous across interfaces. Mathematically we express an arbitrary electromagnetic wave as an *infinite* superposition of the normal modes. It is only that superposition that we expect to be continuous, not its component modes.

4.2 Interface crossing setup

In total, we consider four interface crossings, from left-to-right and from right-to-left at each interfaces. Those four cases are shown in Figure 4.2. Naming of the four crossings as $M_{12}(a)$ etc. is provided for the purpose of further sections.

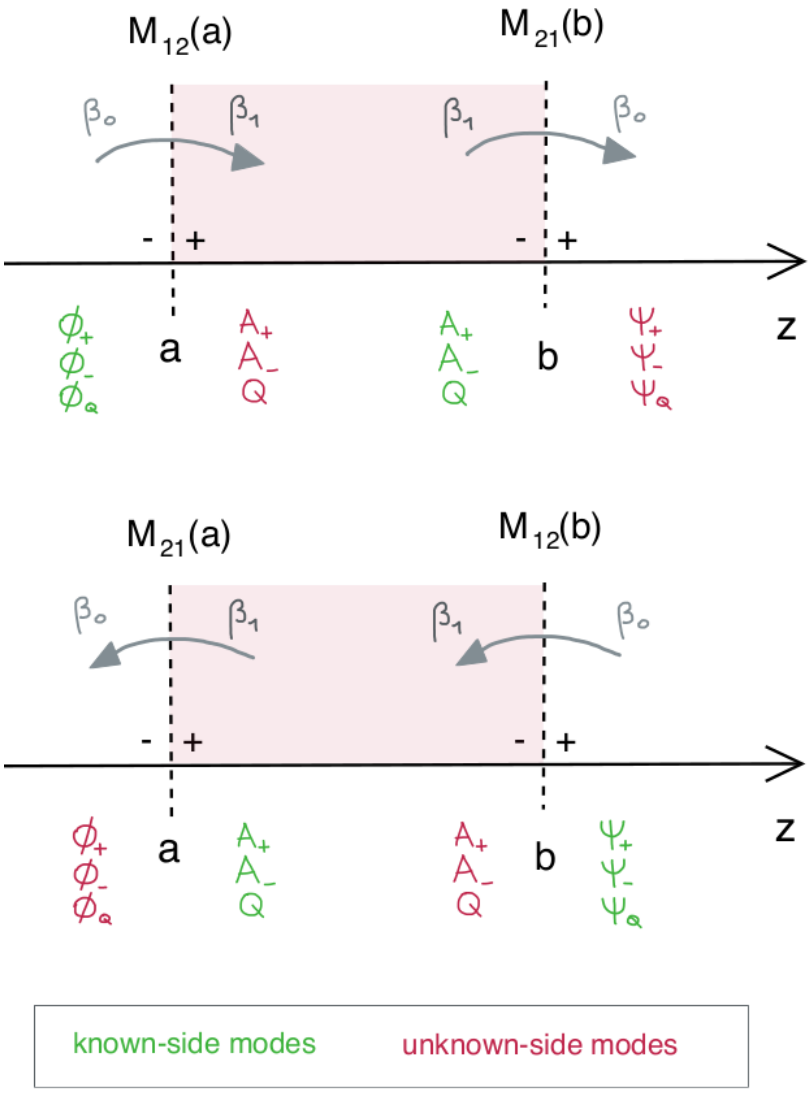

Figure 4.2: Modeled interface crossings.

5

Reality check

5.1 Existence of Q-mode

The Q-mode appears in our equations as a consequence of providing a complete basis for the normal-modes expansion. This mode does not travel along z, as the A_+ and A_- modes do, and it is less intuitive how this mode could manifest itself. In order to take up the topic of the elephant in the room, this section reveals some of the findings of the further sections. This is a spoiler alert.

Analyzing the interface transition conditions, it is not straightforward to deduce whether a non-zero Q mode can arise in the system if it is not already present in the input source to begin with. For a system uniform in x, we have $\xi = 0$. In consequence Q becomes irrelevant in condition (4.9), and (4.8) is reduced to a condition indicating that Q must be zero for a physical system. This is formally shown in section 8.2.2.

Therefore, in order to have a chance of non-zero Q arising, we need to allow for a variability in x direction. In the scaling section, equation (6.20), we reveal that the scale of Q is inversely proportional to the scale of x. The smaller the scale of the input pulse in x-direction, the bigger the scale of Q.

Ensuring a *small* scale in the x-direction means mathematically to represent the input pulse as a *narrow* function of x, e.g. a narrow Gaussian. We are operating with very imprecise terms here, but they serve the purpose of a qualitative discussion. Such a narrow Gaussian pulse represents a laser beam

that is physically focused into a narrow spatial area along x-direction.

Such a setup gives greater chances of producing a non-zero Q, but it is still only a *scale* that we are considering here. It does not guarantee that the dimensionless factor scaled by this scale ever gets to be different than zero. We do see, however, that a case uniform in x-direction corresponds to *focusing* a beam into an infinite region, making the scale of Q inversely proportional to infinity, and thus zero. That confirms the previous findings.

In any case, in order to confirm arising of the Q-mode, it needs to be distinguishable from the numerical errors occurring for particular tolerance thresholds assumed. Also, we expect the shape of Q-mode envelope to follow the one of the input pulse, distinguishing itself clearly from the numerical noise.

5.2 Solvability conditions for b-field

For the existence of magnetic field b consistent with Maxwell's equations, we need to impose the constraint (3.11) at some point of the system. As we have shown in (3.12), this constraint is then preserved by the system. We now show whether that is also true at the interface crossing.

First, let us impose the constraint and derive a solvability condition that ensures the existence of b field. We consider equations (3.11) and (3.8), which involve all electric and magnetic field components of interest: e_1, e_2 and b. Cross-differentiating those two equations by taking ∂_t of (3.11) and ∂_x of (3.8) yields a system

$$\begin{aligned}\partial_{xt} b &= \frac{1}{c^2}\partial_{tt}\left[(1+\mathcal{L})e_2 + p_2\right],\\ \partial_{xt} b &= \partial_{xx} e_2 - \partial_{xz} e_1.\end{aligned}$$

Equating those two together and performing simple algebraic operations we get

$$\partial_{xz} e_1 - \partial_{xx} e_2 = -\frac{1}{c^2}\partial_{tt}\left[(1+\mathcal{L})e_2\right] - \frac{1}{c^2}\partial_{tt} p_2. \tag{5.1}$$

Equation (5.1) is the condition for the solvability of Maxwell's equations, whose solution represents a physical magnetic field.

We will now determine whether condition (5.1) is maintained when crossing an interface according to relations (4.3), (4.4), (4.6). We do it by imposing constraint (5.1) on the LHS of the interface, applying the spatiotemporal interface crossing conditions (4.3), (4.4), (4.6), and checking whether the resulting relation taken to the RHS still meets the solvability condition.

We start with interface condition (4.6) and take the ∂_x derivative of it

$$\begin{aligned}\partial_{xz}e_1^+ - \partial_{xx}e_2^+ &= \partial_{xz}e_1^- - \partial_{xx}e_2^- \\ &\downarrow \text{ using solvability condition (5.1) for RHS} \\ &= -\frac{1}{c^2}\partial_{tt}\left[(1+\mathcal{L}^-)e_2^-\right] - \frac{1}{c^2}\partial_{tt}p_2^- \\ &\downarrow \text{ using interface condition (4.4)} \\ &= -\frac{1}{c^2}\partial_{tt}\left[(1+\mathcal{L}^+)e_2^+ + p_2^+\right],\end{aligned}$$

which is consistent with the form of the solvability condition (5.1) for the RHS of the interface

$$-\frac{1}{c^2}\partial_{tt}\left[(1+\mathcal{L}^+)e_2^+ + p_2^+\right] = \partial_{xz}e_1^+ - \partial_{xx}e_2^+.$$

Note the chain of transformations here. We departed from the RHS of the interface, traversed to the LHS of the interface using interface condition (4.6), then we applied the solvability condition to the LHS, and we traversed back to the RHS using another interface condition (4.4). Going there and back using different interface conditions we arrived at the same result that we departed from. That shows that traversing interfaces using our interface conditions maintains the solvability condition.

We will now transform the solvability condition (5.1) into spectral domain, which will be more convenient later. Taking the FT of (5.1) we get

$$\begin{aligned}i\xi\partial_z\widehat{e_1} + \xi^2\widehat{e_2} &= \frac{\omega^2}{c^2}n^2(\omega)\widehat{e_2} + \frac{\omega^2}{c^2}\widehat{p_2} \\ &\downarrow \text{ using (3.21)} \\ i\xi\partial_z\widehat{e_1} - \beta^2\widehat{e_2} &= \frac{\omega^2}{c^2}\widehat{p_2} \\ &\downarrow \text{ using (3.28) for } \partial_z\widehat{e_1}\text{, (3.27) for } \widehat{e_2} \\ i^2\xi\beta^2\left(A_+e^{i\beta z} - A_-e^{-i\beta z}\right) - \beta^2\left[-\xi\left(A_+e^{i\beta z} - A_-e^{-i\beta z}\right) + Q\right] &= \frac{\omega^2}{c^2}\widehat{p_2} \\ &\Downarrow \\ \cancel{-\xi\beta^2A_+e^{i\beta z}} + \cancel{\xi\beta^2A_-e^{-i\beta z}} + \cancel{\xi\beta^2A_+e^{i\beta z}} - \cancel{\xi\beta^2A_-e^{-i\beta z}} - \beta^2Q &= \frac{\omega^2}{c^2}\widehat{p_2} \\ &\Downarrow \\ Q &= -\frac{\omega^2}{c^2\beta^2}\widehat{p_2}. \end{aligned} \tag{5.2}$$

Equation (5.2) is a spectral equivalent of solvability condition (5.1). It is an implicit relation for Q, where $\widehat{p_2}$ depends on all spectral amplitudes A_+, A_- and

Q. The method for applying such an implicit condition is discussed in Chapter 6.

Showing the continuity of the solvability condition can also be done for its spectral form (5.2), instead of (5.1). This is done for example by inserting spectral interface condition (4.9) into spectral interface condition (4.8) with the application of spectral solvability condition (5.2) along the way.

We determined that the solvability condition (5.1), or (5.2) in spectral form, is maintained when crossing the interface. That allows us to enforce the condition only once, for example through the BC at $z = a^-$, and have it guaranteed to be maintained all along the z-domain.

5.3 Understanding the back-scatter

In this section we discuss some concepts of light propagation through a material slab with a nonlinear polarization response. We do it employing a less mathematical, and more intuitive approach, striving to provide the understanding necessary for appreciating further chapters.

5.3.1 Light scattering

Let us recall the modeling setup presented in section 2.1 and in Figure 5.1. We consider a source laser pulse composed only of the right-traveling wave. It originates from a vacuum environment, travels towards the material slab and hits the first material interface at $z = a^-$. At that point, some of the light gets reflected from the interface back into the vacuum, while the remaining part travels through the slab. Some of the light traveling through the slab gets scattered inside the slab, while the remaining part reaches the second interface at $z = b^-$. At the second interface some of the light gets reflected back into the slab, while the other part goes through the interface, and continues on its path to infinity through the vacuum environment.

From that description we point out several things:

i) The source of light is composed only of the right-traveling wave, with amplitude A_+.

ii) The total electric field on the LHS of the slab is composed also of the reflected radiation, meaning it contains also the A_- component. We do not want this reflected radiation to impact our source, because we desire

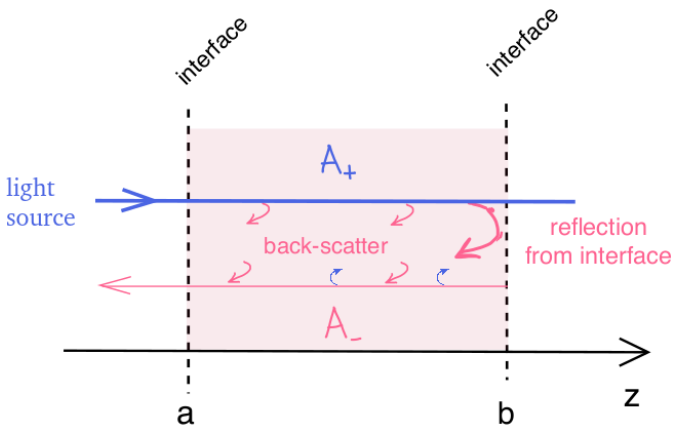

Figure 5.1: Light back-scaterring in nonlinear medium.

to have full control of it. We therefore assume that the source of radiation is shielded from the electromagnetic field reflected from the slab.

iii) On the RHS of the slab there is the light portion that passed the entire slab traveling towards infinity. We do not have any light source at infinity, so we know that in total there is only A_+ component on the RHS of the slab, the A_- component does not exist there.

iv) The existence of Q-mode component in any point of the system is dictated by meeting the solvability condition presented in section 5.2.

How light propagates in vacuum is rather straightforward. We now ponder upon what happens inside the material slab with a nonlinear polarization response.

Light propagation is not instantaneous. It takes certain amount of time, in which the electromagnetic wave progresses through space. The electric field emerging due to the polarization of the medium depends strongly on the interaction with that passing light wave. That is a very dynamical system, where the electric field changes considerably as the wave passes. The two electric fields, one from the light source, and the other from the slab polarization, constantly affect each other, recursively intertwining in an endlessly complicated manner.

Moreover, with nonlinear polarization in play, the arising electric field depends on the cube of the source electric field. That means that the system might produce a response that is *seemingly inadequate* to the input energy. For a constant oscillation of the source wave, the response would not be linear, but rather rise in a cubic manner.

Similarly to being reflected from an interface, light is reflected also within the slab, at *practically* every point of the slab. This occurs at an atomic level, and due to somewhat uneven distribution of atoms, the back-scatter may be *uneven* from point to point. We strive to depict this in Figure 5.1 to certain extent.

We thus have two realms, one inside the slab, where light is constantly scattered in many different directions, and the other, in the vacuum outside the slab, where light propagation in a well-established direction that it never changes.

5.3.2 Boundary between scatter and order

Clearly then, the omnipresent back-scatter produces a rather complicated electric field state at the interface $z = a$, long before the laser pulse manages to travel through the slab, get reflected from the other interface and go back. Our intention is to be able to set up a specific BC at that interface, be able to control it, and do not have it impacted by the back-scatter. And that is indeed guaranteed in out system. Let us explain how.

While the electric field is continuous across the interface, the medium on the two sides of the interface is substantially different. The *chaotic back-scatter* exists only within the slab. The *act* of passing through interface out of the slab deprives the electromagnetic wave of the nonlinear environment which fuels the hard-to-grasp scattering response.

This means that whatever wave we encounter on the LHS of the slab, its right-traveling component can originate *only* from the laser pulse that we control. There is no back-scatter in the vacuum, so the wave coming back from the slab can not *spontaneously* change direction in the vacuum and add to the right-traveling input source. For the same reason we are not expecting any A_- component on the RHS of the slab, because whatever comes out of the slab, traveling to the right, can not change direction in a vacuum and be traveling to the left. No external sources from $+\infty$ are modeled either.

It is clear that the initial state at $z = a^-$, when the laser pulse is just hitting the interface, has only the right-traveling component. It is also clear that this state must evolve in time in order to represent the reflection from the slab interface, giving rise to the left-traveling component there at $z = a^-$. We take this thought to the next chapter. First we introduce the BPPE iterative method, and then, in section 6.1.2, we continue the intuitive approach.

6

The model

6.1 BPPE shooting method

So far we have developed a system of differential equations (3.35) describing the propagation of light in medium according to Maxwell's equations, and we derived three continuity conditions (4.7), (4.8), (4.9) allowing us to propagate light pulse across the material interfaces. In all those equations we use spectral amplitudes A_+, A_-, Q as unknown Fourier coefficients.

It is now time to introduce a method for finding the unknown spectral amplitudes and put everything together into a tool for simulating light propagation in a nonlinear medium. The method we present here is a shooting method proposed in [7] for a TE field[1].

6.1.1 The algorithm

The whole iterative process is illustrated in Figure 6.1, and the rest of this section is dedicated to explaining it.

First, we introduce a notation which is used all throughout the remaining chapters of this document. In order to distinguish the spectral amplitudes inside and outside of the slab, we denote them as stated in Table 6.1.

1. the Q mode is considered in [6], but not in [7]

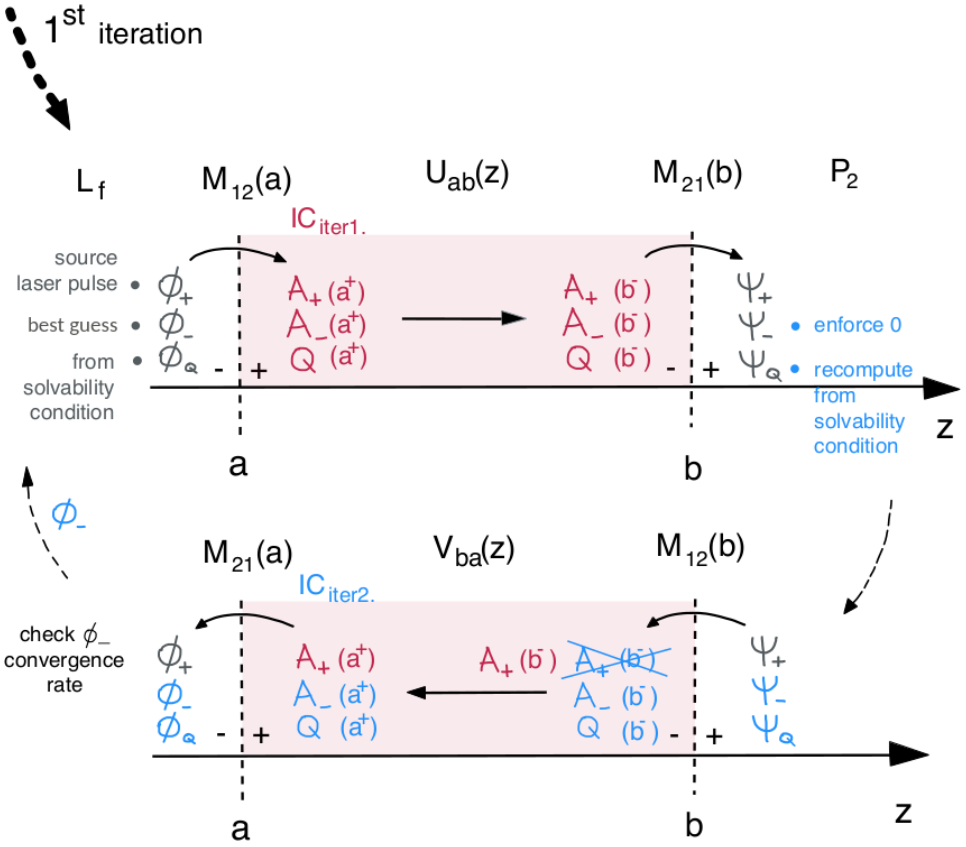

Figure 6.1: Transitions in BPPE iteration map.

Symbol	Spectral amplitudes
Φ_+, Φ_-, Φ_Q A_+, A_-, Q Ψ_+, Ψ_-, Ψ_Q	right-, left-, transversely-traveling modes: · at $z = a^-$ (outside the slab, on the LHS) · between $z = a^+$ and $z = b^-$ (inside the slab) · at $z = b^+$(outside the slab, on the RHS)

Table 6.1: Spectral amplitudes naming conventions.

We drop the dependence of the spectral amplitudes on ω, ξ. The spectral amplitudes inside the slab remain dependent on z.

The main idea of the method is based on two facts

- we are capable of propagating electromagnetic wave through medium and interfaces in both directions along z, meaning we can go *there-and-back*,
- we know there is no electromagnetic source from $+\infty$, meaning that the solution must be such that $\Psi_- = 0$.

The method then starts by solving light propagation system for an arbitrary BC Φ, and checking the state of Ψ_-. If this state is non-zero[2], it is enforced to be zero, and propagated back from $z = b^+$ to $z = a^-$, where it produces an entirely new BC for A_-. This new BC is used in the next iteration, and the process is repeated until Ψ_- is close enough to zero, with certain tolerance range. The spectral amplitudes which are affected by enforcing $\Psi_- = 0$ and propagating back in the slab are marked in blue in in Figure 6.1.

We present the full algorithm of the BPPE shooting method below, with some comments following it. In square brackets we provide the reference to the BPPE iteration steps as they are named in [7].

Algorithm: BPPE iteration map

1. Provide the spectral amplitudes Φ_+, Φ_-, Φ_Q before the first interface at $z = a$. $\left[L_f\right]$
2. Cross the first interface at $z = a$ from $a^- \longrightarrow a^+$, according to continuity conditions (4.7), (4.8), (4.9). $[M_{12}(a), P_1]$
3. Propagate the light pulse through the slab by finding solutions to the spectral form of Maxwell's equations (3.35), with BC given as $A_+(a^+)$, $A_-(a^+)$, $Q(a^+)$, and the RHS nonlinearities as in (3.36) and (3.37). $[U_{ab}(z)]$
4. Cross the second interface at $z = b$, according to interface continuity conditions. $[M_{21}(b)]$
5. Modify the electric field by enforcing $\Psi_- = 0$ and recalculating Ψ_Q according to solvability condition (5.2). $[P_2]$

2. within certain tolerance range for numerical solution

6. Step back into the material slab by crossing the interface at $z = b$ in reverse direction, according to interface continuity conditions. $[M_{12}(b)]$

7. Propagate the wave back through the slab up to $z = a^+$, using constraint (3.25) for A_-, and solvability condition (5.2) for Q. $[V_{ba}]$

8. Step out of the slab by crossing the interface at $z = a$ in reverse direction, according to interface continuity conditions. As a result new values of Φ_- and Φ_Q are obtained, while Φ_+ is not affected. $[M_{21}(a), P_3]$

9. Repeat steps 1.-8. until convergence of Φ_- is reached for certain tolerance range.

10. Reconstruct the electric field components e_1, e_2 from (3.26). (3.27) respectively, by taking IFT of $\widehat{e_1}$, $\widehat{e_2}$.

Comments for the BPPE iterative algorithm on page 41

Ad 1. The values of spectral amplitudes are constructed as follows

- Φ_+ is the laser pulse source that we wish to model for. Mathematically the pulse can be represented with a Gaussian curve.
- Φ_- is an arbitrary initial guess in the first iteration, for example zero. In every next iteration it is the value found in step 8 of the previous iteration.
- Φ_Q is calculated from (5.2) in order to satisfy the solvability condition. Since (5.2) is an *implicit* equation for Q, with highly nonlinear RHS, the solution to Q is found via fixed-point iteration using Newton's method. Depending on the initial guess for the Newton's algorithm, the convergence of the algorithm might be an issue. Feasibility of finding Q in that manner is evaluated in the testing phase.

Ad 5. Justification for the enforcement is that no electromagnetic field sources from $+\infty$ are present in the model.

Ad 5. & 9. The stopping condition is not checked at $z = b^+$, where Ψ_- is enforced to be zero, but rather after going back to $z = a^-$, by comparing the previous and current values of Φ_-. If Ψ_- was already close enough to zero before being enforced to be zero, then the values of the two last consecutive approximations of Φ_- do not vary much. We make the choice to perform

the entire iteration algorithm and propagate back to $z = a^-$ for every iteration, including the one where stopping condition is met.

Ad 7. Equations (3.35) allow us to propagate the system from $a \to b$, not the other way round. What we use instead is the additional constraint (3.25) that has been so conveniently introduced, foreseeing this moment. Using the Fundamental Theorem of Calculus we integrate the constraint (3.25) inside the material slab, as presented in Appendix D. As a result, we obtain an equation for $A_-(a^+)$ in terms of the known state of A_- at the interface $z = b$, where we enforced it to zero, and the known state of A_+, as we propagated it through the slab in step 3. Constraint is integrated as follows

$$A_-\left(z = a^+, \omega, \xi\right) = A_-\left(z = b^-, \omega, \xi\right) + \int_a^b dz\, \partial_z A_+(z, \omega, \xi)\, e^{2i\beta_1 z}. \qquad [I_{ab}] \qquad (6.1)$$

At the end of this step we are in the disposition of

- $A_-(a^+)$, as calculated from (6.1),
- $A_+(a^+)$, as calculated in step 2.,
- $Q(a^+)$ calculated from solvability condition (5.2).

Ad 9. The iterative process is done using Newton's iteration. The tolerance range, and thus the stopping condition, is assessed in the testing phase.

To summarize, the intent of the algorithm is to propagate the equations through the slab there and back, enforcing no left-traveling wave from $+\infty$. Once we do that, in each iteration, we back-propagate the modified electric field to $z = a^-$ and see how much the state of Φ_- has changed. If the change is within a tolerance range, it means that enforcing $\Psi_- = 0$ did not make any significant change to the electric field solution. That in turn means that the spectral amplitudes solution that we just found already meets the assumption of no electric field sources coming from $+\infty$, and we can stop the iterative shooting process. The electric field can be reconstructed inside the slab and at the interfaces for an arbitrary[3] point.

3. in practice according to the discretization of z

6.1.2 System evolution vs. iterative approximation

We return to the intuitive discussion started in section 5.3. We proceed with making a distinction between a temporal evolution of a *physical system*, and the evolution of the *iterative approximation* process underlying the BPPE method.

The change of the approximated solution that we see from iteration to iteration is *not* a reflection of how the physical state of the system evolves in time or space. Consecutive iterations are not progression in time or space, but rather they are consecutive approximations, a *fine-tuning*, of the entire solution state in the entire solution space that we model for. Through the iterative process we approximate the state of the system at spatiotemporal frequency spectrum ξ-ω, for the entire z-range of the slab.

The starting point for *guessing* the state at $z = a^-$ is an arbitrary initial guess for Φ_-, and the solvability condition for Φ_Q. Such a guess is most likely a poor one, and represents a solution where there is a light source at $+\infty$. The guess is modified throughout the iterative process, with the output state Φ_- at one iteration being used as input to the next iteration. Modifying the guess and performing iterations continues until a solution is reached in which $\Psi_- \approx 0$, which is one of the assumptions of the model.

In the imperfect view of the system that we initially obtain, there is a light source at $+\infty$ (represented by $\Psi_- \neq 0$) accommodating for our poor initial guess of Φ_-. By refining the BCs and iterating we bring the non-existing source at $+\infty$ down to zero[4].

For example, if we set the initial guess $\Phi_- = 0$, then we most probably obtain $\Psi_- \neq 0$ after just one iteration. That nonzero Ψ_- represents such a light source from $+\infty$, that it amounts to exactly $\Phi_- = 0$ after passing through the nonlinear slab and the two interfaces. What we obtain on the RHS of the slab, is a consequence of the error that we make in our initial guess on the LHS. Refining the initial guess, brings the left-traveling wave from $+\infty$ down to zero. This is done by iterating and forcing $\Psi_- = 0$ with each iteration. Better-and-better guesses for Φ_- take us closer to the state $\Psi_- = 0$ that we try to achieve.

Once the desired state $\Psi_- = 0$ is achieved, the electric field within the entire slab can be reconstructed. In particular, we can reconstruct the state at the interface $z = a$, and infer how much of the initial pulse energy was reflected and traveled back. That includes the reflections from both slab interfaces, as

4. that is, given the iterative process converges

well as the back-scatter inside the slab. By setting the nonlinear polarization impact to be relatively smaller than the impact of linear polarization, we expect the scattering of light inside the slab to be of significantly less impact than the reflections from the interface planes.

6.1.3 A note on modeling the domain

The time it takes for the laser beam to travel the distance between the two interfaces can be approximated based on the group velocity v_g of the wave. Thus, we can determine at which time point the returning pulse is back at the interface $z = a$. The time domain for modeling should be such that both the source pulse, and the returning reflection are within the domain. Plotting the electric field amplitude for $z = a$ and the entire time domain should reveal two peaks, one belonging to Φ_+ laser source, and the other to Φ_- returning from the slab. The distance between the two peaks corresponds to the time it takes for the light to travel through the slab twice, there and back.

Since we model no horizontal interfaces, the x domain should be wide enough to prevent any *artificial* reflections from the borders of the domain for the given propagation time. That is especially important for modeling oblique angle of incidence, for which the light wave has a component traveling in x-direction. For perpendicular incidence angle only the scatter travels along x. By the assumption of nonlinear polarization having considerably smaller impact, the amplitude of the scatter will in any case be smaller than the amplitude of the main pulse.

We established, that a reasonable model requires harmonizing the z, x and t domains, as well as the proportion of the nonlinear polarization, such that it takes effect but does not dominate the linear response. For that we must perform the scaling and nondimensionalizing of the system.

6.2 Scaling of the system

Before jumping into implementation we scale the BPPE system. The purpose of that is to solve the model independent of physical units, where the dimensionless variables are of similar order of magnitude, as much as possible.

6.2.1 Dimensionless variables

We write out each of the relevant variables as a product of a dimensional constant, with subscript $_0$, and a nondimensional variable, marked with $'$

$$\begin{aligned} z &= z_0\, z', & c &= c_0 c' \\ t &= t_0\, t', & \omega &= \omega_0\, \omega', \\ x &= x_0\, x', & \xi &= \xi_0\, \xi', \\ z &= z_0\, z', & \lambda &= \lambda_0\, \lambda', \\ k &= k_0 k', & \beta &= \beta_0\, \beta', \\ e_1 &= e_{10}\, e_1', & e_2 &= e_{20}\, e_2'. \end{aligned} \tag{6.2}$$

In particular we note the definition of the speed of light c, to be a product of a dimensionless value $c' = 2.998$ and a dimensional constant $c_0 = 10^8 ms^{-1}$. In all our considerations we intend to keep the dimensionless constants of the order of magnitude $O(1)$, and place both the scaling factor, e.g. 10^8, and the *unit* in the dimensional constant.

In the process of scaling, we group the dimensional constants together, into new, combined dimensional parameters of the system. Reducing the number of variables, we reduce the possibility of running the same parameter setup repeatedly in our simulations. Another advantage of scaling is the possibility to perform numerical calculations on dimensionless numbers of similar orders of magnitude, which is beneficial for numerical accuracy.

We follow the same scaling pattern also for quantities such as $\widehat{p_1}$, $\widehat{p_2}$, A_+, A_-, Q, η, $\widehat{NL_A}$, $\widehat{NL_Q}$. Their dimensional constants are expressed with the ones already listed in (6.2). We also introduce relations

$$\begin{aligned} \omega_0 &= \frac{1}{t_0}, & \omega' &= \frac{2\pi}{t'} \\ \xi_0 &= \frac{1}{x_0}, & \xi' &= \frac{2\pi}{x'} \\ k_0 &= \frac{1}{\lambda_0}, & k' &= \frac{2\pi}{\lambda'}, \end{aligned} \tag{6.3}$$

and the relation between spatial and temporal scales resulting from propagation with the speed of light

$$z_0 = c_0 t_0 \qquad \Rightarrow \qquad c' z_0 = c t_0. \tag{6.4}$$

Finally, we introduce dimensionless derivatives. As an example we write $\partial_z e_1$ in terms of $\partial_{z'} e_1'$

$$\partial_z e_1 = \frac{\partial e_1}{\partial z} = \frac{\partial \left(e_{10} e_1'\right)}{\partial z'} \frac{\partial z'}{\partial z} = e_{10} \frac{\partial e_1'}{\partial z'} \frac{1}{z_0} = \frac{e_{10}}{z_0} \partial_{z'} e_1'.$$

We see that each ∂_z derivative introduces a $\frac{1}{z_0}$ factor. The e_{10} in the nominator comes from e_1 term written as $e_{10}e_1'$. Therefore, the second derivative is

$$\partial_{zz}e_1 = \frac{\partial^2}{\partial z^2}\left(e_{10}e_1'\right) = \frac{e_{10}}{z_0^2}\,\partial_{z'z'}e_1'.$$

By analogy, we can derive similar relations for e_2, and the derivatives with respect to the other variables.

In opposition to derivation we have the operation of integration, which we can view as a summation over a distance along a particular direction. Therefore, nondimensional integration is accompanied by a dimensional constant, by analogy to nondimensional derivation preceded by a factor of *an inverse of* a dimensional constant. For example, performing the FT along t introduces a factor of t_0 coming from the operation of integration. We will use this property shortly.

6.2.2 Scaling Maxwell's equations

First, we represent the nonlinear polarization components in terms of the scaled electric fields. Using (3.2) we have

$$\begin{aligned} p_1 &= \eta\left(e_1^2 + e_2^2\right)e_1 \\ &= \eta\left[\left(e_{10}e_1'\right)^2 + \left(e_{20}e_2'\right)^2\right]\left(e_{10}e_1'\right), \\ p_2 &= \eta\left(e_1^2 + e_2^2\right)e_2 \\ &= \eta\left[\left(e_{10}e_1'\right)^2 + \left(e_{20}e_2'\right)^2\right]\left(e_{20}e_2'\right). \end{aligned} \tag{6.5}$$

We now insert the scaled variables into equations (3.17) for the electric fields

$$\begin{aligned} \frac{e_{10}}{z_0^2}\partial_{z'z'}e_1' &= \frac{e_{20}}{x_0 z_0}\partial_{x'z'}e_2' + \frac{e_{10}}{c^2\,t_0^2}\partial_{t't'}\left[(1+\mathcal{L})e_1'\right] \\ &\quad + \frac{\eta\,e_{10}}{c^2\,t_0^2}\partial_{t't'}\left[\left(e_{10}e_1'\right)^2 + \left(e_{20}e_2'\right)^2\right]e_1', \\ \frac{e_{20}}{z_0}\partial_{z'}e_2' &= -\frac{e_{10}}{x_0}\partial_{x'}e_1' \\ &\quad - (1+\mathcal{L})^{-1}\left[\frac{\eta\,e_{10}}{x_0}\partial_{x'}\left[\left(e_{10}e_1'\right)^2 + \left(e_{20}e_2'\right)^2\right]e_1'\right. \\ &\quad \left. + \frac{\eta\,e_{20}}{z_0}\partial_{z'}\left[\left(e_{10}e_1'\right)^2 + \left(e_{20}e_2'\right)^2\right]e_2'\right]. \end{aligned}$$

Using relation (6.4) and performing some algebraic simplifications, namely multiplying the first equation by $\frac{z_0^2}{e_{10}}$, multiplying the second equation by $\frac{z_0}{e_{20}}$,

and taking a factor of e_{10}^2 in front of the square brackets, we get

$$\begin{aligned}
\partial_{z'z'}e_1' &= \frac{z_0}{x_0}\frac{e_{20}}{e_{10}}\,\partial_{x'z'}e_2' + \frac{1}{c'^2}\partial_{t't'}\left[(1+\mathcal{L})e_1'\right] \\
&\quad + \frac{1}{c'^2}\partial_{t't'}\,e_{10}^2\eta\left[\left(e_1'\right)^2 + \left(\frac{e_{20}}{e_{10}}e_2'\right)^2\right]e_1', \\
\partial_{z'}e_2' &= -\frac{z_0}{x_0}\frac{e_{10}}{e_{20}}\,\partial_{x'}e_1' \\
&\quad - (1+\mathcal{L})^{-1}\left[\frac{z_0}{x_0}\frac{e_{10}}{e_{20}}\,\partial_{x'}\,e_{10}^2\eta\left[\left(e_1'\right)^2 + \left(\frac{e_{20}}{e_{10}}e_2'\right)^2\right]e_1'\right. \\
&\qquad \left. + \partial_{z'}\,e_{10}^2\eta\left[\left(e_1'\right)^2 + \left(\frac{e_{20}}{e_{10}}e_2'\right)^2\right]e_2'\right].
\end{aligned}$$

We obtained two dimensionless fractions: $\frac{z_0}{x_0}$ and $\frac{e_{20}}{e_{10}}$. They represent the proportionality between the scales of spatial lengths x and z, and the proportionality of the intensities of electric field components e_1 and e_2, respectively. In general, we expect the scales of the electric field components e_1 and e_2 to be different. In principle we know the scale of the incoming transverse component, but we do not know how big longitudinal component can arise in the course of simulation. That can be determined in the course of experiments, and the scaling factor can be adjusted, if necessary. For simplicity, we assume both spatial distances, and both electric field components to be of the same order of magnitude, making the two proportionality fractions equal to one

$$\begin{aligned}
\frac{e_2}{e_1} = O(1) \quad &\Rightarrow \quad \frac{e_{20}}{e_{10}} = 1 \quad \Rightarrow \quad e_{10} = e_{20}, \\
\frac{z}{x} = O(1) \quad &\Rightarrow \quad \frac{z_0}{x_0} = 1 \quad \Rightarrow \quad z_0 = x_0.
\end{aligned} \tag{6.6}$$

What we mean by $\frac{z}{x} = O(1)$ is that the distances *relevant* for light propagation in both directions are of the same scale.

With that, the above Maxwell's equations simplify to

$$\partial_{z'z'}e_1' = \partial_{x'z'}e_2' + \frac{1}{c'^2}\partial_{t't'}\left[(1+\mathcal{L})e_1'\right] + \frac{1}{c'^2}\partial_{t't'}\,e_{10}^2\underbrace{\eta\left(e_1'^2 + e_2'^2\right)e_1'}_{p_1'},$$

$$\partial_{z'}e_2' = -\partial_{x'}e_1' - (1+\mathcal{L})^{-1}\left[\partial_{x'}\,e_{10}^2\underbrace{\eta\left(e_1'^2 + e_2'^2\right)e_1'}_{p_1'} + \partial_{z'}\,e_{10}^2\underbrace{\eta\left(e_1'^2 + e_2'^2\right)e_2'}_{p_2'}\right]. \tag{6.7}$$

We note that there are two dimensional constants left in those equations, namely e_{10}^2 and η. They always appear together, in the expressions associated

with polarization nonlinearities p_1 and p_2, as indicated by the braces. It must be that the product $e_{10}^2\eta$ is dimensionless in order for the RHS's of the above equations to match the LHS's. The International System of Units (SI) unit of e_{10}^2 is $[V^2m^{-2}]$. The unit of η resulting from equations (3.17) is $[m^2V^{-2}]$. Indeed, we see that the product of $e_{10}^2\eta$ has a unit of $[1]$, the product is dimensionless. We will denote

$$\eta' = e_{10}^2\eta, \tag{6.8}$$

and the dimensionless polarization nonlinearities

$$\begin{aligned} p_1' &= \eta' \left(e_1'^2 + e_2'^2\right) e_1', \\ p_2' &= \eta' \left(e_1'^2 + e_2'^2\right) e_2'. \end{aligned} \tag{6.9}$$

What is left is to be determined is the actual value of η'.

6.2.3 Proportionality of polarization nonlinearity

So far, we managed to reduce all the dimensional constants in Maxwell's equations to fractions equal to one, with the exception of $e_{10}^2\eta$ product. The remaining dimensionless variables present in equations (6.7) are assumed to be of the same order of magnitude. We would now like to determine what is the order of magnitude of the polarization nonlinearity resulting from $e_{10}^2\eta$ factor.

We return to the consideration of the nonlinear polarization resulting from the optical Kerr effect. In equation (3.3) we represented it as nonlinear term $\eta(e_1^2 + e_2^2)$, with η not being specified any further. Following [2], we note that the source of nonlinear polarization is a nonlinear susceptibility component χ_{NL}. We thus reconsider susceptibility to be a sum of linear an nonlinear components

$$\chi = \chi_L + \chi_{NL}.$$

Such χ builds up both the linear $\boldsymbol{P}_L$ and the nonlinear $\boldsymbol{P}_{NL}$ components of polarization. The linear susceptibility is already considered in the refractive index $n(\omega)$, as derived in Appendix B. With the addition of nonlinear susceptibility, we reconsider the refractive index to also be composed of its linear and nonlinear parts

$$n = n_L + n_{NL} = n_L + n_2 I, \tag{6.10}$$

where n_L is the linear refractive index $n(\omega)$ derived in Appendix B, and I is the intensity of the electric field

$$I = \frac{1}{2}\epsilon_0 c n_0 E_0^2 \qquad \Rightarrow \qquad E_0^2 = \frac{2I}{\epsilon_0 c n_0}. \tag{6.11}$$

The units of $n_2[m^2W^{-1}]$ and $I[Wm^{-2}]$ cancel each other out into a dimensionless quantity. We denoted by n_0 the constant refractive index, which in our case is the linear refractive index of the center frequency $n(\omega_c)$. The nonlinear refractive index n_2 is material dependent, and its values are known for different materials. It is given as

$$n_2 = \frac{3}{4}\chi^{(3)}\frac{1}{\epsilon_0 c n_0^2}. \tag{6.12}$$

With the envelope of the nonlinear polarization equivalent to [5]

$$\boldsymbol{P} \equiv \frac{3}{4}\chi^{(3)}E_0^2\boldsymbol{E},$$

and using the product $n_2 I$ according to (6.11) and (6.12)

$$2n_2 I = \frac{3}{4}\chi^{(3)}\frac{1}{n_0}E_0^2,$$

we estimate the nonlinear polarization as

$$\boldsymbol{P} \equiv 2n_0 n_2 I\boldsymbol{E}. \tag{6.13}$$

Comparing equations (6.13) and (2.4) we draw the conclusion that

$$\begin{aligned} \eta E_0^2 \equiv 2n_0 n_2 I &= n_0^2 n_2 \epsilon_0 c E_0^2 \\ \Rightarrow \quad \eta &\equiv \epsilon_0 c n_0^2 n_2. \end{aligned} \tag{6.14}$$

That allows us to determine the actual value of η, since for a particular material all the coefficients on the RHS of (6.14) are known. We do that in section 6.3.

6.2.4 Scaling the normal-mode expansions

We now look into the scaling of the equations for the electric field components expressed as the superposition of the normal modes, namely the equations (3.26) and (3.27). First we express the dispersion relation $\beta(\omega, \xi)$ in equation (3.21) in terms of dimensionless variables, using (6.4), (6.3) and (6.6)

$$\begin{aligned} \beta(\omega,\xi) &= \sqrt{\left(\frac{\omega_0\omega'}{c' z_0 \omega_0} n(\omega_0\omega')\right)^2 - \left(\frac{1}{x_0}\xi'\right)^2} = \sqrt{\frac{\omega'^2}{c'^2 z_0^2} n^2(\omega_0\omega') - \frac{1}{z_0^2}\xi'^2} \\ &= \frac{1}{z_0}\underbrace{\sqrt{\frac{\omega'^2}{c'^2} n^2(\omega_0\omega') - \xi'^2}}_{\beta'}. \end{aligned} \tag{6.15}$$

5. note that we do not include ϵ_0 into the nonlinear polarization, in order to be consistent with (3.3)

For β we obtained the dimensional scale of $\frac{1}{z_0}$, since refractive index $n(\omega_0\omega')$ is a dimensionless quantity. Stating explicitly the following relations

$$t = \frac{1}{\omega_0}t', \qquad \beta = \frac{1}{z_0}\beta', \qquad \xi = \frac{1}{x_0}\xi',$$

we see that the exponents in equations (3.26), (3.27) are dimensionless

$$\begin{aligned}
\pm i\beta z &= \pm i\,\frac{1}{z_0}\beta'\; z_0 z' = \pm i\beta' z', \\
\pm i\xi x &= \pm i\,\frac{1}{x_0}\xi'\; x_0 x' = \pm i\xi' x', \\
\pm i\omega t &= \pm i\;\omega_0\omega'\;\frac{1}{\omega_0}t' = \pm i\omega' t'.
\end{aligned}$$

We also introduce dimensionless amplitudes A'_+, A'_-, Q' with scaling constants A_0 and Q_0. With the same scaling constants for the left- and right-traveling modes we have

$$\begin{aligned}
A_+ &= A_0 A'_+, \\
A_- &= A_0 A'_-, \\
Q &= Q_0 Q' = \frac{A_0}{x_0}Q' \text{ (see below).}
\end{aligned} \tag{6.16}$$

We proceed to writing the normal mode expansion equations in terms of dimensionless variables

$$\begin{aligned}
e_{10}e'_1 &= \frac{1}{2\pi}\frac{\omega_0 A_0}{x_0 z_0}\int_{-\infty}^{+\infty}d\omega'\int_{-\infty}^{+\infty}d\xi'\;\left[\beta'\left(A'_+e^{i\beta' z'} + A'_-e^{-i\beta' z'}\right)\right]e^{i(\xi' x' - \omega' t')}, \\
e_{20}e'_2 &= \frac{1}{2\pi}\frac{\omega_0 A_0}{x_0^2}\int_{-\infty}^{+\infty}d\omega'\int_{-\infty}^{+\infty}d\xi'\left[\xi'\left(-A'_+e^{i\beta' z'} + A'_-e^{-i\beta' z'}\right) + \frac{x_0 Q_0}{A_0}Q'\right] \\
&\qquad e^{i(\xi' x' - \omega' t')}.
\end{aligned} \tag{6.17}$$

All the dimensional constants of the RHSs are gathered in front of the integral signs, except for the constant in front of the Q' mode amplitude. This constant must be dimensionless, in order to be able to sum it up with the other dimensionless quantities in the equation. Therefore, with respect to dimensions we must have

$$e_{10} = e_{20} = \frac{\omega_0 A_0}{x_0 z_0} = \frac{\omega_0 A_0}{x_0^2}, \tag{6.18}$$

which we know is true due to assuming $z_0 = x_0$. From the above we can infer the scale of A_0 to be

$$A_0 = \frac{x_0 z_0 e_{10}}{\omega_0}. \tag{6.19}$$

In order to get dimensional accordance in the second equation of (6.17) we must also have

$$x_0 Q_0 = A_0 \qquad \Rightarrow \qquad Q_0 = \frac{A_0}{x_0} = \frac{z_0 e_{10}}{\omega_0}. \tag{6.20}$$

Note, that the dimensions of Q_0 and A_0 are different. In particular, the smaller the spatial scale we choose to go for in the transverse direction x, the more the scale of Q is amplified. Under experimental setup we would expect to see a *more pronounced* Q mode whenever the along-x *span* of the laser pulse is relatively *small*. Those are very imprecise notions, but they give intuition of the experimental setups where the Q mode might arise more noticeably.

Using relations (6.18) and (6.20) we can write equations (6.17) as

$$\begin{aligned} e_1' &= \frac{1}{2\pi}\int_{-\infty}^{+\infty} d\omega' \int_{-\infty}^{+\infty} d\xi' \left[\beta'\left(A_+' e^{i\beta' z'} + A_-' e^{-i\beta' z'}\right)\right] e^{i(\xi' x' - \omega' t')}, \\ e_2' &= \frac{1}{2\pi}\int_{-\infty}^{+\infty} d\omega' \int_{-\infty}^{+\infty} d\xi' \left[\xi'\left(-A_+' e^{i\beta' z'} + A_-' e^{-i\beta' z'}\right) + Q'\right] e^{i(\xi' x' - \omega' t')}. \end{aligned} \tag{6.21}$$

Those are fully dimensionless equations. Dropping all the primes would give us exactly the same formulas as the original equations (3.26), (3.27). What we have gained, however, are the scaling relations for the amplitudes (6.19) and (6.20). We put the resulting scales in Table 6.2.

6.2.5 Scaling the BPPE system

The final stretch in the scaling process is to determine the dimensionless BPPE system, together with corresponding dimensionless nonlinearities and their scales. We start by writing the LHS of BPPE system (3.35) in terms of dimensionless variables

$$\begin{aligned} \frac{A_0}{z_0^3}\, 2i\beta'^2 \partial_{z'} A_+' e^{i\beta' z'} &= \widehat{NL_A}, \\ -\frac{A_0}{z_0^3}\, 2i\beta'^2 \partial_{z'} A_-' e^{-i\beta' z'} &= \widehat{NL_A}, \\ \frac{A_0}{z_0 x_0}\, \partial_{z'} Q' &= \widehat{NL_Q}. \end{aligned}$$

From the above we infer that the dimensions of spectral nonlinearities are

$$\begin{aligned} dim. \quad \widehat{NL_A} &= \frac{A_0}{z_0^3} = \frac{e_{10}}{\omega_0 z_0}, \\ dim. \quad \widehat{NL_Q} &= \frac{A_0}{z_0^2} = \frac{e_{10}}{\omega_0}, \end{aligned} \tag{6.22}$$

using (6.19). Let us verify this result by expressing the RHS of (3.35) in terms of dimensionless constants. For that we need the dimension of spectral polarization nonlinearities. From (6.7) and (6.5) we have

$$p_1 = e_{10}\, e_{10}^2 \eta \left(e_1'^2 + e_2'^2\right) e_1' = e_{10}\, \eta' \left(e_1'^2 + e_2'^2\right) e_1' = e_{10}\, p_1',$$
$$p_2 = e_{20}\, e_{10}^2 \eta \left(e_1'^2 + e_2'^2\right) e_2' = e_{10}\, \eta' \left(e_1'^2 + e_2'^2\right) e_2' = e_{10}\, p_2'.$$

Taking FT in space and time using dimensionless variables introduces a factor of $\frac{x_0}{\omega_0} = \frac{z_0}{\omega_0}$. We thus have

$$\widehat{p_1} = \frac{z_0}{\omega_0} e_{10}\, \widehat{p_1'},$$
$$\widehat{p_2} = \frac{z_0}{\omega_0} e_{10}\, \widehat{p_2'}.$$

We obtained that the dimension of spectral polarization nonlinearities is $\frac{z_0 e_{10}}{\omega_0}$. Inserting that into BPPE system's RHS nonlinearities (3.36), (3.37), and using relations (6.4), (6.6), (6.3), we get

$$\begin{aligned}
\widehat{NL_A} &= -\frac{e_{10}}{z_0\omega_0} \frac{1}{n^2(\omega_0\omega')} \left(\beta'^2 \widehat{p_1'} + i\xi' \partial_{z'} \widehat{p_2'}\right) &&= \frac{e_{10}}{z_0\omega_0} \widehat{NL_A}', \\
\widehat{NL_Q} &= -\frac{e_{10}}{\omega_0} \frac{\omega'^2}{c'^2\beta'^2} \partial_{z'} \widehat{p_2'} &&= \frac{e_{10}}{\omega_0} \widehat{NL_Q}'.
\end{aligned} \tag{6.23}$$

As expected, we obtained the same dimensional scaling factors as indicated by the LHS (6.22). To some extent that confirms the correctness of out derivations, and it is in accordance with the expectation of non-dimensionality of the laws of physics, in that case the Maxwell's equations, which the BPPE system is derived from. The non-dimensional BPPE system to solve is thus

$$\begin{aligned}
2i\beta'^2 \partial_{z'} A_+' e^{i\beta' z'} &= \widehat{NL_A}', \\
-2i\beta'^2 \partial_{z'} A_-' e^{-i\beta' z'} &= \widehat{NL_A}', \\
\partial_{z'} Q' &= \widehat{NL_Q}',
\end{aligned} \tag{6.24}$$

with nonlinearities defined in (6.23) and all primed variables being dimensionless.

6.3 Physical scales and parameters

6.3.1 Electromagnetic field and polarization nonlinearity

We have presented relations between various coefficients and variables in the previous sections. We now proceed to setting the actual values of the

physical quantities, in order to determine the dimensional constants for scaling equations (6.7). We follow [1] in that regard, where parameters for fused silica medium are used.[6] The listing of all values is provided in Table 6.2. Those values are used for numerical simulations.

We can now determine the values of η and $e_{10}^2\eta$, which were of interest in section 6.2.3. Using the values in Table 6.2 and the relation (6.14) we have

$$\eta = 1.97 \cdot 10^{-22}\ [m^2V^{-2}],$$
$$E_0^2\eta = 4.10 \cdot 10^{-4}.$$

From equation (6.11) we predict the expected magnitude of the electric field solution, which will determine the scales of e_{10}^2 and e_{20}^2

$$E_0^2 = 2.08 \cdot 10^{18}\ [V^2m^{-2}].$$

This is the same result that we would have obtained by dividing $E_0^2\eta$ by η. That confirms that the nonlinearity term is relatively small. For the dimensional constants we have

$$e_{10} = e_{20} = 10^9 Vm^{-1}. \tag{6.25}$$

This is the scaling factor by which the dimensionless solutions e_1', e_2' to system (6.7) will be scaled from the numerical solutions in order to reconstruct the values of physical entities e_1, e_2.

6.3.2 Space-time

In order to find appropriate scales for the space-time dimensions, we return to relations between t, ω, k and λ, where the last two are wave number and wavelength respectively. We would like to choose such scales ω_0, k_0 and λ_0 that the corresponding dimensionless variables are of $O(1)$. We use the usual relations between frequency, wave number and wavelength

$$\omega_0 = v_p k_0 \qquad \Rightarrow \qquad k_0 = \frac{\omega_0}{v_p},$$

where $v_p = \frac{c}{n_0}$ is the phase velocity of the wave, and for vacuum it is equal to the speed of light c. Using (6.3) we have

$$\frac{1}{\lambda_0} = \frac{\omega_0}{v_p} \qquad \Rightarrow \qquad \lambda_0 = \frac{v_p}{\omega_0}.$$

6. We make an exception for the value of electromagnetic field intensity I. In [1] $I = O(10^{17})\ Wm^{-2}$, being the critical level leading to the optical damage of the medium. We use the value of I smaller by two orders of magnitude.

We obtained the formula for the wavelength scale as a function of frequency scale. Electromagnetic oscillation happens at such spatial scale, so it is reasonable to choose λ_0 as the dimensional constant for spatial dimensionless variables. We have

$$\begin{gathered} z_0 = x_0 = \lambda_0 \\ \Downarrow \\ z = \lambda_0 z', \\ x = \lambda_0 x'. \end{gathered}$$

Naturally, from frequency scale we also deduce the dominating time scale $t = \frac{1}{\omega_0} t'$.

Choosing the physical frequency of oscillation of the laser pulse, determines the entire spatiotemporal sizing of the system. High-intensity electric field oscillates with femtosecond periods. This is the *main* frequency of oscillation, meaning that the modes oscillating at that frequency have the largest magnitudes. Based on that, we choose the *center* frequency of the pulse spectrum $\omega_c = \omega_0 \cdot \omega_c'$, and from that we determine the central wavelength and oscillation period, as well as the relevant scales ω_0, λ_0, t_0. We follow [1] for ω_c

$$\begin{aligned} \omega_c = 2.35\ [fs^{-1}] \quad &\Rightarrow \quad \omega_0 = 10^{15}\ [s^{-1}], \\ \lambda_c = 0.880\ [\mu m] \quad &\Rightarrow \quad \lambda_0 = 10^{-7}\ [m], \\ \tau_c = 2.67\ [fs] \quad &\Rightarrow \quad t_0 = 10^{-15}\ [s], \end{aligned}$$

where τ_c denotes the period of oscillation of the central mode, meaning the mode with highest amplitude. Note, that those values are relevant for vacuum, where $v_p = c$. This is of interest to us since the laser pulse which is the input to the model is the one that originates in vacuum. Those values help us design a proper laser pulse input. For calculating values relevant for propagation in slab we would need to take into account the refractive index as well. However, since $n(\omega) = O(1)$ it will not impact the scale, and we can infer about the propagation distance and time based on the above values for vacuum. Those values are also indicated in Table 6.2.

6.3.3 Refractive index

Using now the same scaling approach we introduce dimensionless frequency variables

$$\begin{aligned} \omega_p &= \omega_0 \omega_p', \\ \omega_r &= \omega_0 \omega_r', \\ \gamma &= \omega_0 \gamma', \end{aligned}$$

which allow to express equation (2.5) in fully nondimensional terms as

$$\widehat{\chi}(\omega') = \frac{\omega_0^2 \omega_p'^2}{\omega_0^2 \omega_r'^2 - \omega_0^2 \omega'^2 - i\omega_0 \gamma' \omega_0 \omega'} = \frac{\omega_p'^2}{\omega_r'^2 - \omega'^2 - i\gamma' \omega'}.$$

From that we can directly express n and α in terms of dimensionless frequency ω' according to equations (2.7). We graph $n(\omega')$ and $\alpha(\omega')$ for particular values of ω_r', ω_p' and γ' in Figure 6.2.

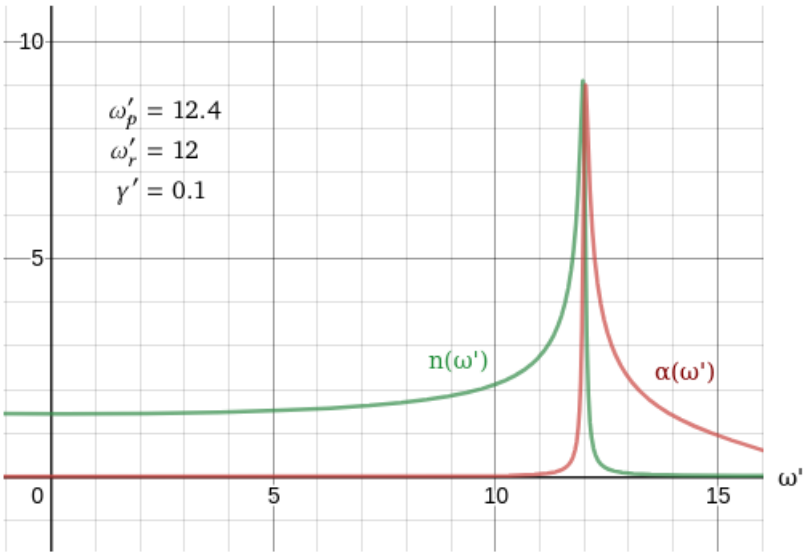

Figure 6.2: Refractive index model.

Looking at Figure 6.2, we note that for certain ranges of frequency ω', the refractive index is practically constant, and the absorption coefficient is zero. Choosing the frequency of our input laser pulse in such a region allows us to reduce the effect of dispersion in the medium. The laser pulse should not be too close to the resonant frequency $\omega_r' = 12$, nor should it be close to the zero frequency. Following [1] we choose $\omega_c' = 2.35$, and that indeed falls in the desired region.

The parameter values we chose are relevant for silica quartz, following [4]. The obtained model is consistent with the values assumed in [1]. Evaluating $n(\omega')$ at the center frequency $\omega_c' = 2.35$ we obtain practically the same result $n(\omega_c') \approx 1.45$[7] and the derivative

$$\frac{dn(\omega')}{d\omega'}|_{\omega_c'} \approx 0. \tag{6.26}$$

7. the nonlinear refractive index part, $n_2 I$, is of negligible proportions

6.3.4 Input laser pulse

We model the input laser pulse as a Gaussian envelope on top of the carrier wave oscillating with frequency ω_c'

$$e(z = a^-, t') = e^{-\sigma t'^2} cos(\omega_c' t').$$

Such pulse has an optical cycle τ_c at the center frequency ω_c

$$\tau_c = \frac{2\pi}{\omega_c} = 2.67\ fs.$$

In [1] the simulations are conducted on *single-cycle regime* pulses, where not much more than one carrier cycle is contained within Full Width at Half Maximum (FWHM) of the envelope, making the pulse width $\tau_p \approx \tau_c$. This is modeled using $\sigma = \left(\frac{1.67}{\tau_c}\right)^2 \approx 0.39$. We allow for slightly more than two oscillations within the FWHM, which we achieve by maintaining the ω_c' but broadening the Gaussian curve by setting $\sigma = 0.1$

$$e(z = a^-, t') = e^{-0.1 t'^2} cos(2.35 t'). \tag{6.27}$$

The pulse width is $\tau_p = 5.27\ fs$. Function in equation (6.27) is graphed in Figure 6.3.

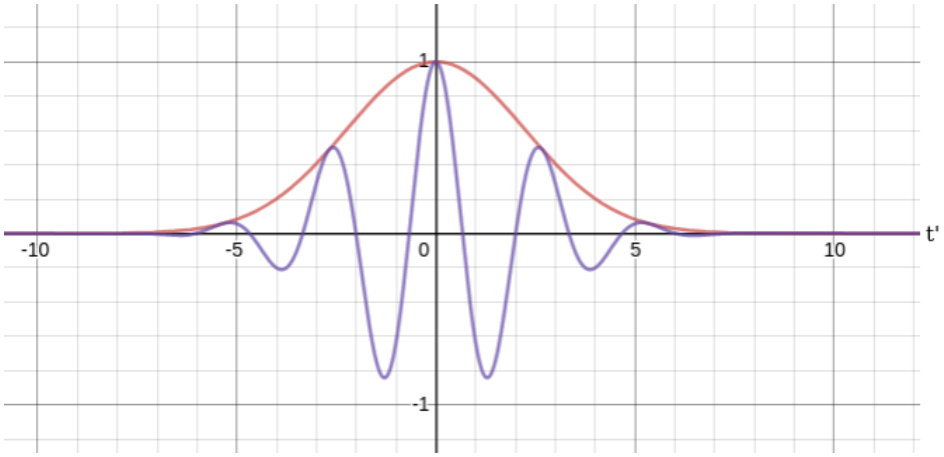

Figure 6.3: Input laser pulse model.

6.3.5 Temporal span of the result

In order to plan for sufficient temporal span of the solution, we would like to predict the travel time of the light pulse. Once a distance in a slab $z_b - z_a$ is established, it determines the time taken for the light pulse to propagate

through the slab, reflect from the interface at z_b and get back to z_a. To catch the electric field amplitude getting back to z_a, we need to know what pulse propagation time to allow for in the simulation.

The peak of the pulse travels through medium with certain *group velocity* v_g. For the direction of propagation $k = \beta(\omega, \xi)$ we have

$$v_g = \frac{\partial \omega}{\partial k} = \frac{\partial \omega}{\partial \beta} = \left(\frac{\partial \beta}{\partial \omega}\right)^{-1}.$$

We use equation (6.15) to compute the derivative of β with respect to ω

$$\frac{\partial \beta}{\partial \omega} = \frac{1}{\omega_0 z_0}\frac{\partial \beta'}{\partial \omega'} = \frac{1}{\omega_0 z_0 c'^2}\frac{\omega' n^2 + \omega'^2 n \frac{dn}{d\omega'}}{\sqrt{\frac{\omega'^2}{c'^2}n^2 - \xi'^2}} \approx \frac{1}{\omega_0 z_0 c'^2}\frac{\omega' n^2}{\sqrt{\frac{\omega'^2}{c'^2}n^2 - \xi'^2}},$$

using (6.26). That expressions is difficult to evaluate exactly, due to the dependence on variable ξ', but we can safely assume that the magnitude of the dimensionless component is $O(1)$. We thus have the approximate scale of v_g

$$v_g = O(\omega_0 z_0) = O(10^8)[ms^{-1}] = O(c).$$

To allow for enough propagation time, we asses the lowest group velocity. We find it by assuming $\xi' = 0$ and evaluating the expression for $\omega' = \omega'_c$. We then obtain

$$v_g \gtrapprox \frac{\omega_0 z_0 c'}{n} \approx 2 \cdot 10^8 [ms^{-1}],$$

being about $2/3$ the speed of light. In nondimensional terms

$$v_g = v_0 v'_g, \qquad v_0 = \frac{z_0}{t_0} = 10^8 ms^{-1}, \qquad v'_g = 2.$$

With such speed the peak of the pulse travels roughly at least $3\mu m$ every $15fs$, or in nondimensional terms it travels a distance $z'_b - z'_a = 30$ in time $t' = 15$. Choosing slab width of 30 units, and allowing the pulse to propagate through the slab there and back, so 60 units in total, we need to allow for propagation time of 30 units. We present the exact simulation setup for the time of propagation and the slab length in the case-study section 9.2.

8. source [11]

Quantity	**Symbol**	**Value**	**SI unit**
Constants			
vacuum permittivity	ϵ_0	$8.8541878128 \cdot 10^{-12}$	Fm^{-1}
light speed	$c = c' \cdot c_0$	$2.99792458 \cdot 10^{8}$	ms^{-1}
vacuum refractive index	n_v	1	1
Physical quantities of choice			
intensity	I	$4 \cdot 10^{15}$	Wm^{-2}
refractive index at ω_c	$n_0 = n(\omega_c)$	1.45	1
nonlinear refractive index[8]	n_2	$3.54 \cdot 10^{-20}$	m^2W^{-1}
central frequency	ω_c	$2.35 \cdot 10^{15}$	s^{-1}
Resulting scales			
electric field scales	e_{10}, e_{20}	10^{9}	Vm^{-1}
frequency scale	ω_0	10^{15}	s^{-1}
length scales	z_0, x_0	10^{-7}	m
time scale	t_0	10^{-15}	s
Resulting parameters of the model			
central wavelength	λ_c	$8.02 \cdot 10^{-7}$	m
central oscillation period	τ_c	$2.67 \cdot 10^{-15}$	s
pulse width (intensity FWHM)	τ_p	$5.27 \cdot 10^{-15}$	s
polarization nonlinearity factor	η	$1.97 \cdot 10^{-22}$	m^2V^{-2}
polarization nonlinearity factor	$\eta' = e_{10}^2\eta$	$1.97 \cdot 10^{-4}$	1
A_+, A_- modes scale	A_0	10^{10}	mVs
Q mode scale	$Q_0 = A_0/x_0$	10^{17}	Vs

Table 6.2: Physical constants, quantities and scales.

7

Verification method

7.1 Artificial source test

We present here a method for verifying the implementation of the BPPE shooting method. The method is of AST type. For an arbitrary solution state at $z = b^+$ it allows to construct the corresponding BC Φ that leads to that state. This is done by solving a single, particularly modified BPPE differential system, *without* the iterative shooting involved. The AST presented here is deeply inspired by [7], yet it is adapted to include the spectral amplitude Q and to be relevant for the TM mode.

Using the AST method we could initialize it with a truly *arbitrary* seed-state, potentially producing a *physically-meaningless* artificial source to be the input for the scatter problem. In consequence, we would design a *non-physical* simulation problem - one that does not have a direct reflection in the physical world, even though it follows the BPPE equations derived from Maxwell's equations. Such problem would still be valid for testing the implementation of mathematics, though.

Our approach, however, will be to combine the testing phase with solving actual physical problems. We achieve it by initializing the AST with particularly designed seed-state, such that the corresponding artificial source is a good representation, a model, of an incoming laser beam. We present the details of how this is achieved in section 9.1.1. It suffices to say now that we pick a model for an incoming laser beam and solve a scatter problem using it as input. As

part of the solution we receive a transmission spectrum at $z = b^+$, which we use as the initialization of the AST. The AST then generates an artificial source, which is numerically close to the original incoming laser beam. We use it[1] as input for solving a new scatter problem, and compare the results against the AST reference.

That is an intuition for the big picture of the testing approach. In this Chapter we present only the particularities of the AST method itself, without prescribing any particular initialization states yet.

7.1.1 Problem

Let us consider a state at $z = a^-$ given by

$$\phi_+(\omega,\xi), \phi_-(\omega,\xi), \phi_Q(\omega,\xi),$$

and a state at $z = b+$ given by

$$\psi_+(\omega,\xi), \psi_-(\omega,\xi), \psi_Q(\omega,\xi).$$

Let us also use the usual notation for the solution to the BPPE system (3.35) within $a < z < b$, with interface continuity conditions (4.7), (4.8), (4.9) expressed in terms of spectral amplitudes

$$A_+(z,\omega,\xi), A_-(z,\omega,\xi), Q(z,\omega,\xi).$$

The challenge is to find such a BC $\left(\phi_+, \phi_-, \phi_Q\right)$ that

$$\begin{pmatrix} \phi_+(\omega,\xi) \\ \phi_-(\omega,\xi) \\ \phi_Q(\omega,\xi) \end{pmatrix} \quad \underset{\longrightarrow}{(4.7),\ (4.8),\ (4.9)} \quad \begin{pmatrix} A_+(a^+,\omega,\xi) \\ A_-(a^+,\omega,\xi) \\ Q(a^+,\omega,\xi) \end{pmatrix} \tag{7.1}$$

and

$$\begin{pmatrix} A_+(b^-,\omega,\xi) \\ A_-(b^-,\omega,\xi) \\ Q(b^-,\omega,\xi) \end{pmatrix} \quad \underset{\longrightarrow}{(4.7),\ (4.8),\ (4.9)} \quad \begin{pmatrix} \psi_+(\omega,\xi) \\ \psi_-(\omega,\xi) \\ \psi_Q(\omega,\xi) \end{pmatrix}, \tag{7.2}$$

where

ψ_+ is arbitrarily chosen,

$\psi_- = 0$, due to no light sources from $+\infty$,

1. only the right-traveling component

ψ_Q follows solvability condition (5.2), $\psi_Q = \psi_Q(\psi_+, \psi_-, \psi_Q)$.

What we are effectively aiming at, is to find a BC ϕ for the end-state ψ controlled by us, such that when solving the BPPE system for that particular BC we know that the solution at $z = b^+$ should be the chosen ψ.

7.1.2 Approach

Let us start with a wordy description of the approach. We solve the above problem by considering a *backwards* problem. The desired arbitrary end-state Ψ is used as a BC for a slightly modified BPPE system, where we solve for spectral amplitudes $B_+(\theta, \omega, \xi)$, $B_-(\theta, \omega, \xi)$, $R(\theta, \omega, \xi)$. This slightly modified system follows all the same rules, but we start with Ψ at $z = b^+$, and after crossing the interface from $z = b+$ to $z = b^-$ we arrive at point $\theta = a$ for the B_+, B_-, R system, where θ is defined in (7.5). This is by no means a physical process, but it does not have to be - it is *just* a mathematical way of generating the artificial source.

Moreover, B_+ mode propagates in the same direction as A_- mode, and B_- in the same direction as A_+. What is an *end* of the journey for a pulse in B_+, B_-, R system, is the *beginning* in A_+, A_-, Q system. An attempt to present this intuition is presented in Figure 7.1, and the mathematical details follow further.

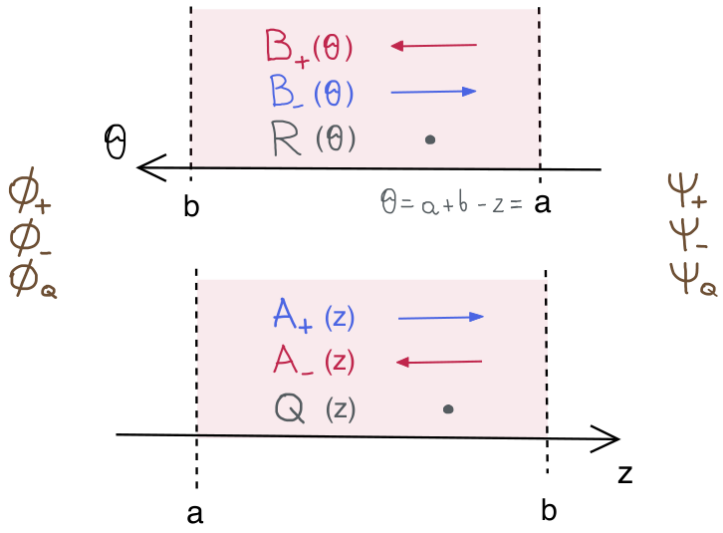

Figure 7.1: Correspondence between two BPPE systems in artificial-source test. Dependence of all spectral amplitudes on ω, ξ is dropped.

Also, since we merely wish to propagate the Ψ BC to the other side of the slab,

we do not need to use the iterative shooting method presented in Chapter 6. Solving a single differential BPPE system inside a slab is enough to obtain the spectral amplitudes solution in the slab. This solution becomes a reference for our original A_+, A_-, Q BPPE problem. Obtaining the Φ BC for the original A_+, A_-, Q problem is done by crossing the interface at $z = a^2$ from inside to outside of the slab.

Summarizing the key points, in order to solve the given problem we consider another BPPE system, where

- the unique spectral amplitudes solution is given by

$$B_+(\theta,\omega,\xi), B_-(\theta,\omega,\xi), R(\theta,\omega,\xi),$$

- the BC of the system is *based on* (ψ_+, ψ_-, ψ_Q),
- the z-dependence in the system is flipped, meaning that the propagation of light progresses in the opposite direction, as depicted in Figure 7.1 (note the direction of arrows representing wave travel direction),
- the nonlinearity on the RHS is modified in a particular manner with respect to the original system, as indicated in (7.3).

For convenience we restate here the original BPPE system (3.35)

$$\begin{aligned} 2i\beta_1^2\,\partial_z A_+(z,\omega,\xi)\,e^{i\beta_1 z} &= \widehat{NL_A}(z,A_+,A_-,Q),\\ -2i\beta_1^2\,\partial_z A_-(z,\omega,\xi)\,e^{-i\beta_1 z} &= \widehat{NL_A}(z,A_+,A_-,Q),\\ \partial_z Q(z,\omega,\xi) &= \widehat{NL_Q}(z,A_+,A_-,Q), \end{aligned}$$

where we made explicit the dependence on arguments, and the value of β is for the slab material. In such context, the modified BPPE system that we consider for the purpose of the artificial-source test is

$$\begin{aligned} 2i\beta_1^2\,\partial_z B_+(\theta,\omega,\xi)\,e^{i\beta_1\theta} &= \widehat{Y}(z,B_+,B_-,R),\\ -2i\beta_1^2\,\partial_z B_-(\theta,\omega,\xi)\,e^{-i\beta_1\theta} &= \widehat{Y}(z,B_+,B_-,R),\\ \partial_z R(\theta,\omega,\xi) &= \widehat{Z}(z,B_+,B_-,R), \end{aligned} \tag{7.3}$$

with a BC such that

$$\begin{pmatrix}\psi_+(\omega,\xi)\\ \psi_-(\omega,\xi)\\ \psi_Q(\omega,\xi)\end{pmatrix} \quad \underset{\rightarrow}{(4.7),\,(4.8),\,(4.9)} \quad J\begin{pmatrix}B_+(a^+,\omega,\xi)\\ B_-(a^+,\omega,\xi)\\ R(a^+,\omega,\xi)\end{pmatrix}, \tag{7.4}$$

2. indeed the interface at $\theta = b$ from the perspective of B_+, B_-, R system

where matrix J is given by

$$J = \begin{bmatrix} 0 & e^{-i\beta_1(a+b)} & 0 \\ e^{i\beta_1(a+b)} & 0 & 0 \\ 0 & 0 & -1 \end{bmatrix}.$$

Note, that despite the fact that in the original setup ψ is the state *after* passing the slab, in the modified setup it forms part of the BC at point $\theta = a^-$. ψ is not exactly the BC due to the occurrence of matrix J on the RHS. The actual BC for the for B_+, B_-, R system depends both on ψ and the inverse matrix J^{-1}. We know that such inverse exists since $\det(J) \neq 0$.

Before proceeding to the application of the newly defined system (7.3) we note several points

- Preserving the solvability condition (5.2) is the property of BPPE system equations, so it is maintained also for the B_+, B_-, R system. By imposing the solvability condition on ψ_Q we introduce it into the modified BPPE system (7.3).

- Multiplication by J matrix stems from how the relation between A_+, A_-, Q and B_+, B_-, R systems is defined in section 7.1.3.

- The nonlinearities for both systems are different, but related to each other. That relation is specified in section 7.1.4. In physical terms it means that the nonlinear response of the material slab is different. In particular, it is *not* the solution A_+, A_-, Q flipped in z-direction, but it is rather an entirely different solution, provoked by different nonlinear properties of a physical material. However, the interface crossings are carried out according to the usual conditions (4.7), (4.8), (4.9), so it is only *strictly inside* the material slab that the nonlinear properties are modified.

7.1.3 Solution

This section provides a link between the two BPPE problems considered so far, and how the A_+, A_-, Q can be constructed from B_+, B_-, R.

Let us define

$$\theta = a + b - z, \qquad \frac{\partial\theta}{\partial z} = -1 \quad \Rightarrow \quad \partial_z = -\partial_\theta. \tag{7.5}$$

The solutions to the original BPPE problem (3.35) are defined in terms of the

solutions to (7.3) as follows

$$\begin{pmatrix} A_+(z,\omega,\xi) \\ A_-(z,\omega,\xi) \\ Q(z,\omega,\xi) \end{pmatrix} = J \begin{pmatrix} B_+(a+b-z,\omega,\xi) \\ B_-(a+b-z,\omega,\xi) \\ R(a+b-z,\omega,\xi) \end{pmatrix} = \begin{pmatrix} B_-(a+b-z,\omega,\xi)\, e^{-i\beta_1(a+b)} \\ B_+(a+b-z,\omega,\xi)\, e^{i\beta_1(a+b)} \\ -R(a+b-z,\omega,\xi) \end{pmatrix}. \tag{7.6}$$

Using relations (7.10), and the reasoning which we elaborate on in section 7.1.4, the LHS of the first equation of (3.35) can be expressed as

$$\begin{aligned}
2i\beta_1^2\, \partial_z A_+(z,\omega,\xi)\, e^{i\beta_1 z} &= -2i\beta_1^2\, \partial_\theta B_-(\theta,\omega,\xi)\, e^{-i\beta_1 \overbrace{(a+b-z)}^{\theta}} \\
&= \widehat{Y}(\theta, B_+, B_-, R) \\
&= f\left(\begin{bmatrix} \widehat{g_1} \\ -\widehat{g_2} \end{bmatrix}\right) \\
&= f\left(\begin{bmatrix} \beta_1 \left(B_+(\theta,\omega,\xi)\, e^{i\beta_1\theta} + B_-(\theta,\omega,\xi)\, e^{-i\beta_1\theta}\right) \\ -\left[-\xi\left(B_+(\theta,\omega,\xi)\, e^{i\beta_1\theta} - B_-(\theta,\omega,\xi)\, e^{-i\beta_1\theta}\right) + R\right] \end{bmatrix}\right) \\
&= f\left(\begin{bmatrix} \beta_1 \left(B_+(\theta,\omega,\xi)\, e^{i\beta_1(a+b)} e^{-i\beta_1 z} + B_-(\theta,\omega,\xi)\, e^{-i\beta_1(a+b)} e^{i\beta_1 z}\right) \\ \xi\left(B_+(\theta,\omega,\xi)\, e^{i\beta_1(a+b)} e^{-i\beta_1 z} - B_-(\theta,\omega,\xi)\, e^{-i\beta_1(a+b)} e^{i\beta_1 z}\right) - R \end{bmatrix}\right) \\
&\quad \downarrow \text{ using (7.6)} \\
&= f\left(\begin{bmatrix} \beta_1 \left(A_-(z,\omega,\xi)\, e^{-i\beta_1 z} + A_+(z,\omega,\xi)\, e^{i\beta_1 z}\right) \\ \xi\left(A_-(z,\omega,\xi)\, e^{-i\beta_1 z} - A_+(z,\omega,\xi)\, e^{i\beta_1 z}\right) + Q \end{bmatrix}\right) \\
&= f\left(\begin{bmatrix} \widehat{e_1} \\ \widehat{e_2} \end{bmatrix}\right) \\
&= \widehat{NL_A}(z, A_+, A_-, Q).
\end{aligned} \tag{7.7}$$

The arguments of function f are arranged in a vector form.

We expressed the LHS of the first equation in (3.35) in terms of B_+, B_-, R, and after some algebraic operations we arrived at the RHS of the same equation. We can perform analogous transformation for the other two equations in the system (3.35). We summarize it below

$$\begin{aligned}
-2i\beta_1^2 \partial_z A_-(z,\omega,\xi)\, e^{-i\beta_1 z} &= 2i\beta_1^2\, \partial_\theta B_+(\theta,\omega,\xi)\, e^{i\beta_1\theta} \\
&= \widehat{Y}(\theta, B_+, B_-, R) \\
&= \widehat{NL_A}(z, A_+, A_-, Q),
\end{aligned}$$

$$\begin{aligned}
\partial_z Q(z,\omega,\xi) &= -\partial_\theta\left(-R(\theta,\omega,\xi)\right) \\
&= \partial_\theta R(\theta,\omega,\xi) \\
&= \widehat{Z}(\theta, B_+, B_-, R) \\
&= \widehat{NL_Q}(z, A_+, A_-, Q).
\end{aligned}$$

Therefore, we conclude that the spectral amplitudes A_+, A_-, Q constructed according to (7.6) from the unique solutions to B_+, B_-, R system (7.3), are the unique solutions to BPPE system (3.35). That allows us to define the BC ϕ_+, ϕ_-, ϕ_Q at $z = a^-$ in terms of A_+, A_-, Q at $z = a^+$ according to (7.1), using the usual interface crossing relations. In other words, we must solve BPPE system (7.3), construct A_+, A_-, Q at $z = a^+$ from (7.6), and construct the BC ϕ_+, ϕ_-, ϕ_Q at $z = a^-$ according to the interface-crossing conditions (4.7), (4.8), (4.9).

7.1.4 Relation between RHS nonlinearities

This section intends to present a formal reasoning for the transformation (7.7) presented in previous section.

The algorithm for constructing nonlinearities $\widehat{NL_A}$ and $\widehat{NL_Q}$ is already addressed in section 3.3.2. We will now specify the algorithm for constructing nonlinearities $\widehat{Y}$ and $\widehat{Z}$ for the RHS of BPPE system (7.3) in relation to that algorithm.

Following the algorithm in section 3.3.2, computing nonlinearities $\widehat{NL_A}$ and $\widehat{NL_Q}$ from spectral amplitudes A_+, A_-, Q consists of performing five consecutive steps

$$\begin{matrix}\widehat{NL_A}\,(z, A_+, A_-, Q)\,, \\ \widehat{NL_Q}\,(z, A_+, A_-, Q)\end{matrix} : \qquad \text{steps: } 1. \to 2. \to 3. \to 4. \to 5.$$

Let us now introduce an additional algorithm step

1a. Flip sign of $\widehat{e_2}$ such that

$$\widehat{e_2} \to -\widehat{e_2}.$$

Using the new step, we define the way of computing nonlinearities $\widehat{Y}$ and $\widehat{Z}$ from spectral amplitudes B_+, B_-, R as

$$\begin{matrix}\widehat{Y}\,(\theta, B_+, B_-, R)\,, \\ \widehat{Z}\,(\theta, B_+, B_-, R)\end{matrix} : \qquad \text{steps: } 1. \to 1a. \to 2. \to 3. \to 4. \to 5.$$

This definition is sufficient to implement the RHS nonlinearity of system (7.3) and perform the AST. In the remaining part of this section we formally show how such definition allows to perform the passages in (7.7).

Let us, for convenience, define certain auxiliary transformations using the six

available algorithm steps. We define

$$\begin{aligned} f_{AUX}: &\quad \text{step:} &&\quad 1. \\ f_{YZ}: &\quad \text{steps:} &&\quad 1a. \to 2. \to 3. \to 4. \to 5. \\ f_{AQ}: &\quad \text{steps:} &&\quad 2. \to 3. \to 4. \to 5., \end{aligned} \tag{7.8}$$

and a definition

$$f \overset{def.}{=} f_{AQ} \circ f_{AUX}. \tag{7.9}$$

The arguments of function f_{AUX} are z, A_+, A_-, Q for system (3.35) or θ, B_+, B_-, R for system (7.3). The arguments of f_{YZ} and f_{AQ} are electric field components in spectral domain, constructed from spectral amplitudes in f_{AUX}. We denote by $\widehat{e}$ the electric field constructed from solutions to system (3.35), and by $\widehat{g}$ the electric field constructed from solutions to system (7.3).

With that we write the full dependence of the functions on their arguments for system (3.35)

$$\begin{aligned} f_{AUX} &= f_{AUX}(z, A_+, A_-, Q), \\ f_{YZ} &= f_{YZ}\left(\widehat{e_1}, \widehat{\partial_x e_1}, \widehat{\partial_z e_1}, \widehat{e_2}\right), \\ f_{AQ} &= f_{AQ}\left(\widehat{e_1}, \widehat{\partial_x e_1}, \widehat{\partial_z e_1}, \widehat{e_2}\right), \\ f &= f\left(\widehat{e_1}, \widehat{\partial_x e_1}, \widehat{\partial_z e_1}, \widehat{e_2}\right), \end{aligned}$$

and by analogy we would have (θ, B_+, B_-, R) and $\left(\widehat{g_1}, \widehat{\partial_x g_1}, \widehat{\partial_\theta g_1}, \widehat{g_2}\right)$ arguments for system (7.3). We drop the dependence on $\widehat{\partial_x e_1}$, $\widehat{\partial_z e_1}$, $\widehat{\partial_x g_1}$ and $\widehat{\partial_\theta g_1}$ for the purpose of clarity, and note from (7.8) that

$$f_{YZ}(\widehat{e_1}, \widehat{e_2}) = f_{AQ}(\widehat{e_1}, -\widehat{e_2})$$

due to the introduction of step 1a. in f_{YZ}.

Going back to the RHS nonlinearities, we define them in terms of transformations (7.8) and (7.9) as

$$\begin{aligned} \widehat{NL_A}(z, A_+, A_-, Q) &= f_{AQ}(\widehat{e_1}, \widehat{e_2}) \circ f_{AUX}(z, A_+, A_-, Q) &&= f(\widehat{e_1}, \widehat{e_2}), \\ \widehat{Y}(\theta, B_+, B_-, R) &= f_{YZ}(\widehat{g_1}, \widehat{g_2}) \circ f_{AUX}(\theta, B_+, B_-, R) \\ &= f_{AQ}(\widehat{g_1}, -\widehat{g_2}) \circ f_{AUX}(\theta, B_+, B_-, R) &&= f(\widehat{g_1}, -\widehat{g_2}). \end{aligned} \tag{7.10}$$

By analogy we can perform similar derivations for RHS nonlinearities $\widehat{NL_Q}$ and $\widehat{Z}$. Those relations allow us to perform the reasoning presented in (7.7).

Part II

Model Implementation & Results

8

Implementation

8.1 Environment

The implementation of the BPPE iteration system was done using *Python 3.6* scripting language. *Python* allows for a fast prototype development and offers a wide range of scientific libraries, primarily available in the well-established mathematical tools, such as *Mathematica* or *MATLAB*. All of the core mathematical transformations were performed using built-in libraries, as it is indicated in more detail in section 8.3. In particular *numpy 1.15.1* and *scipy 1.4.1* libraries were used. *numpy* provides support for handling large matrices and performing combined operations on all their elements without the need of iteration, and *scipy* handles scientific computations.

The simulations were performed on MacBook Pro:
CPU: Intel i5 2x2.3 GHz,
RAM: 16 GB DDR4,
Disk: 128 GB SSD,
OS: Linux Ubuntu 18.04 x86_64.

8.2 Complexity alleviation

8.2.1 Rationale & choices

The more dimensions we allow for in the physical setup, the more the complexity of the system grows. In the mathematical model we are considering a two-dimensional slab, where the TM electric field propagates in time. We thus require a three-dimensional grid of discreet points. While the discretization of z may be fairly low in order to reconstruct a reasonably well-behaved field, the discretizations of x and t need to be fairly high in order to accurately represent the signal in the spectral form, using ξ and ω respectively.

In terms of x and t, dismissing z for the moment, we can say that the computational complexity of the problem is proportional to $O(N^a)$, where N is the number of discrete points for a dimension, and a is the number of spatial dimensions. In order to represent frequencies indicated in the scaling section 6.2, we need at least 256 discrete points for each dimension. We see that the complexity of a $x-t$ problem is 256 times bigger than the complexity of a t-problem.

As we established in the testing phase, a t-problem takes between several seconds to several minutes to be solved, depending on the size of nonlinearity coefficient. Estimated simulation time for the simplest of $x-t$ problems is at least 20 minutes, while the more nonlinear ones reaching hours or days.

For this reason we decided to eliminate the x-direction from the model implementation, effectively reducing the slab to a one-dimensional entity, where the electric field wave propagates. Removing x-dependence can also be thought of as considering a two-dimensional slab, which is perfectly uniform in the x-direction, thus no matter which x position is considered, the electric field remains the same. A similar simplification is used in physics when considering a 2D-flow, where *columns* of liquid constitute a physically three-dimensional volume of liquid.

Such choice has its consequences for the particularities of the mathematical model and the representable results. We discuss this issue in section 8.2.2.

The implementation does not take advantage of the parallelization of operations. This is due to the specifics of Kerr nonlinearity and it is addressed further in section 8.3.2.

8.2.2 Adaptations to mathematical model

The mathematical model presented in the first part of this paper is a general derivation, which applies also to the simplified case with x-dimension removed. The entire reasoning can be repeated, and the derivations can be re-done simply by removing the dependence on x and ξ variables. We do not repeat the derivation process, but we state the resulting most fundamental formulas for completeness.

Dispersion relation

$$\beta(\omega) = \pm\frac{\omega}{c}n(\omega).$$

As indicated in section 8.3.4, numerical computations are performed only for the positive ω-range. The spectral amplitudes for the negative ω-range are reconstructed based on the condition for physical solution, (3.24).

Solutions in terms of normal modes expansions

Electric field components and their respective FT's are

$$e_1(z,t) = \frac{1}{\sqrt{2\pi}}\int_{-\infty}^{+\infty} d\omega \overbrace{\left\{A_+e^{i\beta z} + A_-e^{-i\beta z}\right\}}^{\widehat{e_1}(z,\omega)} e^{-i\omega t}, \tag{8.1}$$

$$e_2(z,t) = \frac{1}{\sqrt{2\pi}}\int_{-\infty}^{+\infty} d\omega \underbrace{\{Q\}}_{\widehat{e_2}(z,\omega)} e^{-i\omega t}. \tag{8.2}$$

BPPE system

The BPPE differential system is

$$\begin{aligned} 2i\beta\partial_z A_+ e^{i\beta z} &= \widehat{NL_A}, \\ -2i\beta\partial_z A_- e^{-i\beta z} &= \widehat{NL_A}, \\ \partial_z Q &= \widehat{NL_Q}, \end{aligned}$$

with nonlinearities

$$\widehat{NL_A} = -\frac{\beta^2(\omega)}{n^2(\omega)}\widehat{p_1}, \tag{8.3}$$

$$\widehat{NL_Q} = -\frac{1}{n^2(\omega)}\partial_z\widehat{p_2}, \tag{8.4}$$

where we have used the new dispersion relation $\beta(\omega)$ to simplify $\widehat{NL_Q}$.

Interface transition

The nonlinear system of three dependent equations describing the interface crossing becomes

$$\begin{aligned} &A_+\left(a^+,\omega\right)e^{i\beta_1 z}+A_-\left(a^+,\omega\right)e^{-i\beta_1 z}\\ &=A_+\left(a^-,\omega\right)e^{i\beta_0 z}+A_-\left(a^-,\omega\right)e^{-i\beta_0 z},\end{aligned}$$

$$\begin{aligned} &n_1^2(\omega)Q\left(a^+,\omega\right)+\widehat{p_2}\left(a^+,\omega\right)\\ &=n_0^2(\omega)\,Q\left(a^-,\omega\right)+\widehat{p_2}\left(a^-,\omega\right),\end{aligned}$$

$$\begin{aligned} &\beta_1\left[A_+\left(a^+,\omega\right)e^{i\beta_1 z}-A_-\left(a^+,\omega\right)e^{-i\beta_1 z}\right],\\ &=\beta_0^2\left[A_+\left(a^-,\omega\right)e^{i\beta_0 z}-A_-\left(a^-,\omega\right)e^{-i\beta_0 z}\right].\end{aligned}$$

It is important to note that the above system is decoupled between the modes A_+, A_- and the Q-mode, and the nonlinearity appears only in the condition for Q. That allows us to solve a *linear* system of the first and the third equation, and then compute Q through iterative root-finding process.

It is also worth noting that the second interface crossing condition has simplified to exactly the same form as the Q-solvability condition has. That explicitly shows that there is no difference between crossing the interface with Q, and computing Q itself, in order to guarantee a physical solution. The interfaces do not exist as far as Q-mode is concerned. In practical terms, whenever a recalculation of Q is needed due to the modification of A_-, this is already handled by the act of crossing the interface.

Scaling

Due to reducing FT to integration only in $\omega - t$, the scaling factors $\frac{1}{x_0}$ and $\frac{1}{z_0}$ are eliminated. The dimensions of the resulting electric field dimensional constants are

$$e_{10}=\omega_0 A_0, \qquad e_{20}=\omega_0 Q_0.$$

We expect the dimension of electric field in both directions to be the same

$$e_{10}=e_{20} \qquad \Rightarrow \qquad Q_0=A_0.$$

Unlike before, we obtained the same dimensions for the amplitudes of all the modes. We remind that in the general case we had

$$Q_0 = \frac{A_0}{x_0}.$$

The difference between those two cases is a reflection of something more profound. In the general case it is possible to *focus* the laser beam into a particular region of x-axis, and the magnitude of Q depends largely on how small that region is. In the simplified case the system is uniform in x-direction, and no focusing is possible. The scale of Q is the same as it is of A_+ or A_-. As we show next, consequences for the Q mode are even more radical.

Q-solvability condition

The solvability condition for Q remains unchanged, but due to a new dispersion relation it can be further simplified into

$$Q(z,\omega) = -\frac{1}{n^2(\omega)}\widehat{p_2}\,(z,\omega)\,.$$

However, to fully understand the consequences of the simplified case for the Q-mode, we need to find the possible solutions to this condition. Using simplified $\widehat{e_2}$ we rewrite (8.2.2) as

$$\widehat{e_2}(z,\omega) + \frac{1}{n^2(\omega)}\widehat{p_2}\,(z,\omega) = 0.$$

As shown in the scaling section 6.2, the refractive index for the ω-range under consideration can be approximated with a constant. Taking the IFT of the above equation and using $n(\omega) \longrightarrow n \sim const.$ we get

$$\begin{gathered}
\mathcal{F}^{-1}\left\{\widehat{e_2} + \frac{1}{n^2}\widehat{p_2}\right\} = \mathcal{F}^{-1}\{0\} \\
\Downarrow \\
e_2 + \frac{1}{n^2}p_2 = 0 \\
\Downarrow \\
e_2 + \frac{1}{n^2}\eta\left(e_1^2 + e_2^2\right)e_2 = 0 \\
\Downarrow \\
e_2\left[\left(1 + \frac{\eta}{n^2}e_1^2\right) + \frac{\eta}{n^2}e_2^2\right] = 0.
\end{gathered}$$

The above equation has a solution when either $e_2 = 0 \Rightarrow Q = 0$ or

$$\left(1 + \frac{\eta}{n^2}e_1^2\right) + \frac{\eta}{n^2}e_2^2 = 0.$$

We recall that e_1 does not depend on Q, it only depends on A_+ and A_-, which are already known at the time of solving the solvability condition. Thus, with known e_1, we rewrite the above expression as an explicit formula for e_2, from which Q is computed by taking FT

$$e_2^2 = -\left(\frac{\eta}{n^2} + e_1^2\right) < 0.$$

Since the expression in parenthesis is always positive, we obtain that for a non-zero solutions to exist we have to have

$$e_2^2 < 0,$$

meaning that e_2 would have to be purely imaginary. This is not a solution we can accept as physical, and therefore the only solution to the solvability condition in the simplified case is $Q = 0 \Rightarrow e_2 = 0$.

As disappointing as it might be, we are not expecting the Q-mode to arise from our simulations. Nevertheless, we will include the amplitude of the longitudinal mode in our implementation in order to observe that it indeed is solved as zero.

The restrictions to the simulation setup mean that we can only simulate a perpendicular angle of incidence with respect to the interface, and we loose variability along x-direction. That results in the absence of e_2 component of the electric field.

8.3 Particularities

8.3.1 Discretization resolution

We allow the discretization of the z-domain to be chosen dynamically by the ODE solver, depending on the rate of change of function, which in practical terms depends on the size of the nonlinearity. As observed during the testing phase, the number of discrete points ranges from a couple to couple of tens for a reasonable size nonlinearity.

The solver used for solving the BPPE differential system is *scipy.integrate.solve_ivp* with explicit Runge-Kutta method of order 5(4) (*RK45*). For performing integration *scipy.integrate.simps* method is used. It performs integration according to Simpson's trapezoidal rule.

For the temporal and spectral resolution we use a fixed number of points required to represent signal oscillation. We establish the number of points in

ω-domain in order to achieve sufficient sampling frequency, and apply the same discretization to the t-domain. The module performing the FT maintains the same discretization when transforming between the two domains. More details regarding the implementation of FT are presented in section 8.3.4.

8.3.2 Spectral nonlinearity

The RHS of the BPPE system involves computing nonlinear polarization terms with each iteration. This is done in analogy to the algorithm presented in section 3.3.2, using the analogical equations for the simplified system. The FT and IFT are taken only in t and ω respectively.

The presence of nonlinearity impacts greatly the possibilities of parallelization of the implementation. It is due to the emergence of new, tripled frequencies in case of Kerr nonlinearity. For a linear case, a system of three BPPE equations for each discrete value of ω could be solved separately, as there would be no interdependence between different frequencies. Such a system is easily parallelizable, into what is called an *embarrassingly parallel problem*.

The presence of nonlinearity requires that all discrete ω's are involved at once, such that a FT (or IFT) can be performed across the entire domain. During that transformation a *mixing* of spectral amplitudes occurs between different ω's. Parallelization of such system is non-trivial to say the least. One could envision a way of decoupling certain frequencies from one another, or devising an algorithm for passing results between smaller sub-tasks. Whether such solution would get a performance boost, considering all the overheads, requires further pondering. For that reason, the implementation performed for the purpose of this thesis is strictly sequential.

8.3.3 Fixed-point iteration

All the nonlinear problems in the implementation are solved using Newton's iterative root-finding algorithm implemented by *scipy.optimize.newton* method. The function whose root is searched is a single iteration of the BPPE iterative process. Since a derivative of such function cannot be provided, a secant method is used, with sub-quadratic convergence[1]. In the testing phase it was confirmed that convergence within a given relative tolerance is obtained for all the discrete points, and within a reasonable number of iterations and processing

1. Following the documentation, for a well-behaved function with quadratic convergence the actual error in the estimated zero after the n-th iteration is approximately the square of the error after the (n-1)-th step.

time.

Different root finding methods were also tested, namely *scipy.optimize.root* with its plethora of available methods, *scipy.optimize.fixed_point*, as well as a naive iteration scheme. None of those methods shown to surpass the Newton's-method implementation, either due to longer processing time or the inability to find the root in the first place. Some of the methods were comparable though.

The Newton's iteration was used to perform the BPPE iterative shooting and solving Q solvability condition. For BPPE iteration the starting guess for the Newton's iteration is obtained from solving equivalent linear BPPE problem. With that we experienced the iterative process to always converge.

For the Q solvability condition also the *scipy.optimize.fsolve* method was tested. Interestingly enough, for that method the obtained solution to Q was a perfect zero, while for the Newton's method implementation it was a negligible noise around zero. We have maintained the Newton's noisy solution to Q in order to demonstrate better that it indeed is computed through iteration.

8.3.4 Fast Fourier Transform

Handling incompatible conventions

Computing FTs is done using methods from *numpy.fft* module, which implements Fast Fourier Transform (FFT) algorithms. However, the FT conventions used by the library differ from the ones presented in Appendix A and used in the derivations in this document. Namely, they are[2]

$$\text{FT:} \qquad \widehat{f}(\omega) = \int_{-\infty}^{+\infty} dt\ f(t)\, e^{-i\omega t}$$

$$\text{IFT:} \qquad f(t) = \frac{1}{2\pi} \int_{-\infty}^{+\infty} d\omega\ \widehat{f}(\omega)\, e^{i\omega t}.$$

For the FT in $t - w$ the above convention differs both by the normalization coefficient in front of the integrals and by the sign of the exponents. That is crucial for distinguishing the left- and right-traveling modes.

Let us consider equation (3.23), where the electric field is expressed in terms of the normal modes. In order to determine the direction of travel of the modes we consider the sign of the exponent. The exponentials in the normal modes

2. following the documentation of Discrete Fourier Transform (DFT) conventions for *numpy.fft* module.

are

$$e^{ikz}e^{\xi x-\omega t}.$$

Let us consider the exponential standing by A_+, thus $k = +\beta > 0$. In such case, for an increasing time t the wave *travels* to the right, since the minus sign in $-\omega t$ introduces a time delay. For $k = -\beta < 0$, which is the case for the exponential by A_-, we have that the wave travels to the left if time t increases. It is the *minus* sign by ωt that inspires such interpretation. Since the FT exponent sign is different in our model and the *numpy.fft* library conventions, the interpretation of which modes are traveling in which directions is the opposite.

In order to align this, we swap the forward and backward FT's that we use in the implementation. That means that for performing a forward FT in our model we can use an Inverse Fast Fourier Transform (IFFT) implementation *numpy.fft.ifft*. Similarly, for performing IFT in the model we can use forward FFT implementation *numpy.fft.fft*.

Making use of the real signal

However, we take our adaptations one step further. Since we model all the temporal signals to be real, namely the electric field $\boldsymbol{e}$, we know that their respective FT's are Hermitian.[3] That allows us to cut by half the ω domain in which the calculations are performed, maintaining only the positive frequencies, and abandoning the negative ones. This is because the spectral amplitudes for the negative frequencies can be fully reconstructed from the positive-frequency amplitudes. Under such regime the IFT function accepts only a signal which is Hermitian (complex), in order to reconstruct a signal that is real.

For such handling *numpy.fft* provides *rfft* and *irfft* functions. However, since we have to use reverse-convention functions in order to account for the direction of travel, we would need to use *rfft* to perform the backward transform. That is not possible, since since *rfft* accepts only real input, while the spectral amplitudes in our model are complex. Therefore, we use yet another pair of *numpy.fft* methods, namely *ihfft* and *hfft* for performing the FT and IFT respectively. Those two methods have similar but opposite expectation about the input signal. The temporal signal is expected to be Hermitian (complex), and the spectral signal, input to inverse transform, is expected to be real. It suits our needs of reversed-convention perfectly, because we can use the inverse transform implementation *ihfft* in order to perform a FT on our real temporal signal. By analogy we use *hfft*, which expects Hermitian, to perform IFT on the spectral signal.

3. meaning that the component at discrete frequency ω_i is the complex conjugate of the component at frequency $-\omega_i$

As complicated as it might sound, the following three methods are used

- *numpy.fft.ihfft* for performing FT,
- *numpy.fft.hfft* for performing IFT,
- *numpy.fft.rfftfreq* for obtaining discretization of ω-domain for non-negative frequencies only.

Normalization coefficient

Using the same library for all FT-related transformations ensures maintaining consistency between the forward and the inverse FTs, and the correct handling of the normalization coefficient. We accept that due to the difference in the normalization coefficient the spectral amplitudes are scaled differently in the implementation than in our model by a factor of $\frac{1}{\sqrt{2\pi}}$. This does not affect the testing or the final solution of the electric field amplitude, because consistency is maintained.

In Appendix B we indicate a particular FT convention that allows for aligning the derivation of the refractive index with the one most common in optics, and applying the $n(\omega)$ model presented in section 2.4. The convention provided through using *numpy.fft* module is *that* named convention.

9 Results

The first section of this chapter is a user manual of sorts, intended to answer any doubts one might have about what the simulation plots actually present. We address the scope of testing and simulation, introduce conventions and configuration used, and cover the topics of how the initialization of AST is done, and how performing the tests is combined with simulating real-life problems.

In the case-study section 9.2 we present both the solutions to certain scatter-problems, as well as the comparison against the reference results obtained from the AST method.

9.1 Presentation approach

9.1.1 AST initialization

What you sow is what you reap

For a better visualization of the narrative of this section we recall Figure 7.1, which intends to encompass the idea behind the AST in a single image.

The AST method presented in Chapter 7 can be initialized with an arbitrary Ψ BC. Clearly, depending on the choice of that BC, the corresponding scatter

problem for which the artificial source is generated resembles an actual physical problem to a different extent. Our aim is to choose such a Ψ BC that the corresponding scatter problem is *realistic*. We now explain how we achieve that.

As shown earlier, there is a correspondence between the B_+, B_-, R and A_+, A_-, Q problems. One can think of propagating B_+, B_-, R once as corresponding to iteratively shooting in reverse direction to get A_+, A_-, Q. We use this correspondence to generate an AST reference for the particular scatter problem that is of interest to us. We use the object under test to initialize an independent testing procedure.

In short, we solve the problem of interest, then we use it to initialize the AST, and then we use the AST to generate a BC for a problem that is very close to the original problem of interest. More systematically, the procedure is performed as indicated below.

AST initialization and testing procedure:

1. Choose a scatter problem of interest, and solve it using BPPE shooting method. As a result, spectral amplitudes inside the slab and on the interfaces are obtained. Collect the transmission state Ψ_+, Ψ_-, Ψ_Q right outside the slab at $z = b^+$.

2. Surely, the Ψ_+, Ψ_-, Ψ_Q state is not an exact representation of the physical state, due to numerical errors and any accuracy limitations of the BPPE method. How much Ψ_+ is distorted is uncertain, but it is known that Ψ_- should be exactly zero, due to no light sources from $+\infty$. Thus, enforce $\Psi_- = 0$, $\Psi_Q = 0$, and together with Ψ_+ use it as the Ψ BC for initializing the AST.

3. Perform the AST generation. This propagates the Ψ BC to the other side of the slab, yielding Φ BC state at $z = a^-$.

4. Construct the input for the new scatter problem, using Φ_+ from point 3. as the incoming laser beam, and zero for both Φ_- and Φ_Q. Solve the scatter problem and compare the results against the ones generated by the AST B_+, B_-, R propagation.

What is immediately apparent here, is that we take the effort to solve almost the same scatter problem[1] twice in order to obtain the reference and the

1. the two scatter problems are very similar due to only minor modification of Ψ_-

iterated results. For the chosen test cases this is not a big computational effort though. We do not compare the results of the first scatter problem against the AST reference for reasons of diligence, and in order to follow the principles of artificial source testing.

We note also that we do not use the left-traveling wave generated by the AST to initialize the Φ_- input for the scatter problem. We set $\Phi_- = 0$, as it would normally be done when solving a scatter problem without the AST involved. This way allows us to verify that the iterative process converges with initial guess for the reflected beam being zero.

The gain discussion

Choosing a physical[2] BC for the first scatter problem guarantees that the second scatter problem simulates a physical system to as much extent as reasonably possible, which we consider a desirable thing. Of course, had we known what the distortion of Ψ_+ is, we could also eliminate it in order to generate an even more realistic reference.

In our simplified case, crossing the interface is a purely linear step, and it does not cause the magnitudes at the $3\omega_c$ range to increase due to Kerr effect. Thus for a Gaussian BC, the nonlinear polarization effect is initially non-existing, and it builds up as the mode propagates through the slab from $z = a$ to $z = b$. After crossing the second interface, the outgoing Ψ at $z = b^+$ is not a perfect Gaussian any more, but has this *bulge* of higher amplitudes in the $3\omega_c$ range, as depicted in Figure 9.1. This is representative of a physical phenomenon of propagation of light through a nonlinear medium. This Ψ is used to initialize AST according to the procedure above.

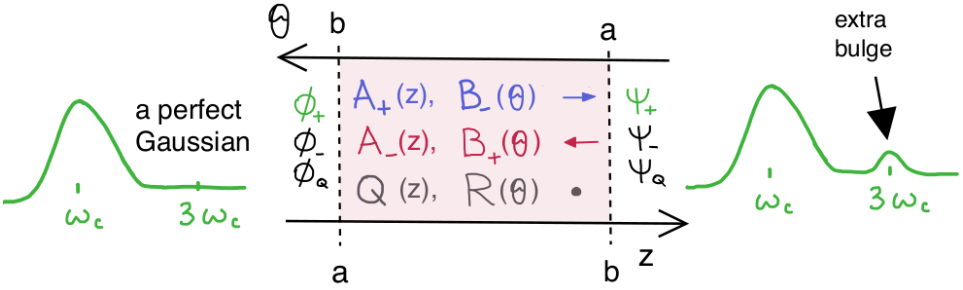

Figure 9.1: Relation between Φ and Ψ states on the two sides of the slab.

If we instead chose to initialize the AST with a perfect Gaussian, not *enriched*

2. one that models a physical laser pulse, e.g. a Gaussian curve

with any higher amplitudes in the $3\omega_c$ range, then propagating B_+, B_-, R effectively backwards, from $z = b$ to $z = a$, might naturally develop those amplitudes. The nonlinear polarization effect in the system would grow from $z = b$ to $z = a$. The state Φ at $z = a^-$ would have a *bulge* of amplitudes in the $3\omega_c$ range. Since Φ is used as BC for the scatter problem under test, we would construct a simulation case where the nonlinear polarization effect dies-off instead of building-up due to passing through the slab. In other words, the input lase pulse would have such a *bulge* of spectral amplitudes in the $3\omega_c$ range, that by passing through the slab and interacting with its material would get *exactly* canceled out, and produce a perfect Gaussian at the other end of the slab, at $z = b^+$. While physically conceivable, this case is quite unlikely to be pursued in the experiments.

For that reason we choose to follow the initialization procedure presented above to generate the reference and iterated results.

9.1.2 Scope of simulations

η nonlinearity factor

What we consider of the biggest interest is the impact of the nonlinear polarization coefficient η on the shape of spectral amplitudes. We present simulation results for two different values of η':

- $\eta' = 1.97 \cdot 10^{-4}$, as resulted from scaling and presented in Table 6.2,
- $\eta' = 5.97 \cdot 10^{-2}$, increased $\sim$ 300-fold with respect to the first choice.

Following equation (6.14), increasing η corresponds to increasing the nonlinear refractive index n_2, and thus changing the properties of the material.

This choice of increasing η' by two orders of magnitude was made in the experimentation phase. Such factor is big enough to demonstrate the Kerr effect clearly, while it is still small enough to not overload the system.

Solution grid

The spectral and temporal state of the system is presented right before the pulse enters the slab at $z = a^-$, right after it goes out of the slab at $z = b^+$, and for certain points inside the slab.

The comparison with the AST reference is made at both faces of both interfaces,

Plot element	Description
Φ_+, Φ_-, Φ_Q, A_+, A_-, Q, Ψ_+, Ψ_-, Ψ_Q	Spectral amplitudes solutions: · at $z = a^-$, right before entering the slab, · inside the slab, · at $z = b^+$, right after exiting the slab.
Re$\{\cdot\}$, Im$\{\cdot\}$	Real and imaginary parts of complex spectral amplitudes.
e_1, e_2	Electric field components, in z and x direction respectively.
reference / iterated	Reference results generated by AST / Scatter results from BPPE iterative shooting.
$z =$	z-coordinate for which the result is presented, e.g. $z = 0$ indicates the first interface.
(inside) / (outside)	A redundant[4]indication of whether the presented state is on the inside or outside of the slab. Maintained for easier orientation.
$\lvert \cdot \rvert$	Denotes absolute value of a complex argument ·, or an envelope of a real signal, computed with *numpy.abs(scipy.signal.hilbert(·))*

Table 9.1: Plotting conventions.

effectively in the four points: $z = a^-$, $z = a^+$, $z = b^-$, $z = b^+$. This is due to the fact that the z-grid where the solution is available inside the slab is dynamically chosen by the ODE solver. As a result, the z-grids of the reference and the iterated solutions are different in the majority of simulations. Nevertheless, through the analysis of the test results we concluded that cross-referencing only at the interface points is representative of the overall accuracy of the method.

9.1.3 Conventions

Table 9.1 presents the conventions used on the plots. We note also that:

- Both the spectral amplitudes solutions and the reconstructed temporal electric field components are presented.
- All quantities are dimensionless. In order to obtain the physical unit and scale the values indicated along the axes ought to be scaled according to Table 6.2.
- The ω' range presented in the spectral plots is wide enough to include the $3\omega'_c$ frequencies, with enough margin from the peak amplitude.

4. names of spectral amplitudes Φ, Ψ and A or Q already indicate that

- Cubic interpolation is used for connecting the discrete solution points.

9.1.4 Configuration

Configuration follows Table 6.2 and the scaling sections 6.2, 6.3, except for the increased value of η' in the second study case. Additionally, we set the propagation-time and slab-length parameters as presented in the first part of Table 9.2.

Dimensionless parameter	**Symbol & formula**	**Value**
group velocity at ω_c'	$v_g' = c'/n(\omega_c')$	2.07
propagation time	t_p'	66
start time	$-\frac{1}{6}t_p'$	−11
stop time	$+\frac{5}{6}t_p'$	+55
nr slab lengths	s	4
slab start point	z_a	0
slab end point (=slab length)	$z_b = v_g' t_p'/s$	34
Discretization status		
nr discrete points for t-domain and ω-domain	N	256
sampling time interval	dt	0.26
sampling frequency	ω_s'	24.28
folding frequency	ω_{max}'	12.14

Table 9.2: Common configuration setup.

For a given propagation time and group velocity, we choose the slab length to be such that the light pulse travels an exact, predefined number of slab lengths s. This allows us to control the number of reflections from the interfaces that we wish to see in the simulation results. In the second section of the table we present the resulting sampling and folding frequency values.

We choose a negative start time of the simulation, such that the peak of the input pulse arrives at the first interface z_a at time $t = 0$. Under this setup the pulse arrives at each interface two times.

With such common configuration the two presented study cases differ only by the order of magnitude of the nonlinearity coefficient η'.

9.2 Case study

We present here the results of experiments, following the approach presented in section 9.1.

9.2.1 Case 1: ordinary nonlinearity

Nonlinearity coefficient in slab, and in vacuum outside of the slab:
$\eta' = 1.97 \cdot 10^{-4}$.

Table 9.3 shows the statistics from the simulation run.

Convergence	
Homogeneous problem:	9 iterations, 256/256[5]points converged.
Full problem:	13 iterations, 256/256 points converged.
Electric field (e1) discrepancies at z=0	
Max magnitude error:	$5e-04$ (0.068% of peak magnitude).
Avg magnitude error:	$7e-05$ (0.009% of peak magnitude).
Electric field (e1) discrepancies at z=34	
Max magnitude error:	$5e-04$ (0.055% of peak magnitude).
Avg magnitude error:	$5e-05$ (0.006% of peak magnitude).

Table 9.3: Case 1 statistics.

Figures 9.2, 9.3, 9.4, 9.5 present the spectral amplitude solutions on both sides of the two interfaces, one figure per each interface face. Different modes are presented in rows, *Re* and *Im* parts of each mode are in different columns.

The state of Ψ_- in Figure 9.5 indicates the level of accuracy obtained with this implementation of the BPPE method. The solution diverges from perfect zero by about $2 \cdot 10^{-5}$.

The obtained amplitudes of the transversely-traveling modes, Φ_Q, Q, Ψ_Q, are of the order of magnitude of numerical noise, $O(10^{-26})$. That confirms the theoretical findings of section 8.2.2, stating that the Q-mode is zero if the system is uniform in x-direction. For that reason, and for clarity of the presentation, we do not include the plots of the Q mode or the e_2 component, which is purely dependent on Q and thus equal to zero as well.

5. The positive ω spectrum for which solution is computed has 128 discrete points, but for each of them convergence of Re and Im parts is traced separately.

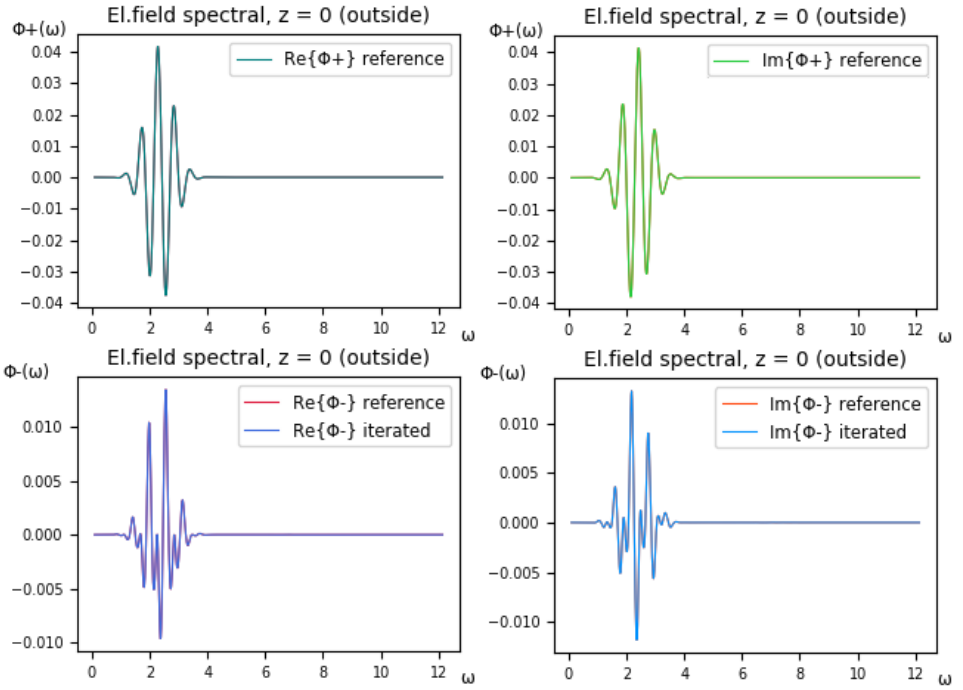

Figure 9.2: Case 1: Spectral amplitudes solutions at the first interface, on the outside of the slab.

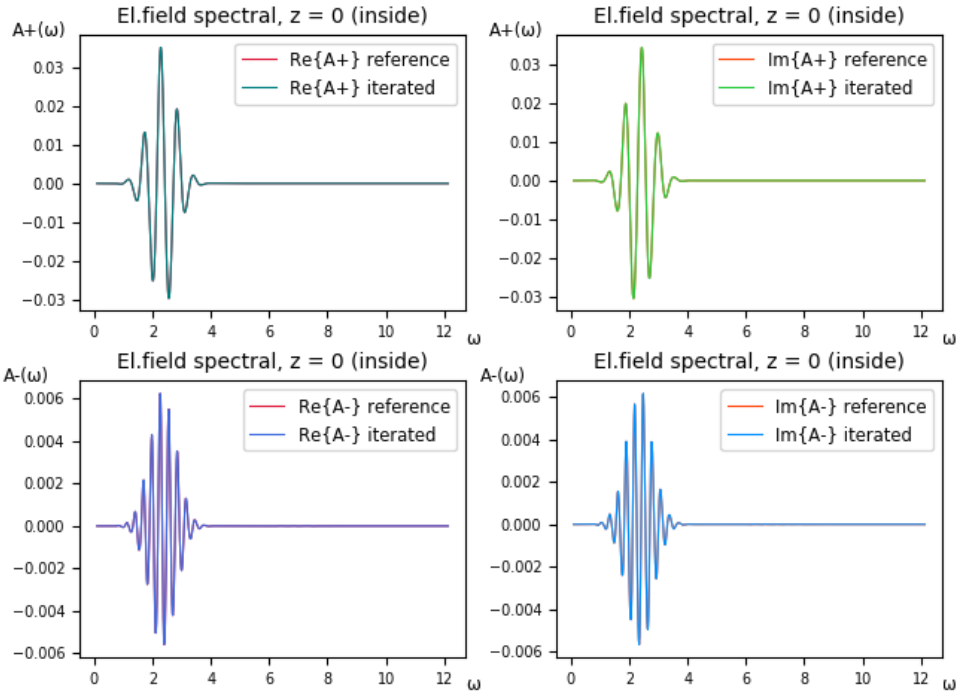

Figure 9.3: Case 1: Spectral amplitudes solutions at the first interface, on the inside of the slab.

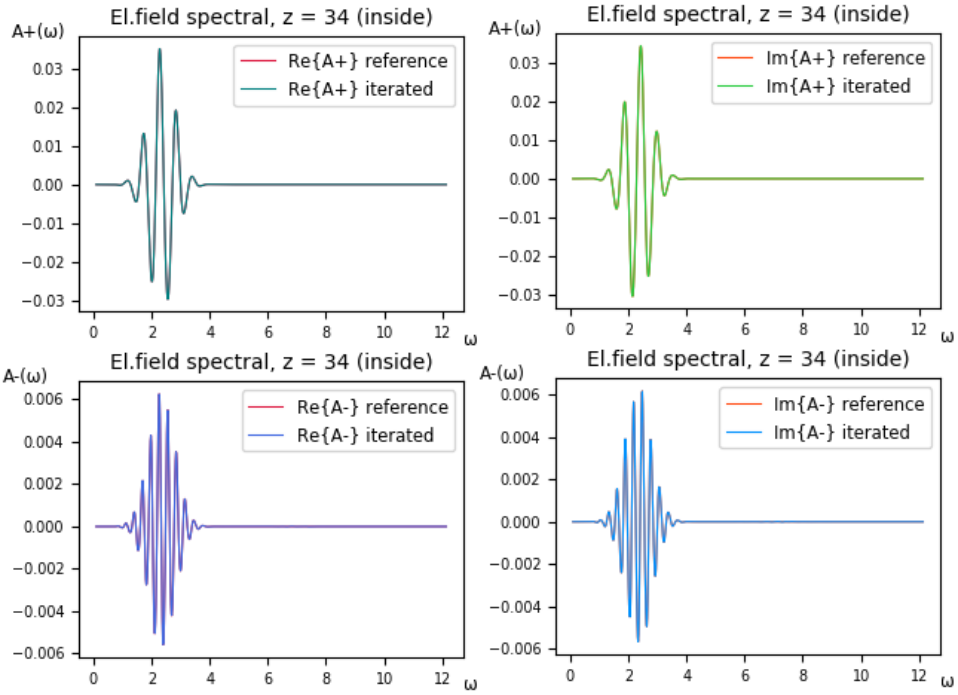

Figure 9.4: Case 1: Spectral amplitudes solutions at the second interface, on the inside of the slab.

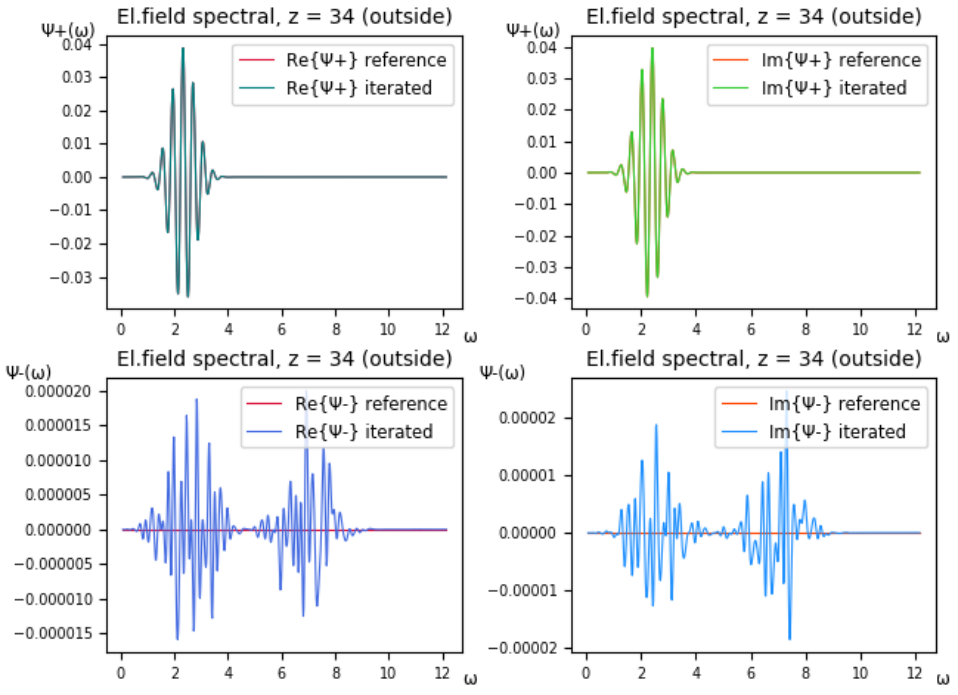

Figure 9.5: Case 1: Spectral amplitudes solutions at the second interface, on the outside of the slab.

Comparing the state at both interfaces we notice that the spectrum changes only very little by going through the slab and the interfaces. The Kerr effect in this study-case is negligible. For a closer look on the emergence of the Kerr effect in this case, in Figures 9.6 and 9.7 we present a zoom on the $3\omega_c'$ range at the same four interface face-points. Only the *Re* part of the complex amplitudes is presented. The scale of the zoom plots is aligned.

At both interfaces the right-traveling mode follows the reference better than the left-traveling mode. At the second interface the left traveling mode struggles to align to a perfect zero, which affects also the accuracy of the right-traveling mode, since both modes are coupled.

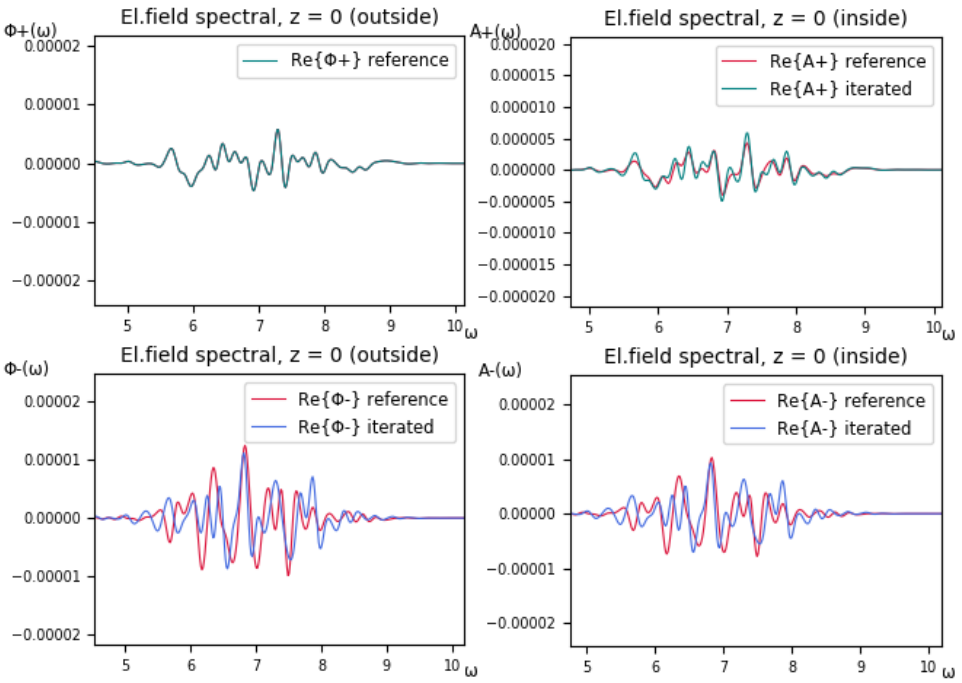

Figure 9.6: Case 1: Spectral amplitudes solutions at the first interface, zoom on Kerr-affected $3\omega_c'$ range.

In Figure 9.8 we present the state of the reconstructed electric field at the two interfaces, only inside the slab. Figure 9.9 shows a zoom on regions between the pulse peaks.

The electric field is reconstructed according to the reference, with the biggest discrepancies between the peak amplitudes. There, the electric field experiences fluctuations, presumably caused by the Kerr effect. The BPPE method implementation has been able to find the prevalent oscillation pattern, but not follow the fluctuations exactly. The discrepancies are $O(10^{-4})$, while the peak magnitude is $O(1)$.

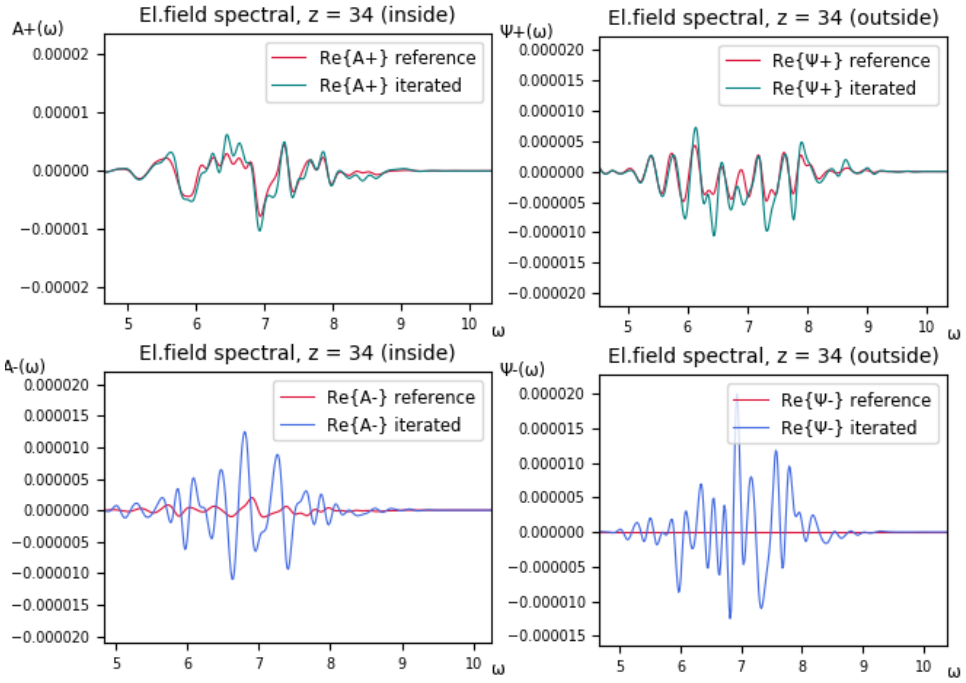

Figure 9.7: Case 1: Spectral amplitudes solutions at the second interface, zoom on Kerr-affected $3\omega_c'$ range.

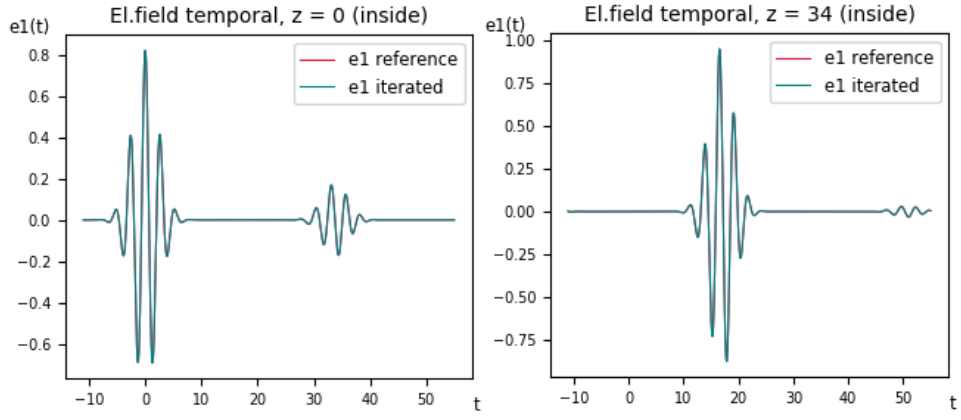

Figure 9.8: Case 1: Electric field solutions at both interfaces.

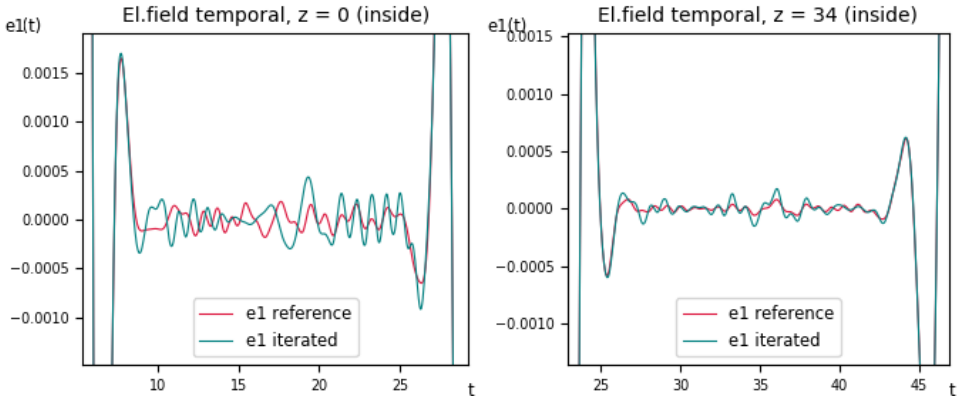

Figure 9.9: Case 1: Electric field solutions at both interfaces, zoom between field peaks.

9.2.2 Case 2: increased nonlinearity

Nonlinearity coefficient in slab, and in vacuum outside of the slab:
$\eta' = 5.97 \cdot 10^{-2}$.

Table 9.4 shows the statistics from the simulation run.

Convergence	
Homogeneous problem:	81 iterations, 256/256 points converged.
Full problem:	268 iterations, 256/256 points converged.
Electric field (e1) discrepancies at z=0	
Max magnitude error:	$1e-02$ (1.458% of peak magnitude).
Avg magnitude error:	$1e-03$ (0.165% of peak magnitude).
Electric field (e1) discrepancies at z=34	
Max magnitude error:	$6e-03$ (0.606% of peak magnitude).
Avg magnitude error:	$1e-03$ (0.110% of peak magnitude).

Table 9.4: Case 2 statistics.

Increasing the nonlinearity factor by two orders of magnitude resulted in a similar increase of the discrepancies of the reconstructed electric field between the AST reference and the iterated solution.

Since the main propagation pattern remains the same, for this case we present only the essential elements linked to Kerr effect boosting. Figure 9.10 presents the spectral amplitudes. Consecutive rows present the state at further points along the z-axis. Right- and left-traveling modes are presented in separate

columns.

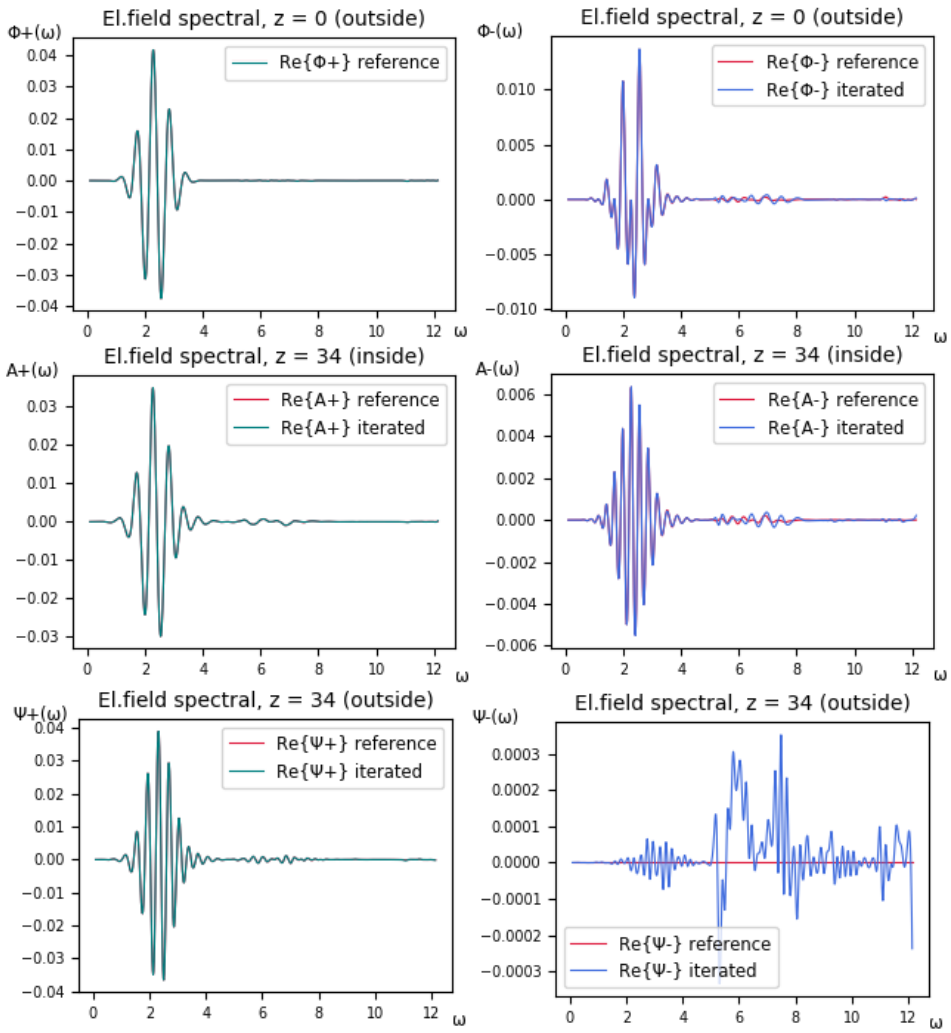

Figure 9.10: Case 2: Spectral amplitudes solutions at both interfaces.

Even without zooming in, the increased amplitude of the frequencies at $3\omega_c' \approx 7$ range is clearly visible. As already observed for Case 1, the right-traveling mode follows its reference much more closely than the left-traveling mode, which diverges notably in the $3\omega_c'$ range. We go back to this observation in the discussion Chapter 10.

The extent of the discrepancies is best visible in the bottom-right plot of Figure 9.10. Ψ_- discrepancies reach $3 \cdot 10^{-4}$.

Figure 9.11 presents the temporal electric field. We note the arising of oscillations at higher frequencies, presumably from the $3\omega_c'$ range. Those oscillations

are of relatively small amplitude on top of the main oscillation pattern.

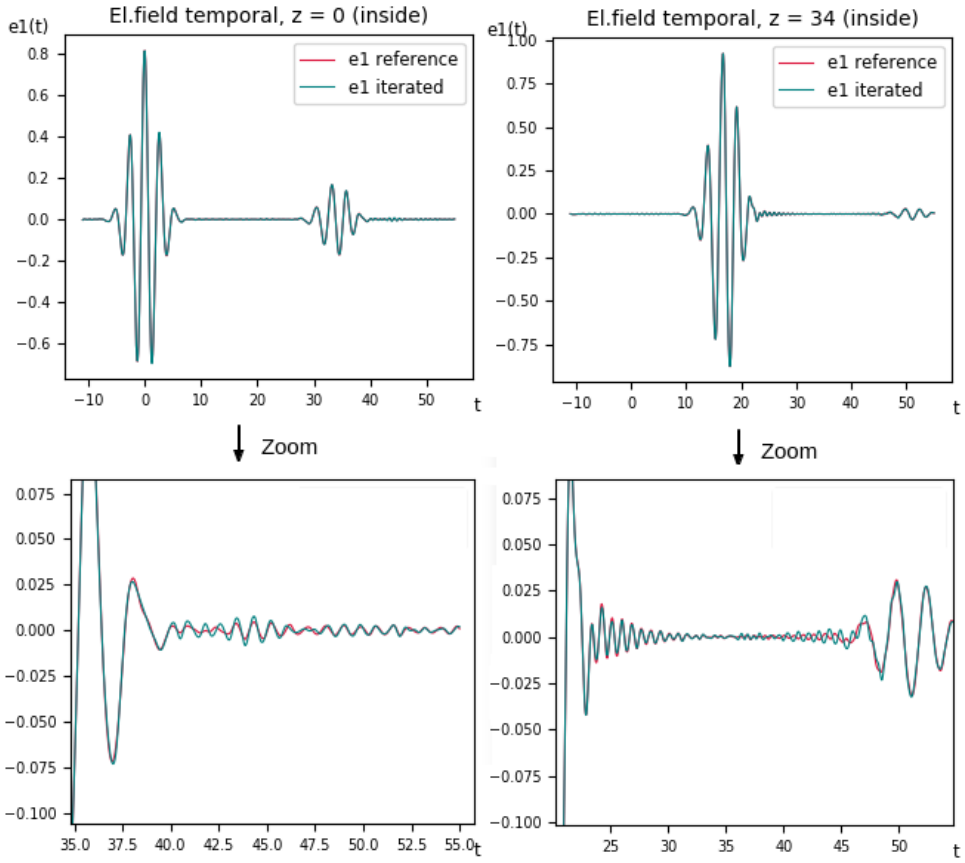

Figure 9.11: Case 2: Electric field solutions at both interfaces.

9.2.3 Bird's-eye view

Last but not least, we present the *entire* state of the system in the slab at once, through a series of quasi-3D plots. The entire slab length falls along the horizontal axis, and the temporal or spectral domain along the vertical axis. Color-coding marks the magnitude of the electric field for each point in the 2D-plane. The configuration follows the high-nonlinearity Case 2.

The plots are generated by solving a scatter-problem directly, not by solving an AST. In a scatter problem we initialize the input pulse as a perfect Gaussian. If we generated the input Φ in the AST regime, it would be a slightly distorted Gaussian, due to the accumulation of numerical errors. We observed that this high-nonlinearity case is already quite sensitive to changes in the BC, and we do not wish to introduce even more noise to it. The 3D plots show certain

emergent structures, which are the more apparent the less noise there is in the system to begin with.

Figure 9.12 shows the magnitude of the temporal electric field. The vertical lines mark the discrete z-points, for which the solution to the BPPE system was found. The Kerr effect is not visible on this plot, but we clearly see how the laser pulse propagates through the slab in time. The first leg, with the highest amplitude, is the initial input pulse propagating through the slab, from $z = 0$ to $z = 34$. Each next leg is a reflected pulse. It is clear how the amplitude quickly diminishes, meaning that the most of the energy of the pulse goes right through the slab, and only about a tenth of it gets reflected from the interface.

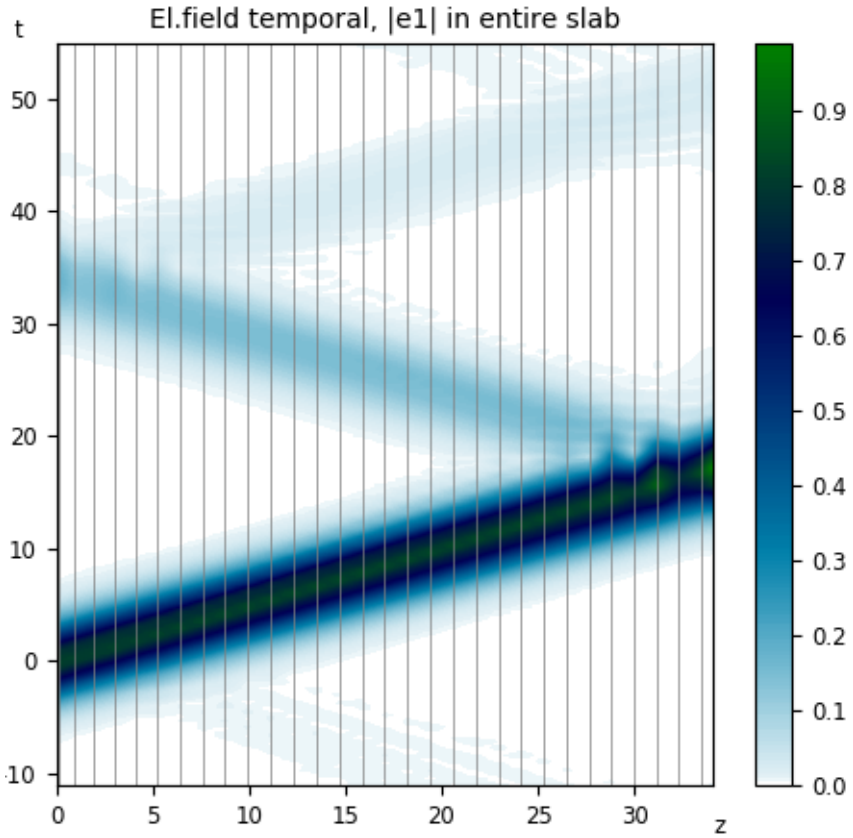

Figure 9.12: Case 2: Electric field solution in the entire slab.

Figure 9.13 presents spectral magnitudes by analogy. We see a relatively strong magnitude around the main frequency $\omega_c' = 2.35$, which does not change noticeably when the wave propagates through the slab.

For the Kerr-excited frequency range, around $3\omega_c' \approx 7$, we se a faint pattern, too week to appreciate in that context. Therefore, we present a zoom on the

$3\omega_c'$ range in Figure 9.14. A new magnitude color-bar is set in order to expose the emerging pattern better. We come back to analyzing those two 3D spectral plots in the discussion Chapter 10.

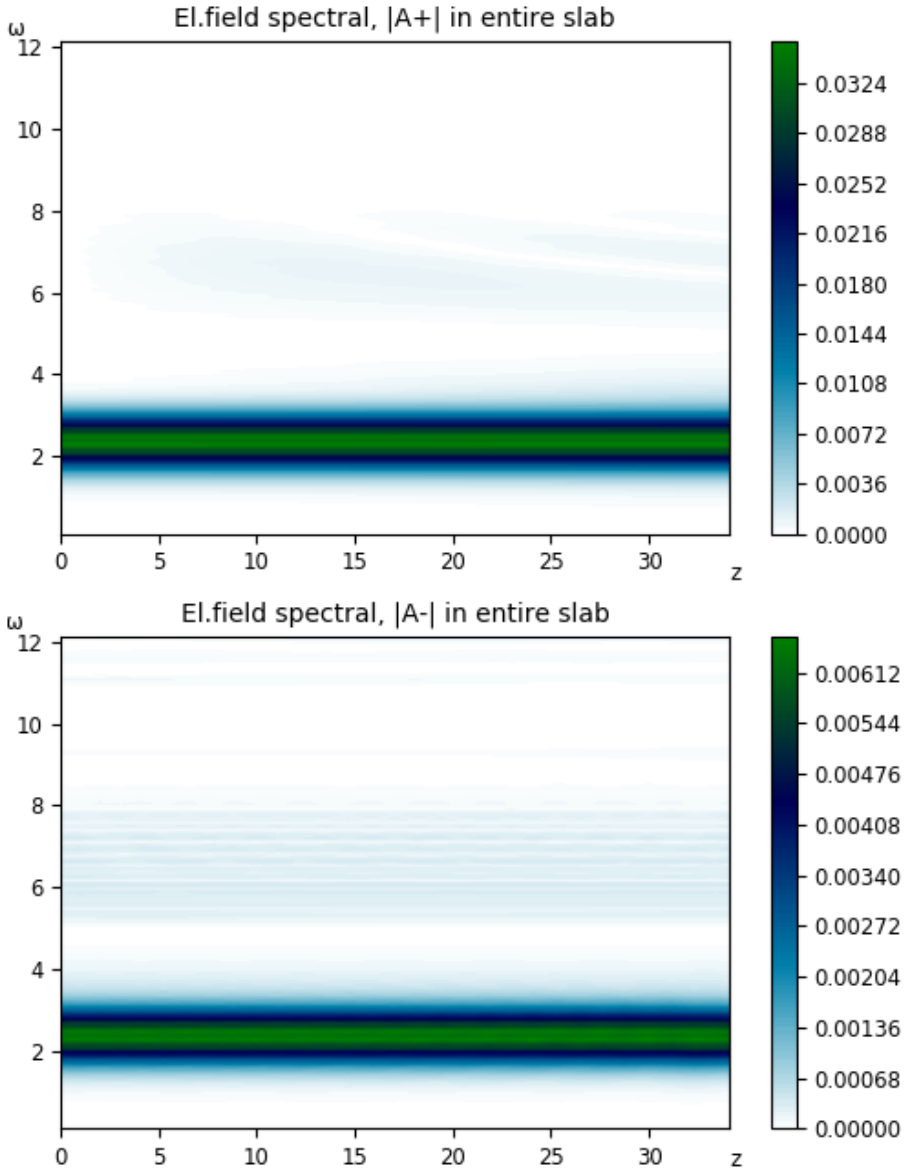

Figure 9.13: Case 2: Spectral amplitudes solution in the entire slab.

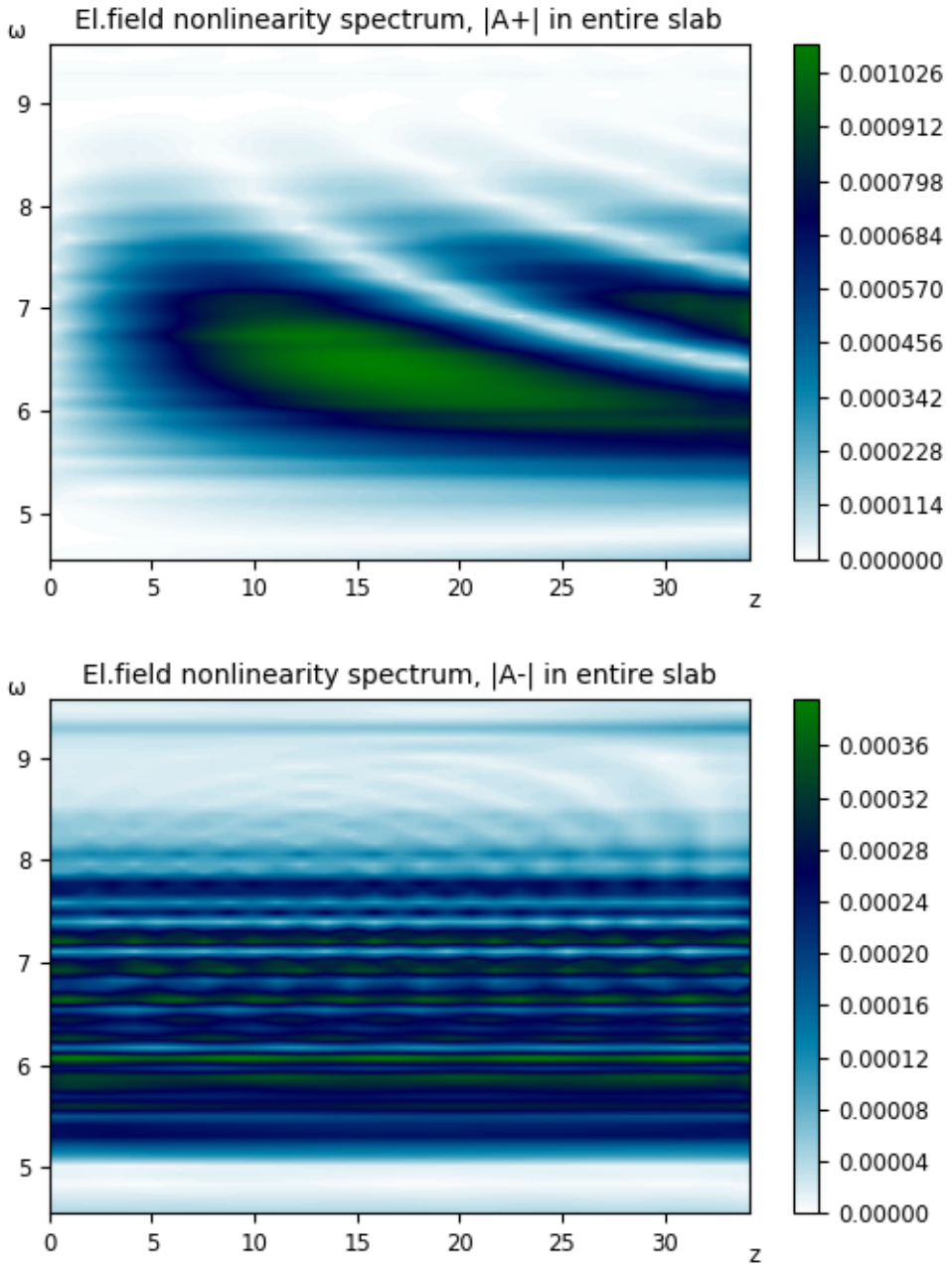

Figure 9.14: Case 2: Spectral amplitudes solution in the entire slab, zoom on Kerr-affected $3\omega_c'$ range.

10 Discussion

10.1 BPPE method accuracy

Error analysis

Addressing the topic of accuracy of the BPPE method we need to keep in mind that we do not have the *exact* solutions available as reference. The AST reference that we use is obtained by solving a nonlinear ODE system with a numerical solver, and as such it is also prone to error.

The tolerance for the numerical ODE solver used is a combination of absolute and relative tolerance thresholds, summing up to $3.6e-5$. This is the accuracy we can expect from the reference solution. Given that the iterated solution depends on repeated calls to the ODE solver, we would expect those errors to accumulate.

Simultaneously, the Newton's algorithm has its own convergence tolerance threshold, expressed as the allowable error of the zero value and set to $1.5e-8$. It tells us about the *backward* error of the approximation (how far the function of approximated root is from the exact zero). We do not know what the *forward* error is, namely what the error of Φ_{-} is. We do know, however, the error of Ψ_{-}. Ψ_{-} should be exactly zero, while we obtain at maximum about $2e-5$ and $3e-4$ discrepancies for Case 1 and Case 2 respectively. This is visible in Figures 9.5 and 9.10. That result seems to be aligned with the ODE solver tolerance.

Decreasing both the ODE solver tolerance and the Newton's method convergence threshold, we observed clearly that the iterative process took considerably more iterations to converge. However, we did not observe the decrease of maximum Ψ_- discrepancies with respect to the exact zero, nor did the reconstructed electric field alignment improved. The issue of what those errors are attributed to requires further investigation, especially in combination with increasing the number of discrete points in the ω-domain. Given the complexity of the system one could expect that the interdependence of errors is also non-trivial.

Nonlinearity-factor impact on accuracy and convergence

We recall that the discrepancies of the reconstructed electric field magnitudes were:

- Case 1 discrepancies: maximum: $1e-4$, average: $1e-5$,
- Case 2 discrepancies: maximum: $1e-2$, average: $1e-3$.

The increase of η' by two orders of magnitude resulted in the increase of the discrepancies with respect to the AST reference also by two orders of magnitude. We have seen that those discrepancies occur practically only between the field peaks, where the electric field received an additional oscillation of small amplitude, likely caused by the increase of amplitudes in the $3\omega_c$ range. We have also seen that in the spectral domain the discrepancies occurred mostly for this $3\omega_c$ range.

Based on those observations we conclude that the presented *implementation* of the BPPE shooting method

- was able to reproduce the linear part of the propagation problem accurately,
- despite having converged, it struggled to reproduce the exact oscillations emerging due to Kerr-nonlinearity, but it was able to reproduce (*mimic*) the prevalent oscillation pattern (we recall Figures 9.6, 9.7 and 9.9),
- has accuracy and convergence rate dependent on the size of the nonlinearity coefficient η'.

Nevertheless, it is fair to note that for higher choices of η', and sufficiently long slab length and propagation time, the iterative process either failed to converge within 500 iterations, or the numerical values exceeded the representable range. We observed a quick build-up of spectral amplitudes, that led to out-

of-range values in numerical terms. Such sensitivity to the increase in η' strongly suggests a cautious optimism towards the numerical results obtained in such cases. Assuming that the convergence properties of the BPPE shooting method itself are not affected by the increase of the nonlinearity coefficient, we conclude that the robustness of the presented implementation requires a thorough investigation, both by analyzing the results against theoretical expectations, and by performing further tests of the implementation.

Forcing left-traveling modes to zero

Throughout the experiments, especially in Figures 9.5 and 9.10, we showed that the discrepancies for the left-traveling modes are much bigger than for the right-traveling modes. This can be explained by the method of initializing the AST. For the AST BC we first solved a BPPE problem, and forced Ψ_- to be to zero, while maintaining Ψ_+ as it was. The new scatter problem was challenged to get aligned to this new, only partially-modified state, while both states (left- and right-traveling modes) are in fact coupled.

Since the amplitude of the right-traveling mode is the dominant one, converging with the left-traveling mode to a modified state must have been more difficult, and we indeed observed larger discrepancies there. In other experiments, where Ψ_- state was not forced to zero in the reference, we observed that the size of the discrepancies decreased.

The BPPE method itself also repeats the step of forcing the left-traveling mode to zero at each iteration. This is the crucial step of the method. It is a matter of further investigation to determine how this step impacts the accuracy of the left-traveling mode solution. Especially when the internal reflection rate in slab is much higher, and the magnitudes of both left- and right-traveling modes are comparable.

Final note on convergence

The convergence of the method has already been addressed in various context in this section. The final remark we would like to stress regards the impact of the BC on the ability to converge.

In section 9.1.1 we make argument for why we choose to initialize the AST with a solution from a previously solved scatter problem, instead of using a perfect Gaussian as AST BC. Apart from the reasons presented there, in our experiments we also observed that setting Ψ_+ to be a perfect Gaussian causes notably worse convergence of the BPPE iteration solving the scatter problem.

This manifested itself in both

- notably higher number of iterations required to converge,
- discrepancies increased by 1 order of magnitude.

We know that in general convergence rate is determined by an initial guess. In this case we observe that it is also determined by the end-result to which the iterative process is expected to converge. Given the coupling of right- and left-traveling modes, it might be that converging to certain results is more difficult than to others. However, making a statement of such loose hypothesis requires further investigation of the convergence properties of the proposed implementation.

10.2 Qualitative results

Light-propagation features

Certain aspects of the qualitative behavior of the simulated system are already mentioned in section 9.2.3. Figure 9.12 is a testimony to the fact that the presented implementation of the BPPE method simulates correctly the following phenomena:

- The reflection of the beam from material interfaces.

  Following Fresnel equations the reflectivity should be about 4% for the center frequency ω_c. What we obtain is that the amplitude of the electric field reflected from the interface at $z = b$ is around 15% of the incoming beam. This result is rather high, but given a relatively high polarization nonlinearity coefficient η', and the fact that the refractive index $n(\omega)$ is not exactly constant, we cannot immediately dismiss it. We have also seen that the error of Ψ_- is non-zero, so we expect certain deviation from the theoretical predictions. Establishing the exact expected reflection rate for this case requires further analysis.

- The rate of propagation of the pulse is consistent with the group velocity v_g computed for the center frequency ω_c.

Also, as we have demonstrated in various figures in Chapter 9:

- Spectral amplitudes in the Kerr-affected frequency range arise as the pulse propagates through the material slab.

- Increase of the amplitudes in the $3\omega_c$ range is also detectable in the reconstructed electric field, as an additional oscillation on top of the main oscillation of the carrier wave (presented in Figure 9.11).

The above observations confirm that the BPPE method, and its implementation presented in this paper, are able to successfully represent the nonlinear polarization impact and the qualitative properties of pulse-propagation through a material medium with interfaces. An important result is that the BPPE method delivered what it was designed for, namely to capture the back-scatter of light beam.

Emergent structures

We return now to the results of Figure 9.14, which presents a zoom on the Kerr-affected frequency range of the spectral amplitudes.

The amplitudes in that range are driven by polarization nonlinearity p_1, which with $e_2 \approx 0$, is practically dependent only on e_1^3. In Figures 9.13, 9.13 we see a clear hierarchy of terms, where

$$\begin{aligned} |A_+|_{\omega_c} &\approx 100\% \text{ of } |A_+|_{\omega_c}, \\ |A_-|_{\omega_c} &\approx \ 18\% \text{ of } |A_+|_{\omega_c}, \\ |A_+|_{3\omega_c} &\approx \ 3\% \text{ of } |A_+|_{\omega_c}, \\ |A_-|_{3\omega_c} &\approx \ 1\% \text{ of } |A_+|_{\omega_c}. \end{aligned}$$

The magnitude $|A_+|_{\omega_c}$ exceeds $|A_-|_{\omega_c}$ approximately by 1 order of magnitude. Building e_1^3 makes that disproportion grow to three orders of magnitude. Thus A_+ seems to be the driving element for both A_+ and A_- amplitudes in $3\omega_c$ range. Presumably, this is why we observe $|A_-|_{3\omega_c}$ to remain fairly constant, being dominated by $|A_+|_{\omega_c}$. On the other hand, $|A_+|_{3\omega_c}$ depends also on itself to a certain degree, which might be enough to generate the *ripple*-pattern visible at the top of Figure 9.14. We are, of course, far from explaining the origin of that pattern, as the underlying interplay of participating elements is rather complex.

The highlight here is that, potentially, by means of applying the BPPE method, we have been able to *uncover* in our simulation an *emergent structure* - a large-scale entity, that is seemingly detached from the properties of individual elements, but that clearly emerges when large collections of those elements are considered. One might say that an emergent structure is *an added value*, which can only be appreciated once many building blocks are assembled together, and it is very hard, if not impossible, to predict from the properties of a single building block.

Had we not obtained any emergent pattern in our results, that would go unnoticed. The structure we see is hard enough to explain once it is already there, yet alone predict and foresee it. It is, of course, easy to get carried away and draw far-fetched conclusions. The pattern that we observe might, after all, be an emergent structure of numerical errors or ODE solver properties, for all we know. Nevertheless, it is not the first time that a structure emerged from a complex system, so we take this as an encouraging result, and one of the starting points for future work.

11

Future work

BPPE method is a fairly new method, and as such it offers many yet-to-be explored directions. With respect to the work presented in this paper, we see the two major focus areas.

The first area is the investigation of the limitations of the method, and of any practical, numerical implementations that it might incarnate as. Many of the ideas were already indicated in the Discussion Chapter 10. They involve, among others, studies of

- accuracy and errors, especially for the left-traveling mode,
- convergence, also in the context of sensitivity to initial conditions,
- the ability to reproduce physical behavior for high-nonlinearity cases.

Another field with much room for improvement is the flexibility and performance of the underlying implementation. That includes

- adding spatial dimensions to the slab representation,
- allowing for non-uniformity in those spatial dimensions, thus allowing for focusing of the beam and simulating oblique incidence angles, and increasing the potential for the emergence of the Q-mode,

- investigating the possibilities of parallelization of the source code for certain types of nonlinearities and implementing them. For the highly-mixing Kerr-type nonlinearity handled in this paper, parallelizing the solution of the BPPE system is non-trivial. However, one can design other types of third-order nonlinearities to promote a more decoupled BPPE system. An example of such *spectrally-local* nonlinearity is presented in [7].

In this paper we have not investigated how the BPPE method implementation reacts to variation of certain parameters. For example, we have treated only very short propagation distances. Allowing for longer slabs would give insight into how the method handles further evolution of the Kerr-effect. Another example is the refractive index. By assuming an almost constant refractive index, we did not leave much room for dispersion to arise. Representing this phenomenon is a crucial feature of the method, and could be investigated further. Also, designing the input pulse to be of even higher intensity and shorter temporal duration would put the method to test in terms of handling the ultra-fast field variations of femtosecond pulses.

Given the well-established reign of UPPE methods in physics of pulse propagation, it would be reasonable to carry out a more thorough comparison of the simulation results yielded by each method, and isolating cases where each of methods is potentially superior to the other one.

Finally, the BPPE method has shown promise of ability to model *emergence* of the underlying complex system. The study of that topic is a completely separate one, and a very young too. Developing a BPPE implementation and pushing it to the limits might also prove to be a tool in the study of the phenomenon of emergence.

12

Summary

In this paper we considered the BPPE method and its capability for modeling the secondary electromagnetic field, arising as a response of a material to an externally applied electric pulse.

We presented the details of derivation for a TM field in a material slab with Kerr-type polarization response, delimited by two material interfaces. We demonstrated that by making a reasonable assumption about the nonlinear polarization being a perturbation on top of the linear response, the system of Maxwell's equations can be transformed into an explicit z-propagation system, such that a boundary-value problem can be formulated for pulse propagation in a natural way. We have shown that solving the system in spectral domain reveals a redundancy in the normal-modes expansion of the electric field solution. That allows for posing an additional constraint, which then plays a key role in supplying the back-propagation capabilities to the BPPE method.

The BPPE shooting method is built around the fact that no incoming modes are expected on the far side of the slab, and iteratively enforcing that expectation onto the intermediate state of the system. By performing case-study simulations, we showed that convergence of such iterative process can indeed be reached, producing a viable solution. However, the size of nonlinearity coefficient η, and the initial conditions, impact the convergence of the numerical iterative process. Separating the limitations of the underlying implementation from the properties of the BPPE method itself requires further investigation.

Apart from the left- and right-traveling modes, we devoted certain attention to the existence of the transversely-propagating mode. The Q-mode cannot arise in a system with a uniformity in the transverse-direction. In general case, the scale of Q is different than the scale of the longitudinally-propagating modes, and it is proportional to the degree of focusing of the beam along the transverse direction.

Employing a dedicated AST procedure allowed for cross-referencing the simulation results and performing an error analysis. We found the errors to be comparable to the tolerance thresholds of the internal solvers, indicating a reasonable accuracy of the solution. The increase of η resulted in a corresponding increase of the errors, which was clearly connected to the arising of high-frequency perturbation on top of the main electric field oscillation. The iterative solution had trouble following the reference perturbation exactly, but it was nonetheless capable of reproducing the overall perturbation pattern, maintaining similar amplitudes and frequencies of oscillation. In the context of the obtained simulation results, we indicated several areas of testing the underlying implementation further.

Qualitatively, we have seen all the key phenomena of light propagation reconstructed in the iterative solution, including partial reflection form the interfaces, group velocity of the temporal pulse, and third harmonic generation due to Kerr effect. For the Kerr-affected frequencies we observed intriguing patterns emerging from the field of spectral magnitudes. That inspires further research directions, related to the ability of the method to capture prevalent patterns of various nature in the system.

Bibliography

[1] Thomas Brabec and Ferenc Krausz. Nonlinear optical pulse propagation in the single-cycle regime. *Physical Review Letters*, 78:3282, 1997.

[2] A. Couairon et al. Practitioner's guide to laser pulse propagation models and simulations. *Eur. Phys. J. Special Topics*, 199:5–76, 2011.

[3] A. Hofstrand, P. Jakobsen, and J. V. Moloney. Bidirectional shooting method for extreme nonlinear optics. *Phys. Rev. A*, 100:053818, 2019.

[4] HORIBA. Lorentz Dispersion Model. Technical report, HORIBA Jobin Yvon, 2006.

[5] Per Jakobsen and J. V. Moloney. The effect of longitudinal electric field components on the propagation of intense ultrashort optical pulses. *Physica D*, 241:1603–1616, 2012.

[6] Per Kristen Jakobsen. Bidirectional pulse propagation equation for extreme nonlinear optics. *Physica Scripta*, 89:095502, 2014.

[7] Per Kristen Jakobsen. A fixpoint formulation of BPPE for TE-electromagnetic waves for a dispersive material in the presence of material interfaces and spectrally local response. 2019.

[8] M. Kolesik and J. V. Moloney. Nonlinear optical pulse propagation simulation: From Maxwell's to unidirectional equations. *Physical review E*, 70:036604, 2004.

[9] M. Kolesik and J. V. Moloney. Modeling and simulation techniques in extreme nonlinear optics of gaseous and condensed media. *Reports on Progress in Physics*, 77:1, 2014.

[10] M. Kolesik, J. V. Moloney, and M. Mlejnek. Unidirectional optical pulse propagation equation. *Physical Review Letters*, 89(28):283902, 2002.

[11] Alexander Q. Wu, Ihtesham H. Chowdhury, and Xianfan Xu. Femtosecond laser absorption in fused silica: Numerical and experimental investigation. *Phys. Rev. B*, 72:085128, 2005.

Appendices

A Fourier Transform conventions

We present here the FT conventions used in this paper. Different conventions are used for the transforms of temporal and spatial variables.

A.1 Convention for spatial variable x

$$\text{FT:} \qquad \widehat{f}(\xi) = \frac{1}{\sqrt{2\pi}} \int_{-\infty}^{+\infty} dx \; f(x) \; e^{-i\xi x}$$
$$\text{IFT:} \qquad f(x) = \frac{1}{\sqrt{2\pi}} \int_{-\infty}^{+\infty} d\xi \; \widehat{f}(\xi) \; e^{i\xi x}$$

We now consider an example showing the FT of the derivative ∂_x.

Example Using IFT to represent $e(x)$ we can write

$$\begin{aligned}
\mathcal{F}\left\{\partial_x e(x)\right\} =& \mathcal{F}\left\{\frac{1}{\sqrt{2\pi}} \int_{-\infty}^{+\infty} d\xi \; \hat{e}(\xi) \; \partial_x \; e^{i\xi x}\right\} \\
&= \mathcal{F}\left\{i\xi \frac{1}{\sqrt{2\pi}} \int_{-\infty}^{+\infty} d\xi \; \widehat{e}(\xi) \; e^{i\xi x}\right\} \\
&= \mathcal{F}\left\{i\xi \; e(x)\right\} \\
&= \frac{1}{\sqrt{2\pi}} \int_{-\infty}^{+\infty} dx \; \left(i\xi \; e(x)\right) \; e^{-i\xi x} \\
&= i\xi \; \frac{1}{\sqrt{2\pi}} \int_{-\infty}^{+\infty} dx \; e(x) \; e^{-i\xi x} \\
&= i\xi \; \widehat{e}(\xi).
\end{aligned}$$

We obtained that under this convention

$$\begin{aligned}
\partial_x &\to i\xi, \\
\partial_{xx} &\to (i\xi)^2 = -\xi^2.
\end{aligned}$$

A.2 Convention for temporal variable t

$$\text{FT:} \qquad \widehat{f}(\omega) = \frac{1}{\sqrt{2\pi}} \int_{-\infty}^{+\infty} dt\ f(t)\ e^{i\omega t}$$
$$\text{IFT:} \qquad f(t) = \frac{1}{\sqrt{2\pi}} \int_{-\infty}^{+\infty} d\omega\ \widehat{f}(\omega)\ e^{-i\omega t}$$

We now consider an example showing the FT of the derivative ∂_t.

Example Using IFT to represent $e(t)$ we can write

$$\begin{aligned}
\mathcal{F}\left\{\partial_t e(t)\right\} =& \mathcal{F}\left\{\frac{1}{\sqrt{2\pi}} \int_{-\infty}^{+\infty} d\omega\ \hat{e}(\omega)\ \partial_t\ e^{-i\omega t}\right\} \\
&= \mathcal{F}\left\{-i\omega \frac{1}{\sqrt{2\pi}} \int_{-\infty}^{+\infty} d\omega\ \widehat{e}(\omega)\ e^{-i\omega t}\right\} \\
&= \mathcal{F}\left\{-i\omega\ e(t)\right\} \\
&= \frac{1}{\sqrt{2\pi}} \int_{-\infty}^{+\infty} dt\ \left(-i\omega\ e(t)\right)\ e^{i\omega t} \\
&= -i\omega\ \frac{1}{\sqrt{2\pi}} \int_{-\infty}^{+\infty} dt\ e(t)\ e^{i\omega t} \\
&= -i\omega\ \widehat{e}(\omega).
\end{aligned}$$

We obtained that under this convention

$$\begin{aligned}
\partial_t &\to -i\omega, \\
\partial_{tt} &\to (-i\omega)^2 = -\omega^2.
\end{aligned}$$

B Origin of refractive index

This section shows how the refractive index $n(\omega)$ originates from the FT of $(1 + \mathcal{L})$ operator acting on an electric field component. We apply FT in x and t variables. For susceptibility χ we consider only temporal dispersion (not spatial) such that $\chi = \chi(t - t')$ and FT of χ is taken only with respect to temporal variable.

We are interested in taking the following FT

$$\mathcal{F}\left\{(1 + \mathcal{L})\boldsymbol{e}\,(z, x, t)\right\} = \mathcal{F}\left\{\boldsymbol{e}\,(z, x, t) + \int_{-\infty}^{t} dt'\ \chi\,(t - t')\,\boldsymbol{e}\,(z, x, t')\right\}. \quad (1)$$

We express $\boldsymbol{e}$ and χ in terms of their respective IFTs as

$$\boldsymbol{e}\,(z,x,t') = \frac{1}{\sqrt{2\pi}^2}\int_{-\infty}^{+\infty} d\omega \int_{-\infty}^{+\infty} d\xi\ \widehat{\boldsymbol{e}}\,(\omega,\xi,z)\ e^{i\xi x - i\omega t'},$$
$$\chi\,(\tau = t - t') = \frac{1}{\sqrt{2\pi}}\int_{-\infty}^{+\infty} d\omega''\ \widehat{\chi}(\omega'')\, e^{-i\omega''\tau}.$$

Now, we extend χ to negative time. For $t' > t$ we have $\chi\,(\tau < 0)$ and $\widehat{\chi}(\omega < 0) = 0$. Thus we can extend the integration scope for χ

$$\int_{-\infty}^{t} dt'\ \chi(\tau) \to \int_{-\infty}^{+\infty} dt'\ \chi(\tau).$$

We can now write (1) as

$$\mathcal{F}\left\{\boldsymbol{e}\,(z,x,t) + \int_{-\infty}^{t} dt'\ \underbrace{\frac{1}{\sqrt{2\pi}}\int_{-\infty}^{+\infty} d\omega''\ \widehat{\chi}(\omega'')\, e^{-i\omega''(t-t')}}_{\chi(\tau)} \underbrace{\frac{1}{\sqrt{2\pi}^2}\int_{-\infty}^{+\infty} d\omega \int_{-\infty}^{+\infty} d\xi\ \ \widehat{\boldsymbol{e}}\,(\omega,\xi,z)\ e^{i\xi x - i\omega t'}}_{\vec{e}(z,x,t')}\right\}.$$

Dropping the dependence on arguments for the electric field, and changing the order of integration we obtain

$$\mathcal{F}\left\{\boldsymbol{e} + \frac{1}{\sqrt{2\pi}^3}\int_{-\infty}^{+\infty} d\omega''\ \widehat{\chi}(\omega'')\, e^{-i\omega'' t} \int_{-\infty}^{+\infty} d\omega \int_{-\infty}^{+\infty} d\xi\ \widehat{\boldsymbol{e}}\, e^{i\xi x} \underbrace{\int_{-\infty}^{t} dt'\ e^{i(\omega''-\omega)t'}}_{2\pi\ \delta(\omega''-\omega)}\right\}.$$

Using the properties of Dirac δ-distribution shown in Appendix C we write

$$
\begin{aligned}
&\mathcal{F}\left\{\boldsymbol{e}+\frac{1}{\sqrt{2\pi}^{3}}\int_{-\infty}^{+\infty}d\omega\int_{-\infty}^{+\infty}d\xi\ \underbrace{\int_{-\infty}^{+\infty}d\omega''\ \widehat{\chi}(\omega'')\,e^{-i\omega'' t}\ 2\pi\ \delta\left(\omega''-\omega\right)}_{\text{no contribution unless } \omega''=\omega}\widehat{\boldsymbol{e}}\ e^{i\xi x}\right\}\\
&=\mathcal{F}\left\{\boldsymbol{e}+\frac{1}{\sqrt{2\pi}}\int_{-\infty}^{+\infty}d\omega\int_{-\infty}^{+\infty}d\xi\ \widehat{\chi}(\omega)\,e^{-i\omega t}\ \widehat{\boldsymbol{e}}\,e^{i\xi x}\right\}\\
&=\widehat{\boldsymbol{e}}+\mathcal{F}\left\{\frac{1}{\sqrt{2\pi}}\int_{-\infty}^{+\infty}d\omega\int_{-\infty}^{+\infty}d\xi\ \widehat{\chi}(\omega)\,\widehat{\boldsymbol{e}}\,e^{i(\xi x-\omega t)}\right\}\\
&=\widehat{\boldsymbol{e}}+\sqrt{2\pi}\,\mathcal{F}\left\{\underbrace{\frac{1}{\sqrt{2\pi}^{2}}\int_{-\infty}^{+\infty}d\omega\int_{-\infty}^{+\infty}d\xi\ \widehat{\chi}(\omega)\,\widehat{\boldsymbol{e}}\,e^{i(\xi x-\omega t)}}_{\mathcal{F}^{-1}\text{ form}}\right\}\\
&=\widehat{\boldsymbol{e}}+\sqrt{2\pi}\,\widehat{\chi}(\omega)\,\widehat{\boldsymbol{e}}\\
&=\underbrace{\left(1+\sqrt{2\pi}\,\widehat{\chi}(\omega)\right)}_{n^2(\omega)}\widehat{\boldsymbol{e}}\,(\omega,\xi,z)\,,
\end{aligned}
$$

where we have used the fact that $\mathcal{F}\left\{\mathcal{F}^{-1}\left\{(\cdot)\right\}\right\}=(\cdot)$.

We have obtained that under FT, the operator is transformed as follows

$$(1+\mathcal{L})\xrightarrow{\mathcal{F}}\left(1+\sqrt{2\pi}\,\widehat{\chi}(\omega)\right)\overset{def.}{=}n^2(\omega).$$

It must be noted that the definition of the refractive index $n(\omega)$ most commonly used in optics is $n^2(\omega)=(1+\widehat{\chi}(\omega))$. That difference stems from the FT conventions used in this paper. Had we chosen a convention where the normalization factor $\frac{1}{2\pi}$ is not evenly distributed among $\mathcal{F}$ and $\mathcal{F}^{-1}$, but rather present in its entirety in $\mathcal{F}^{-1}$, the definition of $n(\omega)$ would be aligned with the one most common in optics.

The take-away point in those considerations is that the refractive index is obtained from the FT of a convolution operator $\mathcal{L}$ acting on $\widehat{e}$, and the exact conventions of the FT do not change the final result of out considerations, as long as consistency between FT and IFT is maintained. As revealed in section 8.3.4, the convention used for the implementation follows the one common in optics, and so does the refractive index model used, presented in section 2.4.

We also use that

$$\mathcal{F}\left\{(1+\mathcal{L})^{-1}\right\} \overset{def.}{=} \frac{1}{n^2(\omega)}.$$

C Dirac δ-distribution

Using FT conventions as in Appendix A, the following relations apply for Dirac δ-distribution

$$\begin{aligned}
\delta(\xi) &= \frac{1}{\sqrt{2\pi}} \int_{-\infty}^{+\infty} dx\ \delta(x)\ e^{-i\xi x} = \frac{1}{\sqrt{2\pi}} \\
&\Downarrow \\
\delta(\xi) &= \frac{1}{\sqrt{2\pi}} \int_{-\infty}^{+\infty} dx\ \frac{1}{\sqrt{2\pi}}\ e^{-i\xi x} \\
&\Downarrow \\
2\pi\delta(\xi) &= \int_{-\infty}^{+\infty} dx\ e^{-i\xi x}.
\end{aligned}$$

By analogy we have

$$\begin{aligned}
\delta(x) &= \frac{1}{\sqrt{2\pi}} \int_{-\infty}^{+\infty} d\xi\ \delta(\xi)\ e^{i\xi x} = \frac{1}{\sqrt{2\pi}} \\
&\Downarrow \\
\delta(x) &= \frac{1}{\sqrt{2\pi}} \int_{-\infty}^{+\infty} d\xi\ \frac{1}{\sqrt{2\pi}}\ e^{i\xi x} \\
&\Downarrow \\
2\pi\delta(x) &= \int_{-\infty}^{+\infty} d\xi\ e^{i\xi x},
\end{aligned}$$

and

$$\begin{aligned}
\delta(\omega) &= \frac{1}{\sqrt{2\pi}} \int_{-\infty}^{+\infty} dt\ \delta(t)\ e^{i\omega t} = \frac{1}{\sqrt{2\pi}} \\
&\Downarrow \\
\delta(\omega) &= \frac{1}{\sqrt{2\pi}} \int_{-\infty}^{+\infty} dt\ \frac{1}{\sqrt{2\pi}}\ e^{i\omega t} \\
&\Downarrow \\
2\pi\delta(\omega) &= \int_{-\infty}^{+\infty} dt\ e^{-i\xi x}.
\end{aligned}$$

Also, we have the basic property of

$$\int_{-\infty}^{\infty} d\alpha\ f(\alpha)\ \delta(\alpha-\gamma) = f(\gamma).$$

D Deriving back-propagation formula from additional constraint

This appendix contains the details of deriving integral formula (6.1) from the constraint (3.25).

We apply the Fundamental Theorem of Calculus (FTC)

$$\begin{aligned}
\int_a^b dz\ \frac{d\ f(z)}{dz} &= \int_a^b dz\ h(z) \\
&\Updownarrow \\
f(b) - f(a) &= \int_a^b dz\ h(z) \\
&\Updownarrow \\
f(a) &= f(b) - \int_a^b dz\ h(z),
\end{aligned}$$

to (3.25), dropping the dependence of A_+ and A_- on arguments (z, ω, ξ)

$$\begin{aligned}
\partial_z A_+ e^{i\beta z} + \partial_z A_- e^{-i\beta z} &= 0 \\
&\Downarrow \\
-\partial_z A_- &= \partial_z A_+ e^{2i\beta z} \\
&\downarrow \text{integrating over } \int_a^b \\
-\int_a^b dz\ \partial_z A_- &= \int_a^b dz\ \partial_z A_+ e^{2i\beta z} \\
&\downarrow \text{FTC} \\
-\left[A_-(b) - A_-(a)\right] &= \int_a^b dz\ \partial_z A_+ e^{2i\beta z} \\
&\Downarrow \\
A_-(a) - A_-(b) &= \int_a^b dz\ \partial_z A_+ e^{2i\beta z} \\
&\Downarrow \\
A_-(a) &= A_-(b) + \int_a^b dz\ \partial_z A_+ e^{2i\beta z}.
\end{aligned}$$